INFORMATION TO USERS

This manuscript has been reproduced from the microfilm master. UMI films the text directly from the original or copy submitted. Thus, some thesis and dissertation copies are in typewriter face, while others may be from any type of computer printer.

The quality of this reproduction is dependent upon the quality of the copy submitted. Broken or indistinct print, colored or poor quality illustrations and photographs, print bleedthrough, substandard margins, and improper alignment can adversely affect reproduction.

In the unlikely event that the author did not send UMI a complete manuscript and there are missing pages, these will be noted. Also, if unauthorized copyright material had to be removed, a note will indicate the deletion.

Oversize materials (e.g., maps, drawings, charts) are reproduced by sectioning the original, beginning at the upper left-hand corner and continuing from left to right in equal sections with small overlaps.

Photographs included in the original manuscript have been reproduced xerographically in this copy. Higher quality 6" x 9" black and white photographic prints are available for any photographs or illustrations appearing in this copy for an additional charge. Contact UMI directly to order.

Bell & Howell Information and Learning
300 North Zeeb Road, Ann Arbor, MI 48106-1346 USA
800-521-0600

THE EFFECT OF ZINC STEARATE ON THE COMPACTION AND SINTERING CHARACTERISTICS OF A Ti-6%Al-4%V HYDRIDE-DEHYDRIDE POWDER

by

Leslie Ederer

A Thesis Submitted to the Faculty of Graduate Studies and Research in Partial Fulfillment of the Requirements for the Degree of Master of Engineering

Department of Mining and Metallurgical Engineering
McGill University
Montreal, Canada
July, 1999

I would like to give thanks to God for blessing me with the opportunity of higher education, and dedicate this thesis to my mother and father whose encouragement and sacrifice will never be forgotten.

ABSTRACT

Powder metallurgy (P/M) processing has become an important technique replacing many casting applications, especially for the fabrication of refractory metals where very high melting temperatures are required. Improvement in powder production, cleanliness and characterization techniques, combined with an increased understanding of basic compaction and sintering principles and a need for metals with high strength to weight ratios has led to an increased interest in titanium powder utilization. P/M techniques for Ti-6Al-4V powder can enable the production of high quality parts at lower processing temperatures and cost. For most applications prealloyed powder produced by the hydride-dehydride process (HDH) is used, due to the lower cost of this powder as compared to Ti-6Al-4V powder produced by other methods.

Lubricant is generally added in powder systems to reduce die wear and ejection pressure, increase compactability and eliminate cracking. The effect lubricants have on the green and sintered density is well documented in such metals as copper, aluminum, tungsten and iron. However, such information is limited for titanium. Thus general characterization of a Ti-6Al-4V HDH powder and the effects of using a zinc stearate on the green and sintered density were examined at different compaction pressures and sintering temperatures. The addition of the lubricant was found to increase the green density by at least 4 percent for all compaction pressures, and the sintered density between 2 to 6 percent depending. The optimum lubricant addition was 0.50 weight percent, above which no significant improvement in the sintered density was observed. The sintered lubricant samples did not exhibit residual contamination and were found to improve sintering kinetics above 1300°C. Therefore, lubricants have the potential to improve consolidation and sintering of Ti-6Al-4V HDH powders at a lower cost.

RÉSUMÉ

Le procédé de la métallurgie des poudres est une technique de pointe qui permet d'obtenir des produits solides sans qu'il y ait fusion, ce qui est très avantageux lors de l'élaboration des métaux réfractaires dont les températures de fusion sont très élevées. L'amélioration de la technique de production des poudres, du contrôle des contaminants et des techniques de caractérisation, combinés à une meilleure connaissance des principes de compaction ainsi que de frittage et du besoin d'utiliser des matériaux à un haut ratio de résistance mécanique versus poids à conduit au développement de la métallurgie des poudres de titane. La poudre Ti-6Al-4V permet de fabriquer des pièces de grande qualité à des coûts et températures inférieurs aux procédés de fonderie traditionnels. Pour la majorité des applications, le procédé d'hydratation–déshydratation (HDH) de fabrication de poudre pré-allié de Ti-6Al-4V est le moins coûteux parmi les méthodes existantes.

Des lubrifiants sont additionnées aux poudres pour diminuer les pressions d'éjection et l'usure des matrices, pour augmenter le degré de compaction et éliminer les fissures. L'effet des lubrifiants sur la densité de la poudre après la compaction et le frittage, est bien connu pour les poudres de cuivre, aluminium, tungstène et fer. Cependant, cette information est peu connue pour le titane. La caractérisation des poudres Ti-6Al-4V HDH et l'effet du lubrifiant de stearate de zinc sur la densité de la poudre après la compaction et après le frittage furent étudié pour différentes pression de compaction et températures de frittage. Il a été établi que l'addition du lubrifiant a augmenté la densité de la poudre après compaction d'un minimum de 4% et la densité après frittage de 2% à 6%. L'addition optimale de lubrifiant est de 0.5% poids. Au-dessus de ce pourcentage il n'y a pas d'augmentation significative de la densité de la poudre après frittage. Les échantillons frittés et fabriqués à l'aide du lubrifiant montrent aucune contamination, tandis que les vitesses de frittage sont améliorées aux températures de frittage supérieures à 1300°C. Par conséquent, les lubrifiants peuvent augmenter le degré de compaction et le frittage des poudres de Ti-6Al-4V HDH d'une manière économique.

ACKNOWLEDGEMENTS

I would like to express my gratitude to my thesis supervisor, Professor Robin A.L. Drew for giving me the opportunity to work in the Ceramic and Composites Processing laboratory at McGill University. I extend my appreciation to him also for his guidance, support and inspiring scientific discussions and suggestions throughout my studies.

I would also like to acknowledge Pratt & Whitney Canada for the support that made this thesis possible, and in particular Denis Blanchet, Jutta DeMers, David Holford, Claude Foucault, Sylvain Gravel, Linda Lang, Francisco Miranda, Christian Picotin, Renald St-Louis and Nicolas Yvon.

I would also like to thank friends and colleagues, past and present, for their invaluable assistance. It is my pleasure to mention here a few names Priti Wanjara, Mona Wanjara, Luis Tavares, Peter Heilmann and my brother Victor Ederer.

Finally, I extend my heartfelt appreciation to my wife, Noosha, and her parents, Diane and Denis Holderberg for their patience, support and understanding during the many years of my study at McGill University. Their love and encouragement have made possible the achievements of this work.

TABLE OF CONTENTS

LIST OF FIGURES

CHAPTER 1

CHAPTER 2

CHAPTER 4

CHAPTER 5

LIST OF TABLES

CHAPTER 2

CHAPTER 4

CHAPTER 5

CHAPTER 1:

INTRODUCTION

Powder metallurgy (P/M) is a term used to describe the processing, fabrication and characterization of metallic powders (which may also contain non-metallic particles) that are used for consolidation into discrete and usable shapes[1,2]. Powder metallurgy generally involves compaction, which is the forming of the powder into a green compact of the desired shape, and sintering, which is the consolidation of the compact at some temperature below its melting point.

The application of powder metallurgy originated in the Near East where the earliest civilizations formed tools, weapons and ornaments from sponge iron during the so called "Iron Age" to form wrought iron. Examples of these include Egyptian iron implements dating from 3,000 BC and the Delhi column in India, 300 AD, consisting of approximately 6 tonnes of reduced iron. The beginning of modern P/M is generally associated with the process development for the production of fine platinum powder which was then pressed into a cake for forging in 1834 by the British Wollaston and Russian Sobolewskoy[2]. The first commercial development was in 1910 to form tungsten wire filament for lamps[3]. From the 1920's up to World War II, P/M was used mainly for the manufacturing of exotic components such as oil-less bearings and cemented carbides. However, from World War II and onwards the need for reduced labor costs and improved

dimensional control spurred the development of P/M manufacturing techniques. These techniques minimize segregation of alloying elements, allow compositional flexibility and promote the production of unique fine scale microstructures[2]. Thus, by the 1940's, conventional press and sintering was being applied to ferrous materials, by the 60's ferrous and non-ferrous and by the 70's specialty alloys.

The ability of P/M to reduce material costs has been the stimulus for the development of newer cost-effective high volume processes, which in turn increase the range of industrial applications. Since the 1970's powder metallurgy has become an increasingly more important technique for specialty metals. The reasons for this can be seen from the Venn diagram shown in Figure 1.1. The economic portion of the diagram represents high productivity and low cost fabrication of parts with high final tolerances versus casting where there are increased problems and associated costs with precision, machining, and segregation. The unique portion of the diagram represents the ability to fabricate unique microstructures that cannot be obtained by other methods. These include oxide and fiber dispersion strengthened alloys and porous metals. The final circle represents the refractory and reactive metal applications where fusion techniques are not practical. The overlap of the Venn diagram in all three categories exists in most practical P/M applications justifying the usage of P/M for specialty metals[1].

The potential of P/M is demonstrated with titanium, which has a high reactivity, particularly in the molten statc. P/M techniques utilize temperatures below the melting point of titanium, and by controlling the process environment (e.g. using a vacuum or inert atmosphere) it can minimize titanium from reacting. Titanium alloys are particularly attractive to the aerospace industry due to their strength to density ratio, toughness, fatigue, creep and corrosion resistance[4].

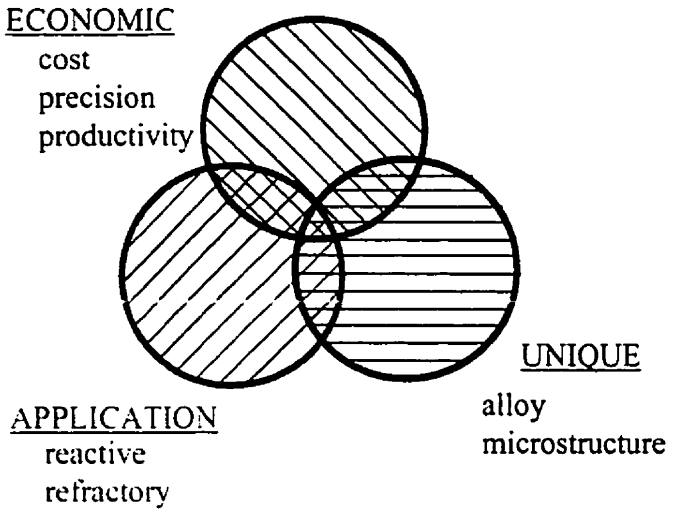

Figure 1.1: Venn diagram justifying the application of powder metallurgy[1].

Titanium was first discovered in minerals in England and Germany around 1790. It occurs mostly in the form of ilmenite, $FeTiO_3$, that consists of hematite, Fe_3O_3, in which half the iron has been replaced by titanium, and rutile, TiO_2. The earth crust contains approx. 0.6% titanium making it the ninth most abundant element and the fourth most abundant structural metal after aluminum, iron and magnesium[5]. Titanium is the 22nd element in the Periodic Table with an atomic weight of 47.88g/mole and a density in the alpha phase of 4.51g/cm^3 (value at 20°C) and beta phase of 4.35g/cm^3 (value at 885°C). The melting point of titanium is ≈1670°C. Pure titanium undergoes an allotropic transformation from hexagonal closed packed alpha phase to body centered cubic beta phase above 882.5°C. Elements that when added to titanium produce little change or an increase in the phase transformation temperature are known as "alpha stabilizers" such as tin, aluminum and interstitial elements. Elements such as the transition metals molybdenum and vanadium that decrease the phase transformation temperature are called "beta stabilizers"[5].

Alpha alloys, typified by Ti-5Al-2.5Sn have satisfactory strength, toughness, creep resistance and weldability. Furthermore, the lack of a ductile-to-brittle transformation

makes alpha alloys suitable for cryogenic applications. Beta-alloys such as Ti-15Mo-5Zr are extremely formable, have high strength (yield strength up to 1380 GPa) but are not suitable for low temperature applications. Alpha + beta alloys such as Ti-6%Al-4%V have good fabrication characteristics, high room temperature strength (900-1030 MPa) and moderate high temperature strength. These can contain from 10 to 50% beta at room temperature but if the content is over 20% then they cannot be welded. These alloys properties are controlled by heat treatment of the beta phase[5].

Ti-6%Al-4%V can acquire a large variety of microstructures with different arrangements of the alpha and beta phase. When quenched from above the beta transus temperature (approximately 988°C ± 10°C) the microstructure forms an acicular (needle) or fine-laminar structure called hexagonal closed packed martensite, α', which is crystallography related to the alpha phase. The rate of cooling also effects the shape of the martensite. For example slow cooling results in α-phase plate structure, air cooling results in acicular alpha and water quenching results in hexagonal closed packed martensite. Ti-6%Al-4%V quenched from between 750°C and 900°C produces an orthorhombic martensite α''[5]. Equiaxed microstructures are obtained by mechanical working (>75% reduction) of the mixed alpha and beta phases and then subsequent annealing at temperatures between 700°C and 925°C.

The titanium industry is able to rely on a copious and stable supply of basic ore developed in order to cope with the large demand for TiO_2 pigment which was 3,770,000 tonnes in 1994 or over 90% of the titanium demand[6]. Metallic titanium sponge accounts only for a few percent of this production because of the energy required to produce a ton of sponge-titanium (228 kcal/mole), which is 16 times that needed to produce a ton of steel, or 1.7 times that for a ton of aluminum[5]. Comparing 1994 world titanium metal production to other metals in Table 1.1, the relatively small titanium metal market which although growing (8% annually) is still limited[6].

Table 1.1: 1994 WORLD METAL PRODUCTION[5].

METAL	TONNAGE
Steel	724,000,000
Aluminum	19,100,000
Copper	8,995,000
Zinc	7,096,000
Lead	4,489,000
Nickel	830,000
Magnesium	279,500
Titanium Sponge	86,900

Of the total sponge production figure, approximately 75% is for aerospace use and only a few percent is for titanium powder applications[7]. Of all the titanium alloys used, Ti-6%Al-4%V accounts for more than 50% of titanium tonnage of which over 80% is used by the aerospace industry[5]. Although applications continue to expand for titanium alloys, aerospace usage remains the largest because of the relatively high cost of these materials as compared with other common metals and their alloys. However, the use of the powder metallurgy techniques for the production of titanium based components from low cost powders may provide a means of reducing the manufacturing costs whilst achieving properties similar to cast or wrought products. Research and development in this area is especially critical as titanium alloys are increasingly penetrating consumer markets (e.g. sporting goods such as bicycles and golf clubs).

Traditional titanium powders used for many applications are of the spherical type. The cost for these types of powders made by methods such as rotating electrode process and plasma rotating electrode process can range from $200 to $1000/lb[8]. The cost of Ti-6%Al-4%V powder produced by the hydride-dehydride method is about $50/lb[9]. Thus, hydride-dehydride powders offer a low cost alternative for non-critical P/M applications such as bicycle frames, connecting rods and valve components. However,

hydride-dehydride powders are angular in shape and consequently have different flow and packing characteristics than spherical powders. To improve the aforementioned characteristics, a lubricant can be added. Generally, lubricants used for most metal powders are mixed with the metal prior to compaction. The most common lubricants used are the stearates, based on aluminum, zinc, lithium, magnesium or calcium[1]. Binders can also be used to improve the strength properties of the powder after compaction by enhancing adhesion between the powder particles. Binders can be derived from either polysaccharides or natural organics such as cellulose[10].

The aim of this research is to investigate the effect of a lubricant on the compaction and sintering behavior of a hydride-dehydride titanium alloy powder. The literature review, presented in Chapter 2, will cover the theory and technology of titanium powder production, as well as conventional compaction and sintering. Chapter 3 outlines the objectives and Chapter 4 covers the experimental procedure. In Chapter 5, the results are shown and discussed with the conclusions given in Chapter 6.

CHAPTER 2:

LITERATURE REVIEW

2.1 TITANIUM POWDER METALLURGY

Powder metallurgy (P/M) technology is used as a viable processing alternative to the difficult and costly casting operations required when products are fabricated from titanium and titanium alloys[1,11]. During the past two decades the P/M of titanium alloys has been the subject of research and development efforts with cost reduction and material savings being the end objectives of the two processing approaches: the pre-alloyed method and the blended elemental method. Although both processes effectively use automated operations with savings in material, energy and capital costs, major drawbacks hindering both techniques are related to the cost, quality and availability of titanium alloy powders. Several processes can achieve the production of titanium powders. The choice of process depends on the category of powder, purity and quantity requirements as well as cost[4,12]. Ti-6%Al-4%V can be produced by all existing methods most of which are listed in Table 2.1.

Titanium powders processed by P/M techniques are divided into two general categories: blended elemental and pre-alloyed powders. Blended elemental powders are

made by blending elemental powders with master alloys. Pre-alloyed powders are produced either by comminution of hydrogen embrittled alloy stock (also known as the hydride-dehydride process) or by various methods of melting and rapid solidification[1,4,11,13-15].

TABLE 2.1: TITANIUM POWDER MAKING PROCESSES [4,15].

POWDER MAKING PROCESS	DESIGNATION	PARTICLE SHAPE
Na Reduction (elemental sponge)		Angular
Mg Reduction (elemental sponge)		Angular
Electrolytic (elemental sponge)		Angular
Hydride-Dehydride	HDH	Angular
Rotating Electrode Process	REP	Spherical
Plasma Rotating Electrode Process	PREP	Spherical
Hydrogen Evolution	C-T	Spherical
Electron Beam Rotating Disc	EBRD	Spherical
Powder Under Vacuum	PSV	Spherical
Gas Atomization	GA	Spherical
Pendant Drop	PD	Elliptical
Strain Energizing Process	SEP	Disc
Vacuum Plasma Spray*	VPS	Spherical

2.1.1. BLENDED ELEMENTAL

The blended elemental method of blending elemental powders to achieve the required alloy is commonly processed by the use of conventional consolidation techniques, namely cold pressing followed by sintering. Blended elemental is more economical than other methods, producing parts that have good density, strength, fracture

* PyroGenesis Inc. Process

toughness and near-net shape. Fatigue strength however is inferior to pre-alloyed parts due to the porosity caused by residual chloride impurities from the elemental powder making processes[4,12,14]. Consequently blended elemental powders are used for P/M parts that are not fatigue-critical.

In this technique, elemental titanium is produced by the Kroll process, Hunter process and by variations of the two[16,17]. For small batches of high purity elemental powders, electrolytic or vapor phase reduction methods can also be used. The Kroll process involves the reduction of titanium tetrachloride (from rutile or ilmenite) by magnesium.

$$TiCl_{4(l)} + 2Mg_{(s)} \rightarrow Ti_{(s)} + 2\,MgCl_{2(s)} \qquad 2.1$$

At temperatures as high as 1040°C the metal dissolves and forms a sponge, hence the name titanium sponge. The Hunter process reduces titanium dichloride with sodium. Sodium reduced sponge yields larger amounts of fines and the chloride content is lower than magnesium reduced sponge. Regardless of the method, the titanium sponge is then crushed, producing elemental titanium powders from the generated fines. These powders are typically -100 mesh (<150 microns) and have an irregular shape as illustrated in Figure 2.1[3].

For component fabrication by the blended elemental method, these titanium sponge fines are combined with elemental or master alloy powders to achieve the desired composition of the alloy. Currently, there has been much work on powder metallurgy processing of titanium based materials using this approach. Although the most attractive aspect of blended elemental processing is the low cost of the titanium powder, residual chloride levels in the particles deteriorate the dynamic properties of the component and reduce the overall potential of the technique and product. Commercially pure titanium powders with low chloride levels, 10 ppm, can be produced by the AlTi process, which is based on reacting TiO_2 with fluorine salts followed by reducing with aluminum in a zinc

carrier medium[18]. Although the processing of such powders gives properties similar to that of wrought or cast materials, as compared to titanium sponge fines, these are more expensive, and their processing using the blended elemental approach still involves relatively high temperatures and long sintering times to homogenize the matrix alloy chemistry. Additionally post processing using hot isostatic pressing is necessary to attain full density. which adds to the processing time and overall costs.

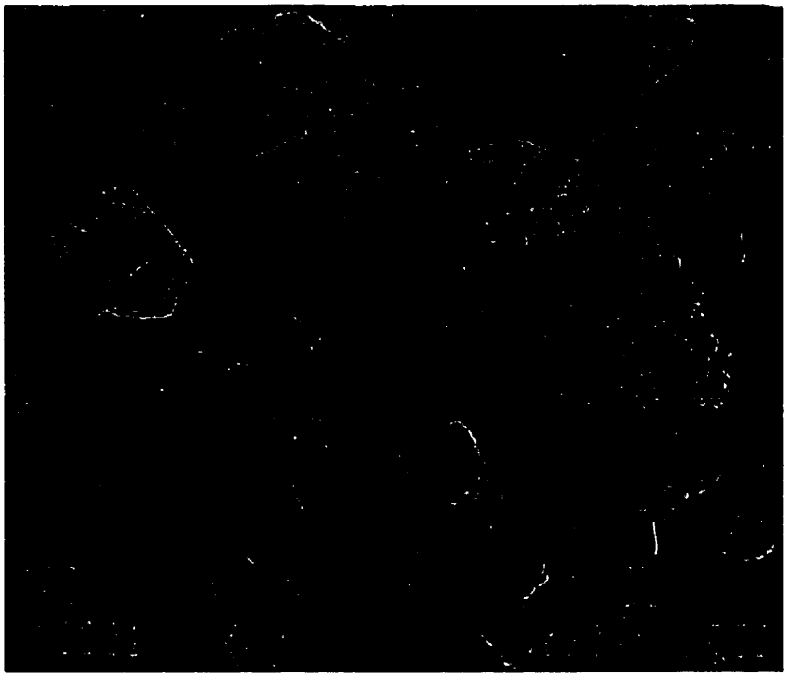

Figure 2.1: Scanning electron microscopy imaging of -140 mesh titanium sponge fines.

2.1.2. PRE-ALLOYED

Pre-alloyed powders are produced either by comminution of hydrogen embrittled alloy stock or by various methods of melting and rapid solidification. Production of pre-alloyed Ti-6%Al-4%V powder is made using typically hydride-dehydride, rotating electrode process, plasma rotating electrode process, gas atomization and vacuum plasma spraying[4,16]. Pre-alloyed powders offer increased homogeneity and improved

mechanical properties in the final part where strength and toughness are comparable to wrought materials with an added plus of net shape capabilities[4,16]. Because of the increased work hardening rate of pre-alloyed powders, these cannot be easily formed by conventional compaction methods[16]. Combined with the conventional processing problems and the aerospace requirements of fully densified consolidated parts, the pre-alloyed powder is usually consolidated by methods that combine the entire operation of consolidation into one step such as hot isostatic pressing and vacuum hot pressing[4,12,14].

2.1.2.1 HYDRIDE-DEHYDRIDE

Among the various techniques for titanium powder production, the hydride-dehydride method offers good quality titanium commercial powder at the lowest cost and the potential for mechanical property levels equivalent to those attainable by ingot and cast metallurgy. The ductile nature of titanium and its alloys require that they be converted to a more brittle state before comminution. This is achieved by hydrogen embrittlement in the hydride-dehydride process. The feedstock for titanium hydride-dehydride processing is generally scrap, machine turnings, ingot and billets that have been sorted, cleaned and dried. The cleaned feedstock is then loaded into a hydride furnace where it is hydrided by an exothermic reaction with very high purity hydrogen at 400°C to 700°C. The brittled hydrided feedstock is removed and ground in a ball mill. Argon is often introduced before and after grinding to reduce the oxygen content and hence oxidation of the particles. After grinding, the product is screened into the required size fractions. The hydrided powders are then dehydrided in a vacuum at temperatures between 600°C to 700°C[4,14].

Hydride-dehydride particles (Figure 2.2) are seen to have an angular morphology, and depending on the starting stock may, or may not contain residual chloride. Generally, the titanium powders produced by the hydride-dehydride method are lower in chloride content than those produced by the Kroll or Hunter reduction processes.

To reduce the overall cost of the process further, a hydride-dehydride pre-alloyed titanium powder may be beneficial since the cost of producing hydride-dehydride powder is nearly the same for commercial purity titanium or an alloy, but processing the latter should reduce the consolidation requirements because homogenization will not be of concern. Also, the use of pre-alloyed powders over blended elemental powders has an added advantage of reducing the activity of titanium, thereby decreasing its affinity for oxygen in the alloyed state.

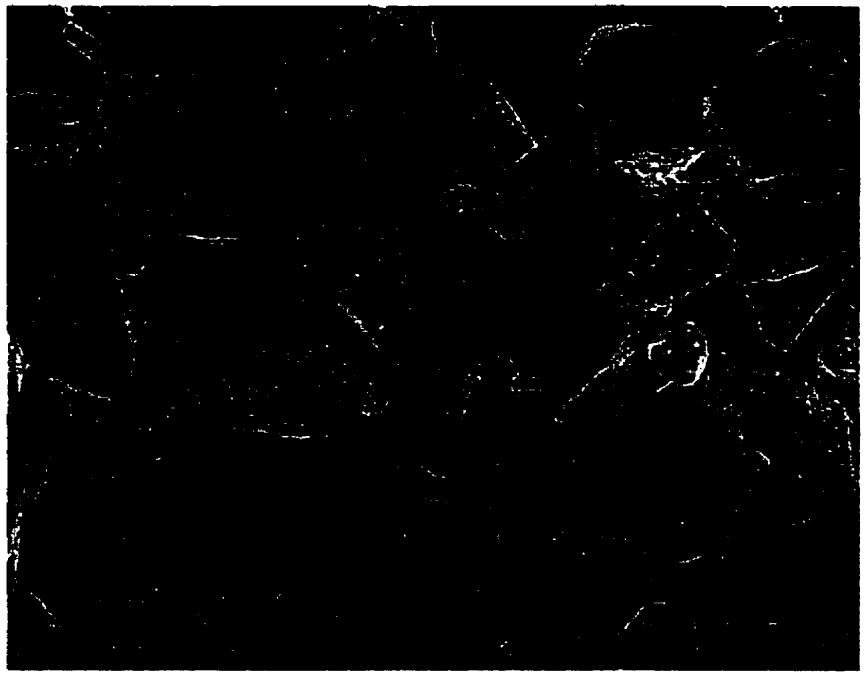

Figure 2.2: Scanning electron microscopy imaging of -200 mesh hydride-dehydride Ti-6%Al-4%V powder, x150.

Use of a pre-alloyed powder produced by the hydride-dehydride process appears to have considerable potential for near net shape processing by powder metallurgy techniques and attaining superior overall properties. Shortcomings to the application of hydride-dehydride pre-alloyed powders in industry however lie in the angular shape and alloyed condition of the powder particles, which tend to require higher compaction pressures and/or give greater die wear. A common practice in industry to facilitate compaction and minimize tooling wear is to mix a lubricant and/or binder with the

powder prior to compaction. In the case of Ti-6%Al-4%V powder, effects of such additions on P/M processing have not been fully investigated and are the subject of this work. In the following sections, the stages corresponding to powder processing are reviewed. To begin with, characterization of the starting powder defines the basic properties of the process and the final component. Handling and adjusting the powder properties prior to compaction are necessary for easier processing. Compaction provides the basic shape to the metal powder and the resulting green properties enable ease of handling. Finally, sintering is necessary to initiate inter-particle bonding and improve the properties of the component.

2.2 POWDER CHARACTERIZATION

To tailor a component according to the needs of the end user, the fundamental characteristics of the starting material must be determined to ensure proper selection of subsequent processing requirements. A well characterized powder may have a higher initial cost but in the end it will be more cost effective. This importance will be seen as compaction and sintering are discussed. The fundamental characteristics generally used are the size, size distribution, shape, specific surface area, flow, packing characteristics, compressibility, and chemical characterization. The importance of these parameters used to characterize particles and bulk powders becomes apparent by the influence of these on producing a low cost high quality product[1-2,19].

2.2.1. PARTICLE SIZE AND SIZE DISTRIBUTION

Information on the particle size of the powder generally involves determining the size distribution of the powder, which is useful in determining the powder's packing characteristics as well as determining the temperature and time needed for final consolidation. Typically, a range of particle sizes is used to aid consolidation by maximizing particle packing, while finer particle sizes are used to reduce the time and temperature needed for final consolidation[10]. For size and distribution measurements the

particles are often regarded as spheres and the particle size is defined as the equivalent spherical diameter that has the same physical properties. Thus, nearly all measurement methods use one geometric parameter in terms of a single linear measurement, (i.e. sieve diameter is the width of the minimum square aperture through which the particle will pass even though the particle may be elongated and can only pass on one axis). Hence, the actual particle size is only an approximation relative to the specific testing method. As a result, a particle size analysis should convey the information on the particle size distribution, particle shape and the basis for measuring the particle size[1-2].

Once the size is determined the size distribution is usually found by plotting particle size versus the weight fraction of particles of that size[19]. Some of the common methods used for titanium particle size analysis are listed in Table 2.2.

TABLE 2.2: COMMON SIZE ANALYSIS METHODS[1-2,17,20].

CLASS	METHOD	PARAMETER MEASURED	SIZE RANGE (μm)
Sieving	Woven wire screens Micromesh	Sieve diameter	>38 5 - 50
Microscopy	Visible light Electron microscopy	Perimeter diameter (projection area)	>1 >0.001
Sedimentation (Elutriation)	Gravitational Centrifugal	Stokes Diameter	2 - 300 0.05 - 60
Electrical Conductivity	Coulter counter	Volume Diameter	0.5 - 800
Light Scattering	Monochromatic laser light	Volume Diameter	1 - 1800

2.2.2. SHAPE

To be able to employ sizing techniques, it is necessary to determine the shape of the particles[1-2]. Shape is a relatively more difficult property to measure and as such is reduced to a single parameter for size measurements. For characterization, the shape is generally described qualitatively. The powder fabrication process itself can be used to predict the shape of the particles[2]. For example, hydride-dehydride results in angular shaped particles[4]. If the surface tension of the cooling liquid has time to minimize the surface area, the result is a spherical shape similar to that produced by rapid solidification processes[16]. Thus, shape depends on the surface energy of the particle which can be varied through the chemical composition of the melt and the energy input of the process[1,4]. The final shape of the particle can be compared to existing pictorial and numerical classifications (Figure 2.3).

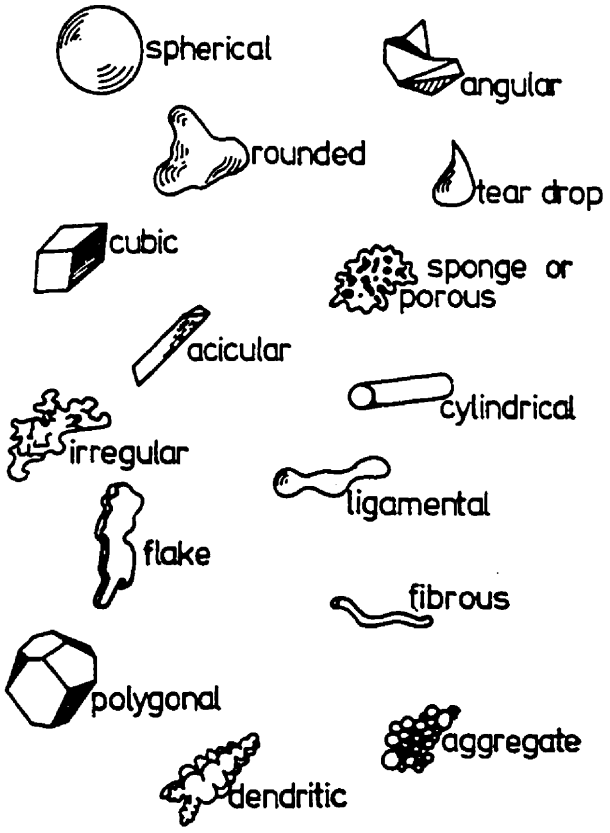

Figure 2.3: Common qualitative shape classifications[1].

2.2.3 FLOW

The ability of a powder to flow is important if the powder is to fill a specific volume in a quick, reproducible manner. The factors that effect flow are shape, size and size distribution. These factors influence the inter-particle friction. As the surface area of a powder increases (i.e. fine particles and irregular shaped), the amount of inter-particle friction also increases, hence resisting flow. Thus, due to the angular shape of Ti-6%Al-4%V hydride-dehydride powders, the inter-particle friction reduces its ability to flow. Factors that reduce inter-particle friction are coarse, smooth spherical shapes and lubricants that improve the flow. Also oxidized powders have lower inter-particle friction than clean powders because of the hardened surface which reduces the friction.[1] Fine particles can also be agglomerated to produce a coarser particle size that is free flowing.

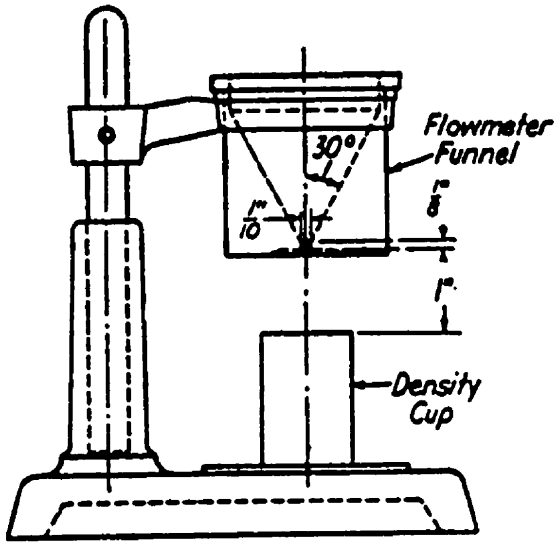

Metric Equivalents

in.	mm
1/10	2.54
1/8	3
1	25

Figure 2.4: Hall flowmeter[21].

The measurement method used for determining the flow rate is usually the time it takes for 50 grams of powder to flow through a Hall flow-meter funnel (ASTM B213) as seen in Figure 2.4. If the powder is non-free-flowing then a Carney flow-meter funnel (ASTM B417) is used. If the powder is a refractory the Scott volumeter (ASTM B329) can be used.

2.2.4 POWDER PACKING

Classification of the size and shape of powder particles is used to determine the packing density also referred to as the apparent density. The apparent density is expressed as the weight per a unit volume of powder in the loose state (unshaken) and is found using the Hall flow-meter funnel (ASTM B212) along with a 25 cm^3 volume cup. The apparent density is an important value because of its use for controlling the volume or weight of a pressed compact. If the weight of the powder changes for a fixed volume, the result is a change in the pressed density also called the green density[22].

One effect of the size and shape, as with the flow, is inter-particle friction. If this friction increases, the apparent density decreases due to poor flow past neighboring particles. Hence, the apparent density depends, in part, on the friction conditions between the particles. The apparent density also depends on another effect of the size and shape. This effect is related to a packing coordination number, which is the number of touching neighbors that any particle has in a bulk powder. The higher the coordination number, N_c, the higher the powder density[1]. The relation between the coordination number and the apparent density expressed on a fractional basis is as follows[1]:

$$\rho = ((N_c - 1)/ N_c) \qquad 2.2$$

where ρ is the fractional density and is also called the packing factor. A packing factor value of one would be the equivalent to that of uniformly sized polyhedral particles that are perfectly packed and suggests that the apparent density approaches the theoretical

density of the solid material. For example, simple cubic, body-centered cubic (BCC), face centered cubic (FCC) and hexagonal close-packed (HCP) crystal structures having monosized spheres have packing factor values of 0.52, 0.68, 0.74 and 0.74, respectively[2]. Blending powders with different size distributions can increase the packing factor to as high as 0.98 because smaller particles fill the gaps of the larger particles, as illustrated in Figure 2.5, increasing the packing factor. However, a critical limit exists for this addition and adding large quantities of small particles can actually diminish the packing factor by causing the separation of the larger particles, as shown in Figure 2.6. This effect is called bridging and results in increased porosity. Tapping the powder also helps to improve the packing density. The density of a powder that has been tapped at a specific frequency for a predetermined time is called the tap density.

Figure 2.5: Smaller particles increase packing factor by filling voids[2].

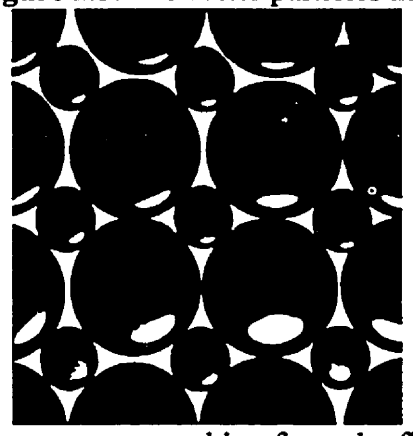

Figure 2.6: Packing factor decreases due to bridging effect[2].

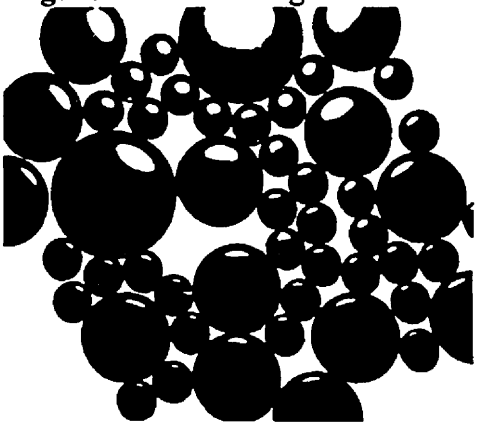

2.2.5 COMPRESSIBILITY AND COMPRESSIBILITY RATIO

Compressibility is the measure of the amount by which a powder densifies under pressure. Typically, compressibility is the density reported at a pressure of 415 MPa (30 tons/in^2) in an uniaxial die specified by the ASTM Standard B331. Compressibility is greatly influenced by inter-particle friction and by the internal structure of the particles

(i.e. particle porosity). Another measure of compressibility is the densification parameter. This value is dependent on the apparent density[2]:

$$\text{densification parameter} = \frac{\text{green density} - \text{apparent density}}{\text{theoretical density}} \qquad 2.3$$

The densification parameter is used to represent the fraction of the maximum density possible for a given apparent density. This parameter is also used to compare the densification of different powders for a given green density and pressure[23].

The compression ratio is the ratio of the apparent density to the green density for a given pressure. This ratio must be known to be able to properly design the compaction tooling[1,23]. To determine this ratio the following equation is used:

$$\text{Compression ratio} = \frac{\text{green density}}{\text{apparent density}} \qquad 2.4$$

Equation 2.4 yields the multiplier used to determine the fill volume of a powder in a die to achieve a specific final height. However, care must be taken when using this ratio since the plot of green density versus compaction pressure for different powders may not necessarily be linear and, as a result, the relationship between the green density and apparent density also may not be linear (Figure 2.7). Therefore, when a multiplier is found, it is only valid for the specific pressure used. Factors that increase the apparent density, such as lubrication, also reduce the compression ratio required and increase the compressibility. This results in lower compaction pressures, reduced tool wear, faster die fill (less volume required), higher green density, reduced press motion and higher production rates.

2.2.6 CHEMICAL CHARACTERIZATION

Chemical characterization is used to focus on the impurity concentration for elemental powders as well as alloy composition for pre-alloyed powders. Normal analytical chemistry techniques such as emission spectroscopy and X-ray fluorescence are used. Internal defects which can affect compaction and sintered densities are examined by metallographic techniques[1,2].

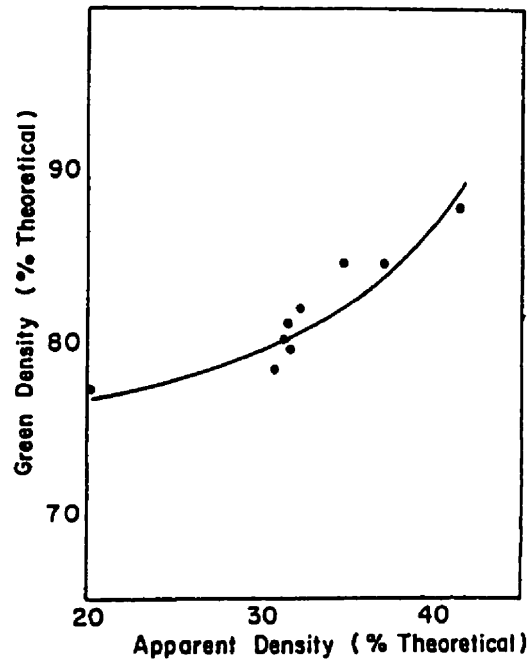

Figure 2.7: Dependence of green density on apparent density[2].

2.3 POWDER PRE-COMPACTION

Generally, powders are tailored to meet specific properties, compositions and for improved compaction and sintering. This usually requires one or more pre-compaction steps. The most common pre-compaction steps used are classification, mixing or blending and lubrication. Other pre-compaction steps which can be used include attrition milling to reduce particle size, removal of surface oxidation to improve sintering and minimize agglomeration of fine particles thereby improving powder flow[24].

Classification involves the preparation of the powder into specific size fractions to improve powder quality (if impurities are in a specific size fraction), particle packing and sintering characteristics. Coarse size fractions improve compaction, while finer size fractions aid the final consolidation stage[24]. The tailoring of the powder to a specific size fraction is achieved by one or more methods of classification discussed earlier. The specific size fractions are then either blended or mixed to produce the required size distribution. Generally, blending refers to the combination of like materials, while mixing refers to the combination of powders of different composition[24]. Thus, to achieve new compositions as required for the blended elemental method the powders are mixed. Mixing or blending can take place in 3 ways: diffusion, convection and shear. Both blending and mixing require that the end product be consistent[24].

2.3.1 LUBRICATION

For the preparation of parts by P/M techniques, the stages related to dry-pressing are: the filling of the die, conventional compaction and ejection of the pressed part. All three stages involve the use of a lubricant as will be seen in the following sections. The type of lubricants most often used for metal powders are the stearates based on aluminum, zinc, lithium, magnesium or calcium. For the purpose of this work only zinc stearate will be examined.

Zinc stearates are made by two different methods.[25] The first involves the formation of sodium stearate from stearic acid plus an alkali, which is then treated with zinc salt to form zinc stearate (precipitate). The second method involves the fusion of molten stearic acid with zinc oxide, which forms a solid zinc stearate (atomized). The resulting products from both methods are ground to the required size and size distribution. Zinc stearate has a melting temperature of 130°C and a density of 1.09 g/cm^3. The low melting point helps to facilitate burn off of the lubricant prior to sintering while the low density implies relatively low residual contamination after burn off. The stearate molecular chains are 12 to 22 carbon atoms long and have a polar character.[1]

Hence, in a metal powder, the zinc stearate lubricates the surface through short-range repulsive forces.[24]

2.3.1.1 LUBRICANT IN DIE FILLING STAGE

The die filling stage requires that a specific volume be filled in a quick and reproducible manner. Irregular shapes and small particles have high surface areas, which increase inter-particle friction and can interfere with consistent die filling. The addition of a lubricant reduces the effect of the surface area resulting in improved and controlled flow and apparent density. The powder may be purchased premixed with a lubricant or admixed in house. Admixing a lubricant with the powder in industry is usually performed in a twin shell mixer called a V-mixer. The V-mixer is chosen because the mixing pattern (Figure 2.8) minimizes segregation due to particle size, shape and density variations.[26]

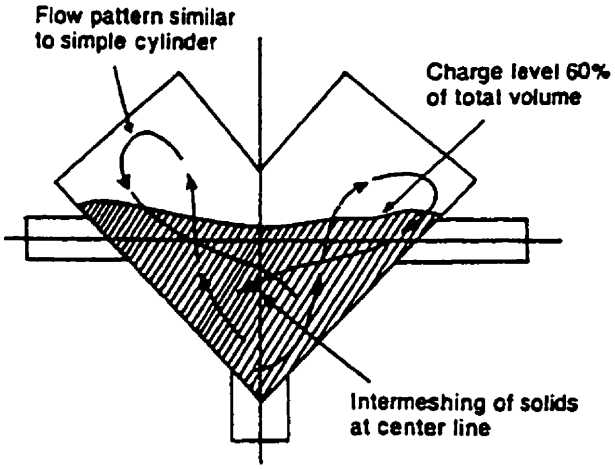

Figure 2.8: V-mixer flow pattern[26]

The extent of mixing is very important. Inadequate mixing will result in poor flow, while excessive mixing can overheat the lubricant until it becomes sticky and promotes particle agglomeration. The effect on the flow using a lubricant can be measured using a Hall flowmeter. By plotting the flow time versus mixing time, an optimum can be determined (Figure 2.9). Similarly, the effect of a lubricant and mixing

time on the apparent density can be seen in Figure 2.10. The apparent density increases with mixing time and decreases with increasing lubricant. The decrease in apparent density is due to the increased volume that is being occupied by the lower density lubricant.[1]

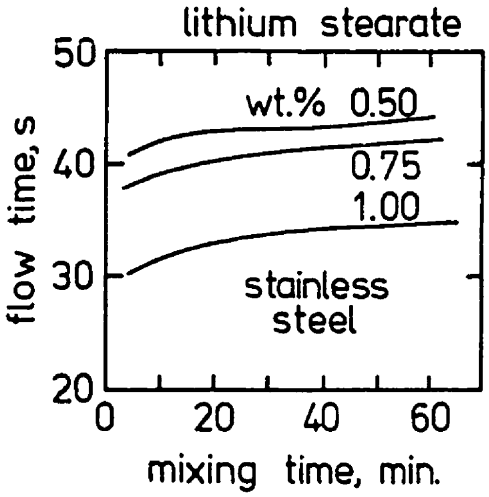

Figure 2.9: Effect of a Li- stearate on flow time versus mixing time[1].

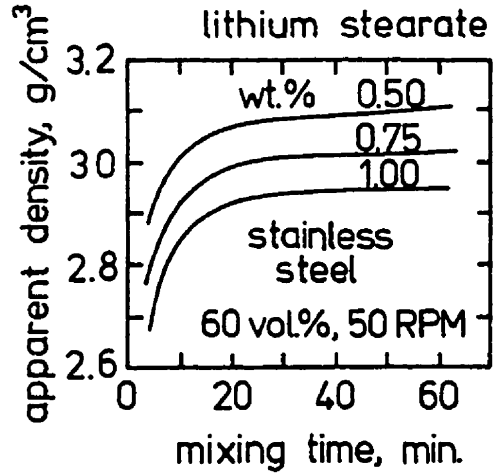

Figure 2.10: Apparent density as a function of mixing time and wt% lubricant[1].

2.3.1.2 LUBRICANT IN THE COMPACTION STAGE

During uniaxial compaction of metal powders, inter-particle bonds develop through cold welding, weak attractive forces and mechanical interlocking. The strength developed at this stage is called the green strength, while the pressed density, as mentioned before, is termed the green density. Characteristics that improve the green density also improve green strength.[1] One of the most important methods used to improve the green density is to add a lubricant. The lubricant reduces frictional losses, which results in an increased effective pressure for the same applied pressure[19].

The lubricant can be added to the die wall or mixed into the powder. Clean powder surfaces are desirable to improve inter-particle welding. Since the addition of a lubricant reduces the inter-particle contact through the formation of a thin surface film, it

is preferable to add the lubricant only to the die wall. However, die wall lubrication is generally uncommon because of the difficulties in applying exactly the right amount of lubricant within a carrier, and the complete elimination of the carrier between lubricating and powder filling cycles. Mixing the lubricant into the powder is easier to achieve. However, green strength and dimensional control are affected.[26] Regardless, the goal is to achieve the desired powder properties with minimal friction between particles and the die wall.

The optimal amount of lubricant decreases as the compaction pressure increases (Figure 2.11). The reduction in lubricant is necessary because otherwise pore filling by the excess lubricant occurs which lowers the green density.[1] Using the lubricant sparingly also helps reduce springback that occurs after the compaction pressure is removed.[10] Springback can cause cracks to form and results from the release of the stored elastic energy in the pressed part.

2.3.1.3 LUBRICANT IN EJECTION STAGE

The last stage of pressing involves the use of a lubricant for reducing the ejection force required. During automated pressing, the force required to eject the pressed part increases rapidly without lubrication for each successive part. This would result in the part seizing in the die after only a few compacts have been pressed. The lubricant acts to separate the metal surfaces by a thin film of low shear strength. Some friction remains, since complete separation of the surfaces (due to high points) is not possible. As the amount of lubricant added is increased, the ejection force and consequently the die wear decreases (Figure 2.12).

From the previous sections, it can be seen that the amount of lubricant added is a balance between the desired flow, apparent density, compaction pressure and ejection force. In industry, a lubricant addition in the range of 0.2 to 1.0 percent is most commonly used to achieve the desired results.[1]

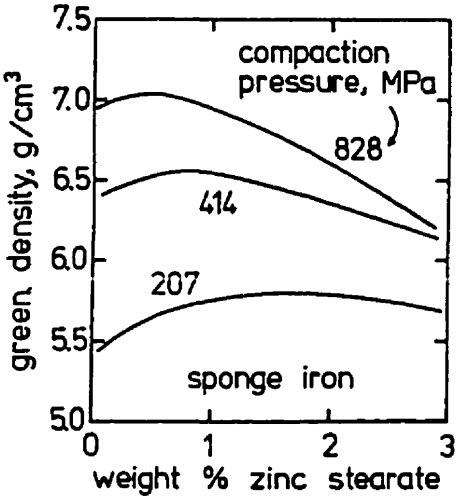

Figure 2.11: Zinc stearate effect on green density of sponge iron at three compaction pressures[1].

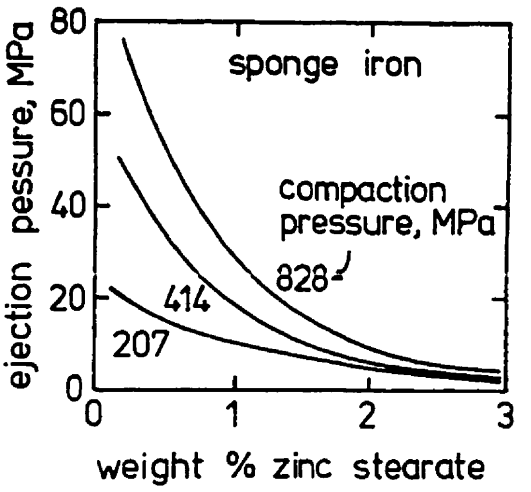

Figure 2.12: Ejection force required as a function of the amount of lubricant used during pressing[1].

2.4 COMPACTION

Powder compaction can be summed up as the operation that provides shape, dimensional control, desired density and strength for subsequent handling. Conventional compaction occurs in the following manner, as shown in Figure 2.13. Initially, as pressure is applied, the loose arrays of particles are packed closer and particle bridging is eliminated. At this stage the density attained is at most equivalent to the tap density. As the pressure is further increased the contact area grows through rearrangement and sliding. At high pressures the contact area increases through plastic deformation[1-2,4].

The inter-particle bonds develop through cold welding, weak attractive forces and mechanical interlocking. The strength developed at this stage is called the green strength, while the pressed density is termed the green density. Generally, due to interlocking, rounded but irregular large shaped particles result in the highest green strength. The higher the hardness of the particles the lower the green density. Also if the particles are small, the finer pores will require higher pressures to collapse and the pressed density will

be low. In general, characteristics that improve the green density also improve green strength[1-2,4,17].

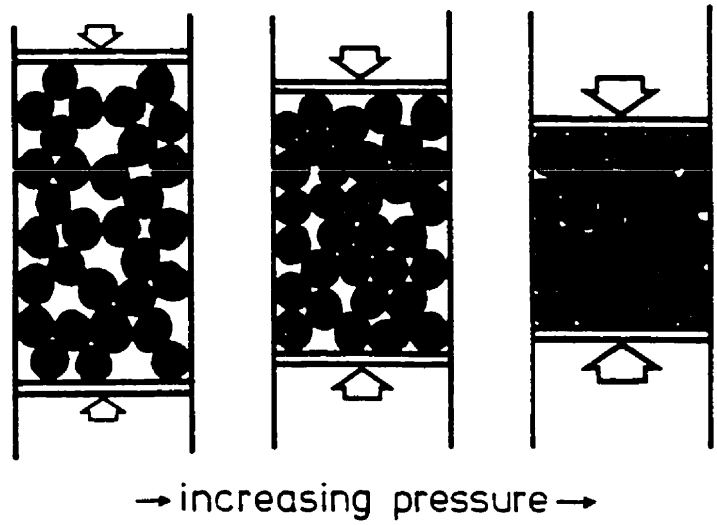

Figure 2.13: Stages of compaction, tap density, rearrangement and green density[1].

The methods of compaction all have the same goal, which is to achieve the desired properties with minimal wall friction. This results in reduced tool wear and improved pressing efficiency. For compaction to be successful (i.e. uniform compact properties), the ratio of compact height (H) to the compact diameter (D) must not exceed five. A method to further increase the ability to gauge the pressing operation is the *zu*H/D ratio, where *z* is the ratio of the radial stress to the axial stress and *u* is the die wall friction coefficient. As the *zu*H/D ratio increases, the successfulness of the pressing operation decreases with increased inhomogeneity in pressure and density. The effect of the die wall friction (*u*) is to reduce the efficiency of compaction. The addition of a lubricant decreases *u*, but when added directly to the powder, it increases the *z* parameter. This improves pressing homogeneity[1].

2.4.1 COMPACTION DEVICES

Compaction devices can be classified into two categories. They are pressure and pressureless techniques. Pressure techniques include single and double action dies, isostatic, forging, extrusion, vibratory and continuous. The pressureless techniques are slip casting, gravity and continuous[1-2,4].

2.4.1.1 PRESSURE TECHNIQUES

Die compaction is the most common method. It can be preformed in atmospheric conditions or in a vacuum. If the compact is heated during compaction the technique is referred to as hot or warm pressing. Regardless of the pressing conditions, the die is a rigid and solid mass with a cavity that is formed in the desired shape. A punch compacts the powder in the die into the required shape. Single action dies have only one dynamic pressing action. This results in a lower density at the bottom of the die due to decreased particle rearrangement, as the particles have less free space to move through. Trapped gases also decrease particle movement. Double action compaction uses punches at opposite ends. This method results in the lowest density values to occur in the middle of the compact (Figure 2.14).

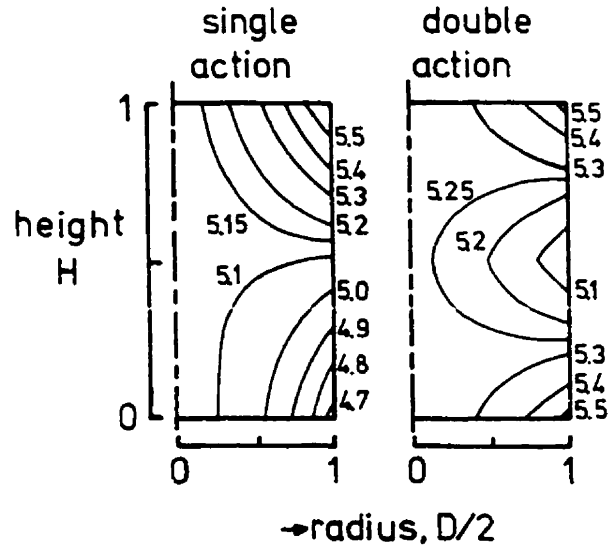

Figure 2.14: Comparison of single versus double action compaction density zones[1].

2.5 SINTERING

Once adequate green strength has been achieved for handling of the part, the next stage is sintering. Sintering is the process by which the application of heat below the melting point of a compacted or confined powder causes chemical bonding into a solid structure[27-28]. Sintering can be performed simultaneously with compaction (hot pressing or hot isostatic pressing) or afterwards[29]. The effects include heat treatment, alloying, joining and densification. If the temperature is sufficient to include one or more phases in liquid form, the process is called liquid phase sintering. The fundamental aspects of sintering consist of the basic sintering stages, driving forces and transport mechanisms[1-2].

2.5.1 SINTERING STAGES

Sintering initially causes the particles that are in contact to form grain boundaries at the point of contact through diffusion[1-2]. This is the point contact stage (Figure 2.15a) and does not result in any dimensional changes[2]. The greater the initial density of compaction (increased particle contact and potential grain boundary area), the higher the

degree of coherency in the material[1]. Newly formed bonds take on the appearance of necks. This stage is therefore referred to as the "neck growth" stage (Figure 2.15b)[1-2]. No change in the dimensions is observed nor does porosity decrease. This stage continues well into the intermediate stage.

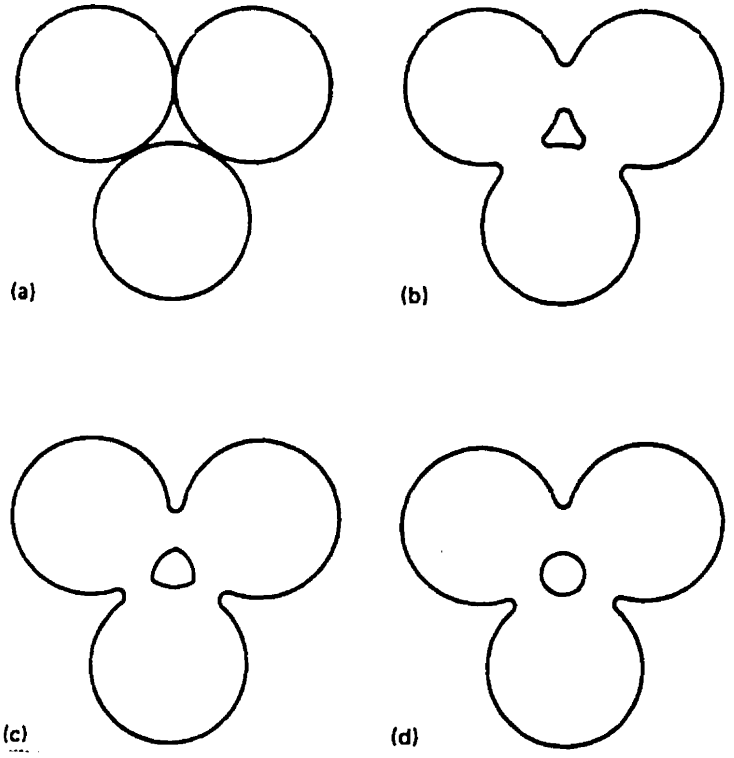

Figure 2.15: Three sphere sintering model: a) point contact, b) neck growth, c) pore closure and d) pore rounding[2].

The intermediate stage is pore channel closure (Figure 2.15c) where interconnected pore channels are closed off isolating porosity[1]. One of the causes of pore channel closure is neck growth. Another cause is the creation of new contact points by pore shrinkage within the pore itself.

Pore rounding and pore shrinkage belong to the final stage (Figure 2.15d). Material transport from the neck regions to the pore surface results in the pore becoming more rounded. Pore shrinkage is the most important stage in sintering. For this stage to occur, solids must be transported into the pores and a means must exist by which the gas

in the pores can escape to the surface. The resultant effect is to decrease the volume of the sintering mass[1-2]. Normally, a few isolated spherical pores remain in the material since complete elimination is impractical[17]. In the final stage, there is also a possibility of pore coarsening, but this does not always occur. If it does, the number of pores decrease but the average size of the remaining pores increase. This does not cause any major consequence for most non-critical commercial applications[2].

2.5.2 DRIVING FORCES AND TRANSPORT MECHANISMS

The most important driving force is fundamentally related to thermodynamic principles. The ability for the process of sintering to work depends on the free energy change of the system, ΔF. The thermodynamic free energy change due to chemical reaction is represented as the chemical volume free energy change, ΔF_C. The sintered mass undergoes changes in order to decrease the surface area[2,25]. The reduced contribution of the surface term ΔF_S in the free energy equation: $\Delta F = \Delta F_C + \Delta F_S$ results in a lower total free energy which is the driving force for the process. Thus, the greater the amount of surface area in the initial mass the larger the driving force for sintering[2]. During sintering, the activity of the powder depends on the available free energy, the exposed surface area and the number of lattice vacancies or defects[25]. The two transport mechanisms that occur in response to the activity of the powder are surface transport and bulk transport as seen in Figure 2.16[1-2,25].

2.5.2.1 SURFACE TRANSPORT MECHANISMS

Surface transfer mechanisms are initially the dominating methods of neck growth due to the sharp curvature gradients that exist near small inter-particle necks[1-2]. These surface transport mechanisms are evaporation-condensation, surface diffusion and volume diffusion[1]. Evaporation-condensation and surface diffusion is the result of a higher vapor pressure and lower surface tension on the convex surface than the concave

neck area. This creates the driving force for mass flow into the neck region[1,25]. Initially, due to the sharp curvature gradients and large surface area available, evaporation-condensation and surface diffusion are the main surface transfer mechanisms. Volume diffusion is dependent on the high gradient of vacancies found in the neck region. The concentration increases with increased surface tension and concave curvature[1-2,25]. However, since surface transfer by volume diffusion occurs by the movement of atoms from a surface source to a surface sink through the solid lattice structure, it is the least important of the surface transport mechanisms. Surface transport contributes to necking. However, the net change in dimension and density is insignificant[1].

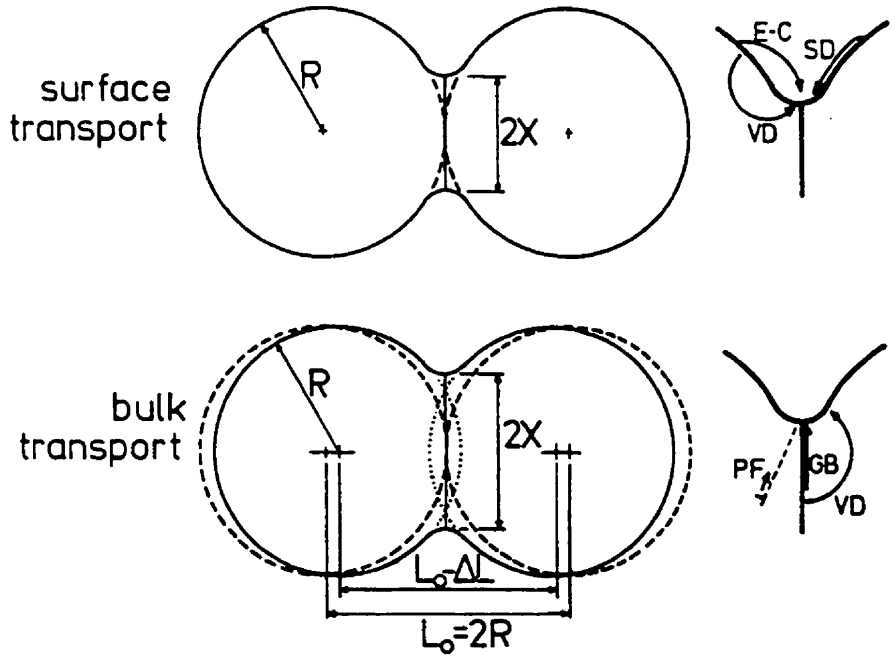

Figure 2.16. Surface transport and bulk transport[1].

2.5.2.2 BULK TRANSPORT MECHANISMS

Bulk transport occurs in the later stages of sintering due to high surface tensions at the weld neck. The methods of transport that promote neck growth and pore shrinkage are plastic flow, grain boundary diffusion and volume or lattice diffusion[1,25]. Since plastic deformation takes place under constant load and elevated temperature, creep occurs. The

process by which creep takes place is slip and climb of edge-dislocations during heating. Thus, plastic flow is not very significant with its effects limited to the heating period. For a given temperature and material, grain boundary diffusion is generally greater than volume diffusion. This is due to the smaller grain boundary volume with respect to the lattice volume and the lower activation energy of the grain boundary diffusion mechanism. With increasing temperature the difference between volume diffusion and grain boundary diffusion decreases. In the later stages of sintering, for any further grain boundary diffusion to occur, the atoms must move through the lattice and volume diffusion becomes rate controlling. The prevalent method of atomic motion in volume diffusion is by "vacancy exchange". The magnitude of the transport of atoms into vacancies is quantified by the diffusion rate (D) given by:

$$D = D_0 \exp(-Q/RT)^{(2)} \qquad 2.5$$

Where D_O = material constant
Q = activation energy
R = gas constant
T = temperature (K)

Grain boundary diffusion is effective until the grain growth or diminishing pore pinning force causes pore breakaway. This makes full densification difficult because the pores must diffuse vacancies to a distant grain boundary. Attempting to heat for extended periods of time will only cause the mean pore size to increase through the smaller pores being consumed by the larger ones (Oswald ripening). However, unlike surface transport mechanisms, these bulk transport mechanisms result in dimensional changes[1,2].

2.5.3 SINTERING VARIABLES

Factors that effect sintering efficiency are particle size, shape, structure and composition as well as green density, temperature and time. Decreasing particle size results in increased sintering. This is due to the increased ratio of surface area to volume, which results in a higher driving force. Shapes that result in increased contact area also increase sintering rates. The rougher the surface is, the greater the contact area. The

grain structure of crystalline powders has the most significant effect for sintering. The tendency in polycrystalline structures is towards very small grain sizes to improve the final mechanical properties such as tensile strength and dimensional stability. A fine grain structure improves the effect of material transport, which in turn allows for higher rates of sintering. After sintering, the grain size tends to remain small even though grain growth during sintering may occur. Usually the final grain size depends on the initial particle size. The smaller the initial size of the powder particle, the finer the final grain size.

The structure of sintered powders tend to be stable, since the major driving force for recrystallization (reduction of dislocations) is not present in powders[1,2]. A structure with large amounts of defects, such as dislocations, enhances diffusional processes. Particle composition such as surface oxidation reduces the surface energy and acts as a barrier for surface transport mechanisms, hence diminishing the effectiveness of sintering. Dispersed phases promote sintering by increasing the available vacancies and by reducing the grain motion through limited grain growth. This prevents pore breakaway.

If the initial green density is high, the change in final density and hence shrinkage after sintering will be small. High green density also yields better final properties such as increased strength, shape definition and density. Increasing the green density has the same effect as increasing the contact area. Methods that increase the rate of sintering reduce sintering time or temperature and hence decrease production cost. The rate of sintering decreases with time to a point where the degree of sintering with any further time becomes small and impractical. Finally, increasing either the processing temperature or time increases the sintering with the former having a greater effect due to the existence of an exponential relationship.

2.5.3 SINTERING FURNACES

Sintering furnace should ideally consist of three zones. These are a burn-off and entrance zone, a high temperature sintering zone and a cooling zone. The burn-off zone is used to volatilize the admixed lubricant and is designed to heat the part slowly to reduce the possibilities of expansion and fracture. The high temperature zone is where the sintering occurs. This zone is designed to be of sufficient length to insure that the temperature and the time required are attained. The sintering atmosphere can consist of one of the following: hydrogen, nitrogen, hydrogen-nitrogen mixture, hydrocarbon gases, argon, helium or a vacuum. It should be noted that the oxidation behavior of Ti-6%Al-4%V is similar to unalloyed titanium with the reaction rate laws ranging from logarithmic at 300-500°C to parabolic at 500-750°C to linear above 750°C. Figure 2.17 shows the oxidation behavior at various temperatures[5]. The cooling zone consists of two sections. In one section the cooling rate is sufficiently slow to prevent thermal shock. The latter is a water cooled section where the temperature is reduced enough to prevent oxidation of the material on exposure to air but not too low as to cause condensation on the walls of the furnace[1-2].

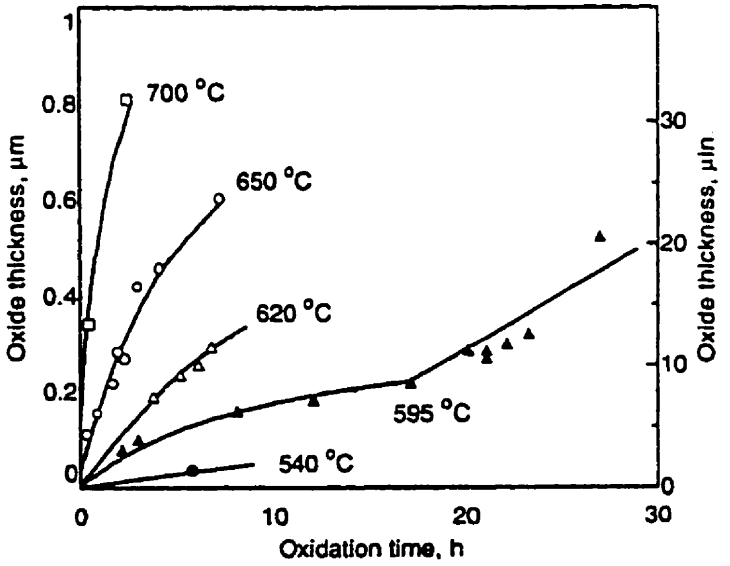

Figure 2.17. Oxidation behavior of Ti-6%Al-4%V at various temperatures[5].

CHAPTER 3:

OBJECTIVES

The purpose of this work was to investigate the influence of lubricant addition on powder metallurgy processing of hydride-dehydride Ti-6%Al-4%V powder. The main objectives of this research are outlined as follows:

(1) To characterize the effect of varying amounts of lubricant addition on the flow and apparent density of Ti-6%Al-4%V hydride-dehydride powder.

(2) To observe the effect of varying lubricant content and compaction pressures on green density.

(3) To determine the optimum quantity of lubricant addition for high apparent and green densities.

(4) To determine the temperature and time required too complete the burnout of the lubricant.

(5) To investigate the degree of shrinkage and densification with varying green densities and sintering temperatures.

(6) To investigate the influence of the processing parameters on the sintered microstructure.

(7) To define the optimum processing parameters (e.g. lubricant quantity, compaction pressure, sintering temperature and holding time) for powder metallurgy consolidation of hydride-dehydride Ti-6%al-4%V powder.

CHAPTER 4:

EXPERIMENTAL PROCEDURE

The Ti-6%Al-4%V powder was characterized, compacted and consolidated with and without lubricant addition. These experimental techniques used for processing the titanium alloy as well those associated with measuring the effectiveness of lubricant addition are described in this section.

4.1 POWDER AND LUBRICANT CHARACTERIZATION

The titanium alloy powder used in this experiment was a -200 mesh Ti-6%Al-4%V master alloy powder obtained from Micron Metals Inc., Salt Lake City, Utah, USA. The as-received powder had a density of 4.43 g/cm^3 and a chemical composition as given in Table 4.1. The Ti-6%Al-4%V powder was characterized by scanning electron microscopy (SEM) examination, sieving, attrition milling and sieving, mixing, flow and apparent density measurement.

The lubricant used was zinc stearate powder purchased from Johnson Matthey Alfa Aesar. The zinc stearate consisted of stearic acid salt, $Zn(C_{18}H35O_2)_2$. The flash point was 276.7°C (530F) with auto ignition at 421.1°C (790F).

Table 4.1: Certified analysis of Ti-6%Al-4%V powder

Analysis	Al (%)	V (%)	O_2 (%)	N_2(PPM)	C (%)	H_2(PPM)	Fe (%)
	6.00	4.00	0.13	200	0.02	100	0.06

4.1.1 SEM AND EDX EXAMINATION

Samples from the as received Ti-6%Al-4%V powder were examined for general morphology, surface topography and alloying distribution using a Hitachi variable pressure scanning electron microscope model S-3500N. This model features PC controlled electronics with Windows 95, as well as a variable pressure chamber that allows for wet, oily and non-conductive samples. The system has an accelerating voltage range of 0.3 to 30 kV, with a 3.5nm resolution at 25 kV. For the analysis, no metallic coating or conductive bridge was required for the samples with this system. Both secondary electron and backscatter imaging was utilized. The elemental microanalysis was carried out using the integrated energy dispersive X-ray spectrometer (EDX). X-ray dot mapping of the elements was performed using the high speed digital X-ray mapping, line scanning and image processing software also integral to the SEM.

4.1.2 SIEVING

The size distribution was verified using Tyler sieves (140,200,270,325 and 400 mesh). The sieving was carried out using 100g of powder placed on the uppermost sieve in the stack. The stack of sieves was placed into the roto-tap for 15 minutes. The mass fraction remaining on each sieve was weighed and recorded. This sequence was carried out for three batches of Ti-6%Al-4%V powder.

4.1.3 ATTRITION MILLING

To minimize the surface oxide layer on the Ti-6%Al-4%V particles, the powder was attrition milled prior to powder metallurgy processing. This was performed by wet attrition milling with alumina grinding balls and isopropyl alcohol in a 4L Teflon cylindrical mill similar to that shown in Figure 4.1, for 30 minutes at 200 rpm. The isopropyl alcohol was used to protect the freshly exposed surface from oxidation and reduce the risk of explosion (titanium powder is pyrophoric). A solid:liquid ratio of 1:5 by weight was used. The milled slurry was passed through a 212 μm screen to separate the powder slurry from the grinding media. Subsequently, the powder slurry was decanted and then placed in an oven at 200°C for 4 hours to remove the isopropyl alcohol. The sieving stage was then repeated for the milled powder to determine the effect of attrition milling on the Ti-6%Al-4%V particle size and size distribution.

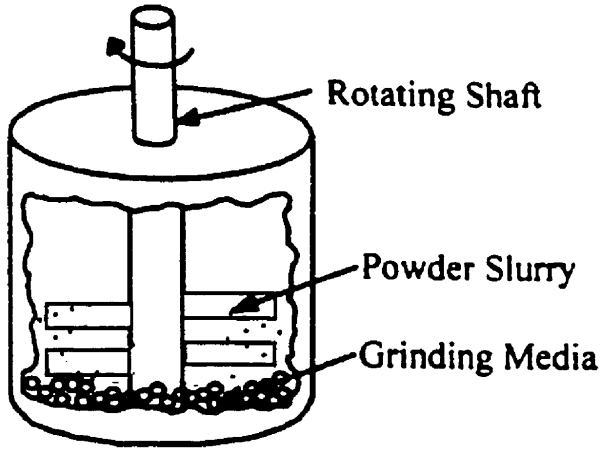

Figure 4.1: Schematic of an attrition mill.

4.1.4 MIXING

Using a Y-cone mixer at 50 rpm, admixed powder was prepared using 1/4 wt.%, 1/2 wt.% and 1 wt.% zinc stearate. Initially 60g of each of the three lubricants were mixed for 5, 10, 20 and 40 minutes. This was performed to determine the optimum mixing time necessary for the lubricant addition to the Ti-6%Al-4%V powder. This

mixing time optimum was extrapolated from the results of the flow and apparent density measurements described in the next section. An optimum time of 35 minutes was determined and used for all subsequent samples prepared for examination.

4.1.5 Flow and Apparent Density Measurements

The flow rate (ASTM B213) for all the powders (as received, milled and admixed) was measured using a Hall flowmeter (Figure 2.4). The Hall flowmeter required the use of 50-gram samples. The sample was placed into the Hall flowmeter whose bottom orifice was held closed by the strategic placement of a finger. Using a stopwatch, the flow time to empty the flowmeter was recorded upon removing the finger from the orifice.

The apparent density test (ASTM B212) was carried out at the same time as each flow test. The $25cm^3$-volume flow cup was placed under the flowmeter orifice and allowed to fill. Care was taken not to shake the cup to prevent further settling. The powder at the top of the cup was carefully leveled and the mass of the powder in the cup measured. The apparent density was found by multiplying the mass of the powder by 0.04. It was observed that the non-lubricated powder, whether as received or milled did not flow freely and as a result the flow and apparent density tests could not be performed for these powders.

4.2 Compaction and Green Density Measurement

Using a uniaxial, single action, hydraulic press, the milled powder (with and without lubricant) was pressed into 2.5g compacts. The size and shape of the compacts were determined by the use of cylindrical, tool steel punch and die sets having an inside diameter of 19mm (3/4 inch). The pressures used were 207, 241, 276, 310 and 343MPa (30, 35, 40, 45 and 50 ksi, respectively). The green density measurement of each

compact was obtained by using the dry weight and the average of three measurements taken 45° apart on the diameter and thickness of each sample with Vernier calipers. The average of the measurements was used to calculate the volume. The density of each sample was determined using the following equations:

$$V = \pi r^2 h \qquad 4.1$$

$$D = m/V \qquad 4.2$$

Where V is the volume in cm^3, h is the height of sample, r is the radius of sample, m is the weight and D is the density in g/cm^3.

4.3 SINTERING

4.3.1 LUBRICANT BURNOUT

To determine the temperature at which the lubricant burns out within the sintering environment the change in weight of the sample was monitored using a Thermo-Gravimetric Analyzer (TGA). The water-cooled furnace was custom-built using an open ended 6 cm diameter mullite tube surrounded by heating elements. The bottom end was closed except for one port attached to a vacuum rotary pump. The top end was sealed by a glass tube in which one end of a molybdenum wire was used to suspend the sample into the furnace and the other was attached to the Cahn D-100 balance that was controlled and monitored by a personal computer. The set-up is shown in Figure 4.2. The sample being investigated was placed on a boron nitride bed within an alumina crucible fabricated in house specifically for this purpose. The crucible was suspended from the wire within the glass tube, counter balanced and then positioned into the center of the hot section of the furnace. The TGA was then evacuated to approximately 5 Pa and the balance tarred. The furnace was heated to 600°C at a rate of approximately 12°C per minute. The temperature was measured using a

type B thermocouple located near the center of the hot zone adjacent to the outside wall of the mullite tube. Temperature calibration was performed by inserting a similar thermocouple of known resistance error through a temporary self sealing opening in the bottom of the mullite tube. The temperatures obtained were compared and the junction resistance of the working thermocouple adjusted to compensate for any deviation. The change in weight was monitored every 10 seconds and recorded by the computer.

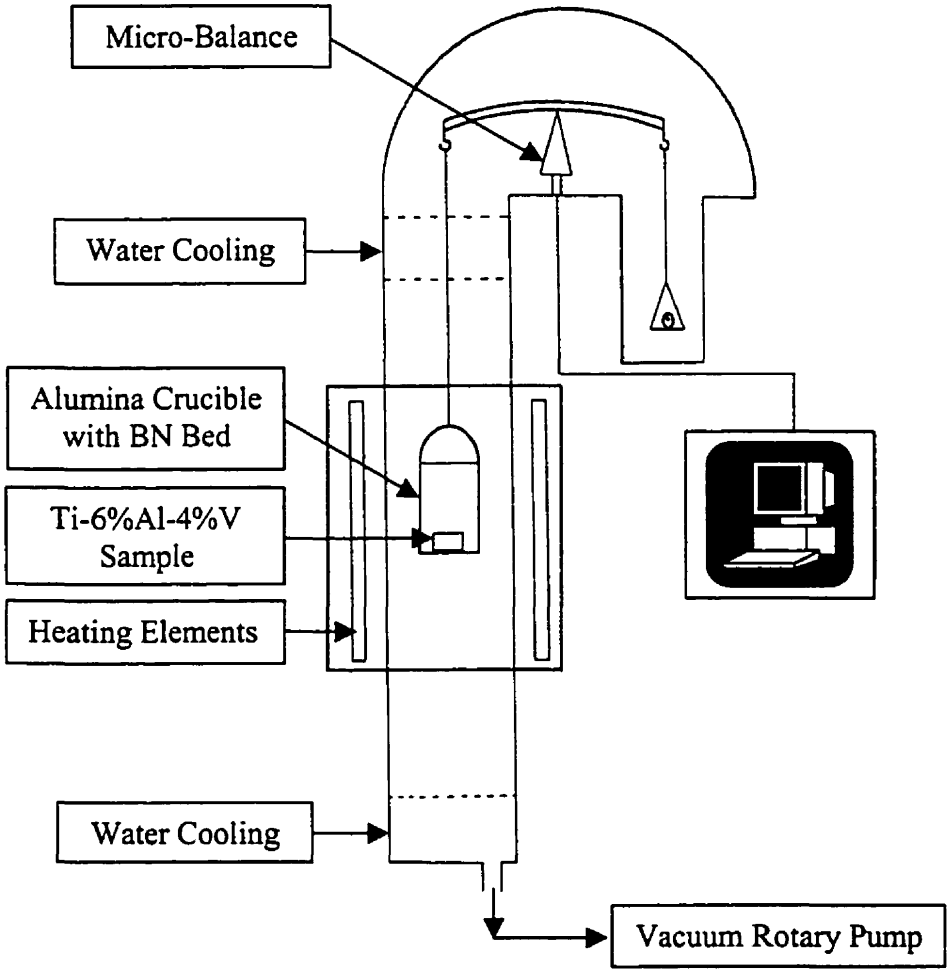

Figure 4.2: Schematic diagram of the Thermo-Gravimetric Analyzer.

4.3.2 SINTERING FURNACE

Within a boron nitride crucible, the green compacts were placed onto a boron nitride powder bed and completely covered using boron nitride powder. The crucible, along with some sponge titanium (used as a getter), was then placed into a water-cooled graphite-element furnace (Figure 4.3). The furnace was back-filled with industrial grade nitrogen gas and then placed under a vacuum. Initially the vacuum was approximately between 25 to 30 Pa dropping to approximately 5 Pa by time the sintering temperature was reached. The heating rate and temperature was maintained using a digital controller coupled to a Type C shielded thermocouple having an accuracy of ± 2°C. Calibration of the thermocouple was performed by using pure alloys of known melting temperature and comparing the actual temperature of the furnace at which first evidence of melting occurs. The sintering temperatures used were 1100°C, 1300°C, 1400°C, and 1500°C. The furnace was heated at a rate of 20°C/min. To insure complete lubricant burnout, the furnace was held at 540°C for 10 minutes before continuing to the required final temperature. The compacts were allowed to cool to room temperature within the furnace (under a vacuum) before being removed.

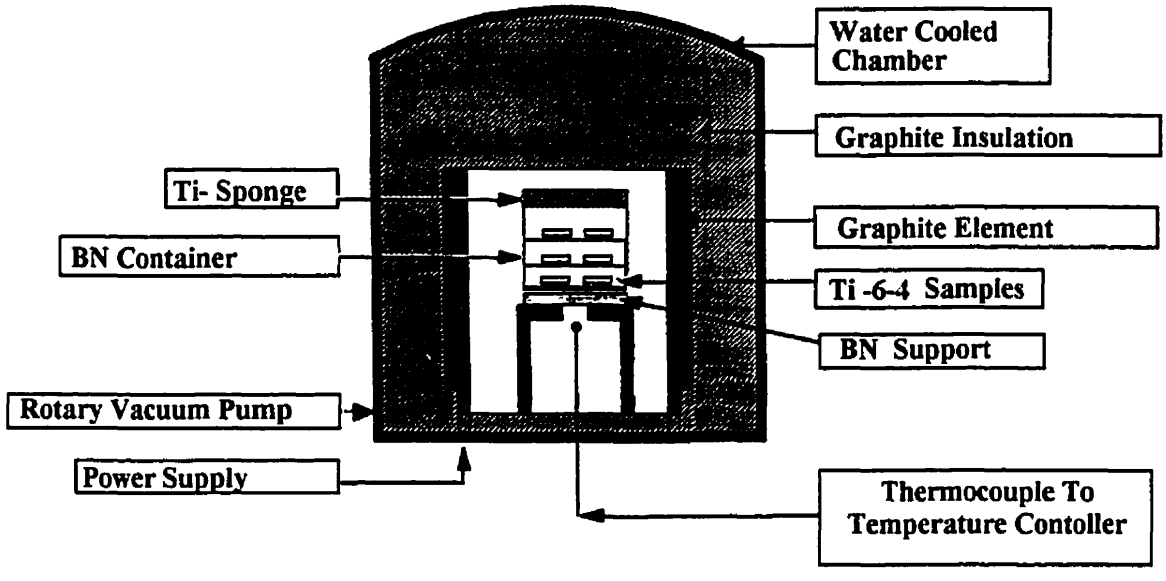

Figure 4.3: Diagram of the graphite-element vacuum furnace.

4.3.3 SINTERED DENSITY MEASUREMENT

Density measurement was performed according to ASTM standard C373-72 and depends on the Archimedes' principle: the volume of an object is the difference in wet weight of the object in air and that of the object's weight suspended in water. The procedure used was as follows:

1. After the sintered compact had cooled, the dry weight (D) was measured.
2. The compacts were then placed into a flask of distilled water and placed under a vacuum until bubble formation was no longer observed on the surface of the compacts.
3. The wet suspended weight in water (S) and the wet weight in air (M) were measured.
4. The following equations were used to determine the volume (V) and bulk density (ρ) also called the sintered density:

$$V = \frac{M - S}{\rho_{water}} \qquad 4.3$$

$$\rho = \frac{D}{V} \qquad 4.4$$

Where ρ_{water} is density of water.

4.4 MICROSTRUCTURAL EVALUATION

4.4.1 METALLOGRAPHIC PREPARATION

The sintered samples were sectioned longitudinally using a Leco CM-15 cut-off machine mounted with a diamond-wafering blade (Extec Technologies, Enfield, PA). One section from each sample was then mounted in an epoxy resin (EPO-THIN, Buehler) using vacuum impregnation to fill the pores and to provide superior edge retention. The polishing was performed on the Leco VP-150 VARI/POL automatic grinding/polishing machine, also equipped with a Leco AP-50 polishing pressure control unit. The polishing procedure

followed was prepared and optimized by Buehler Ltd. at Lake Bluff, Illinois using actual samples sintered for this thesis and was as follows in Table 4.2.

Table 4.2: GRINDING AND POLISHING PROCEDURE FOR TI-6%AL-4%V

Stage	Surface (Buehler tradename)	Lubricant extender	Abrasive type/ size carrier	Time (min:s)	Force per sample	Speed setting (rpm)	Relative rotation
Planar Grinding	Buehler-met 2	Water	240 grit	Until plane	1.5 kg	150	Comp
Sample Integrity	Ultra-Pad 8" cloth		9μ Oil based suspension	3:00	2 kg	150	Comp
	Texmet 1000	Distilled water 1:1	Mastermet	4:00	3.5 kg	120	Comp
Final Polishing	Mastertex	Distilled water 1:1	Mastermet	1:00	1.5 kg	80	Comp
Remarks	Clean with ultrasonic for each step						

For microstructural evaluation, the samples were etched using Kroll's Reagent (6 ml HNO_3, 3 ml HF and 100 ml of distilled H_2O). This consisted of submersing the sample for 15 to 20 seconds in the reagent depending on the degree of contrast required between the phases and grain boundaries. To prevent etchant stains, immediately upon removal from the etchant the sample's surface was flooded and washed with ethanol and then dried using a hair dryer.

4.4.2 IMAGE ANALYSIS

Image analysis was used for determining the percent porosity and hence density of the samples for comparison with the densities determined by the Archimedes as well as

verifying the trends observed for the varying sintering parameters. The LECO L2002 image analysis system uses a binary digitized image constructed from a gray scale employing 0 to 255 shades. This allows distinguishing between the dark porous phase and lighter phase of the unetched matrix. The results are calculated as a percentage of the area of the view frame, which was determined at a magnification of x125. Generally at this magnification the average of 30 frames were sufficient to result in a good representation of the bulk porosity, but care had to be exercised not to include the porous surface region which would bias the density measurements.

4.5 VICKERS MICROHARDNESS

Microhardness measurements were preformed using a computerized Buehler Omnimet Micro Hardness Tester (MHT). The MHT employs an image analysis software package called Micromet 2001, version 1.1. The automated analysis works on the same principles described for the microstructural image analysis, with 0 to 255 degrees of grays. The indentation, which appeared as a different shade was automatically measured and converted to Vickers hardness. The system is self-calibrating and once the indentation parameters (number of indentations, load, time and magnification) are entered, the only parameter to control is the location of the indentation. The indent location was displayed at the desired magnification on a computer screen and could be relocated using a joystick. Seven readings were taken for each sample. The mean from these readings along with its standard deviation was automatically calculated and given as a Vickers hardness value (HV).

4.6 RADIOGRAPHIC TESTING

Industrial radiography is a nondestructive method of inspecting materials frequently used for detecting discontinuities and imperfections in castings and welds. The material being inspected is bombarded by electromagnetic radiation of short

wavelength, which in turn is absorbed to varying degrees, depending on the material composition and thickness. As a result of this absorption the amount of radiation emerging from the opposite side of the material varies. This variation is detected on radiographic film, which has a layer of x-ray emulsion on ether side producing a composite radiographic image. The sensitivity of the radiographs to small changes in material thickness and/or density permits observation of the corresponding small changes in the film blackness.

The source of radiation was a Philips constant potential X-ray System Model MG320. The uni-directional x-ray tube was a Philips MCN 321 with a maximum output of 320kV. The X-ray tube contained a tungsten target with a focus of 4.0mm^2 at 10mA. The radiographic film was an AGFA D4 Structurix fine grain film inserted between a 0.005" lead screen on the top and 0.010" lead screen on the bottom. The lead screen and sensitivity rating combined to reduce backscatter, which can reduce the image sharpness. A more sensitive D2 film with even finer grain could be used but this film is also slower and thus more sensitive to backscatter, and as a result the X-ray parameters would be difficult to optimize given the range of densities for these samples.

The kilovoltage, milliamperage, time and distance control exposure of the film. The kilovoltage effects the X-ray beam intensity; increasing the kilovoltage increases penetration. The milliamperage is used to control the X-ray beam density for contrast and quality of image. The time is used to fine tune between the X-ray intensity and beam density. The distance of the object to the source of radiation controls the geometric unsharpness caused by the penumbra effect (light shadow). The relationship between milliamperage, time and distance is called the Exposure Factor (E.F.) and is expressed as:

$$\frac{\text{Milliamperes x time [seconds]}}{\text{Distance}^2\text{ [centimeters]}} \qquad 4.5$$

However, since for this test the kilovoltage was kept at 75 kV and the object to film distance was fixed at 137 centimeters, the exposure was controlled by the X-ray

relationship of milliamperes x seconds referred to as mA·s. The best results for this test were obtained using a mA·s of 840.

The last tool that is required for this radiographic test is the penetrameter. Penetrameters provide an ability to check on the overall X-ray quality. The penetrameter is made of the same or similar material (in this case AMS 4928) with a thickness (T) of approximately 2% of the part being measured. Hence a penetrameter of 0.10", has an actual thickness of 0.002". The penetrameter also contains three small holes that represent a penetrameter thickness of 1T, 2T and 4T. When the radiograph is viewed the hole or holes visible indicate the sensitivity of the film. Since the sintered samples showed a range in thickness at different temperatures. A combination of several flat penetrameters of different thickness forming a step wedge was placed on the source side of each film.

The radiographic film was developed using a Kodak XO-Matic automated film processor. The processor performs the development, fixing and rinsing, with premixed solutions that are maintained at the appropriate temperature and periodically verified. After processing, the film's density (blackness) was verified on a Macbeth TD 504 densitometer to insure that the industrial minimum acceptable optical density of 2.00 was met. All the films prepared for this thesis measured 2.07, meeting this requirement. A film viewer with a minimum of 540 foot/candle was required for interpreting the results. The X-rays were then converted to positives using an X-ray film scanner and associated computer software.

CHAPTER 5:

RESULTS AND DISCUSSION

Existing literature on the characterization of powder with the presence of lubricants has been researched for less reactive metals such as ferrous alloys and copper alloys. The present work is aimed at determining the effect of lubrication on titanium powder metallurgy processing and examining similarities and/or disparities in relation to other work on lubricants. The results discussed in this chapter are broken into two sections. In the first the titanium alloy powder, with and without zinc stearate lubricant, is characterized for particle size, distribution, morphology and composition as well as for flow, apparent density and green density. The second section examines the effect of lubricant addition on sintering through the measurement of the sintered density, microstructure and hardness.

5.1 POWDER CHARACTERIZATION

5.1.1 SHAPE AND COMPOSITION

The as-received Ti-6%Al-4%V powder was characterized for general appearance of the particles using a scanning electron microscope. Figure 5.1 shows the angular

morphology of the titanium alloy particles, which is characteristic of the hydride-dehydride process used for the manufacturing of this powder (compare with Figure 2.2).

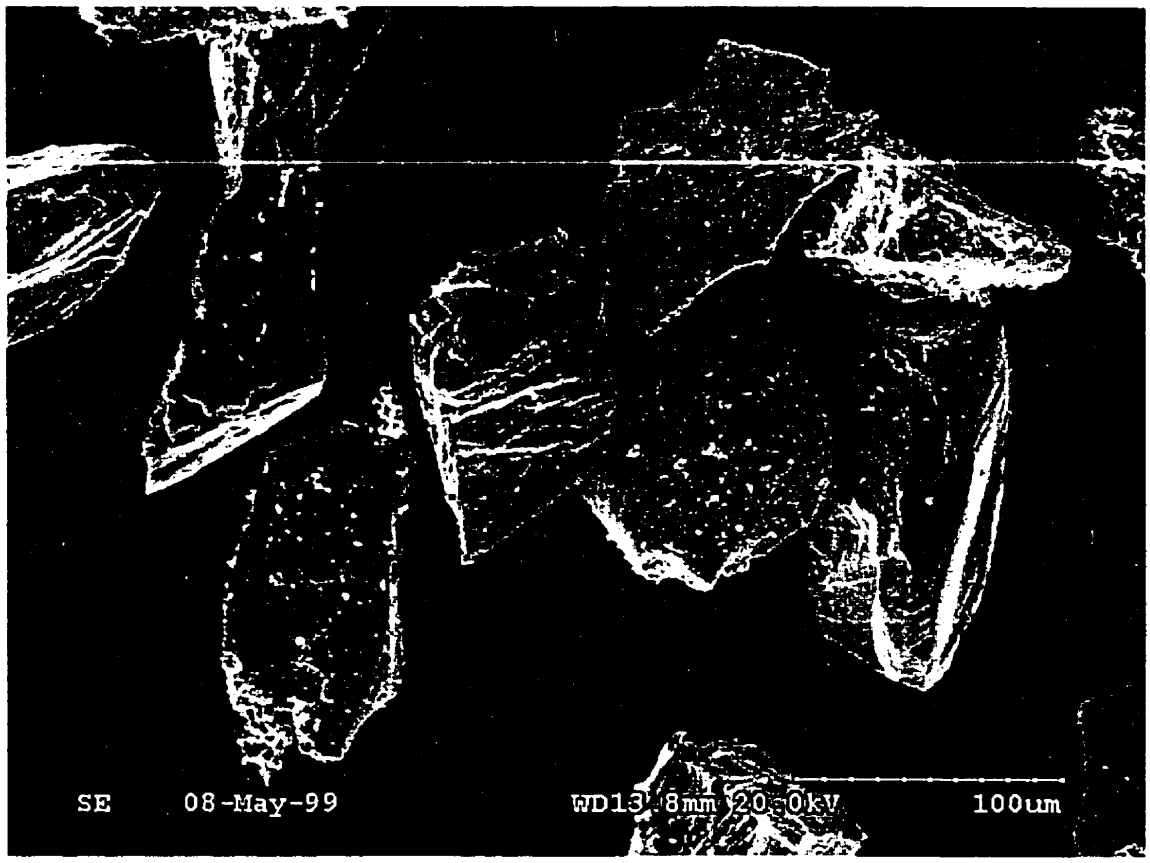

Figure 5.1: Particulates showing typical angular shape of the as received hydride-dehydride titanium alloy powder.

Chemical compositional analysis by energy dispersive x-ray analysis revealed no significant impurities with the only detectable elements being titanium, aluminum and vanadium, as indicated in Figure 5.2. Dot mapping for these elements revealed an homogeneous distribution for titanium, aluminum and vanadium on each particle supporting the pre-alloyed condition of the powder as shown in Figure 5.3.

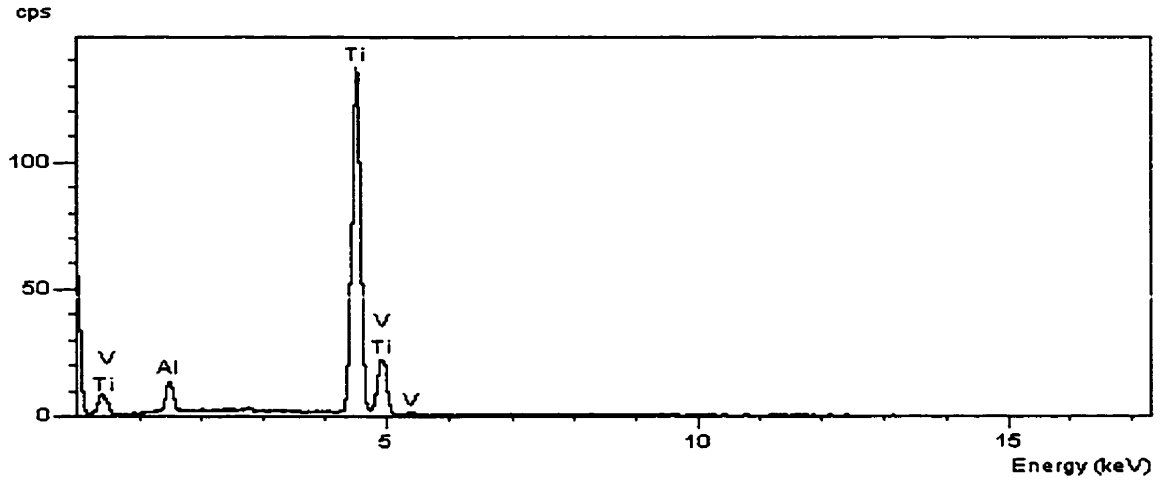

Figure 5.2: Energy dispersive analysis of the as received powder shows the presence of titanium, aluminum and vanadium.

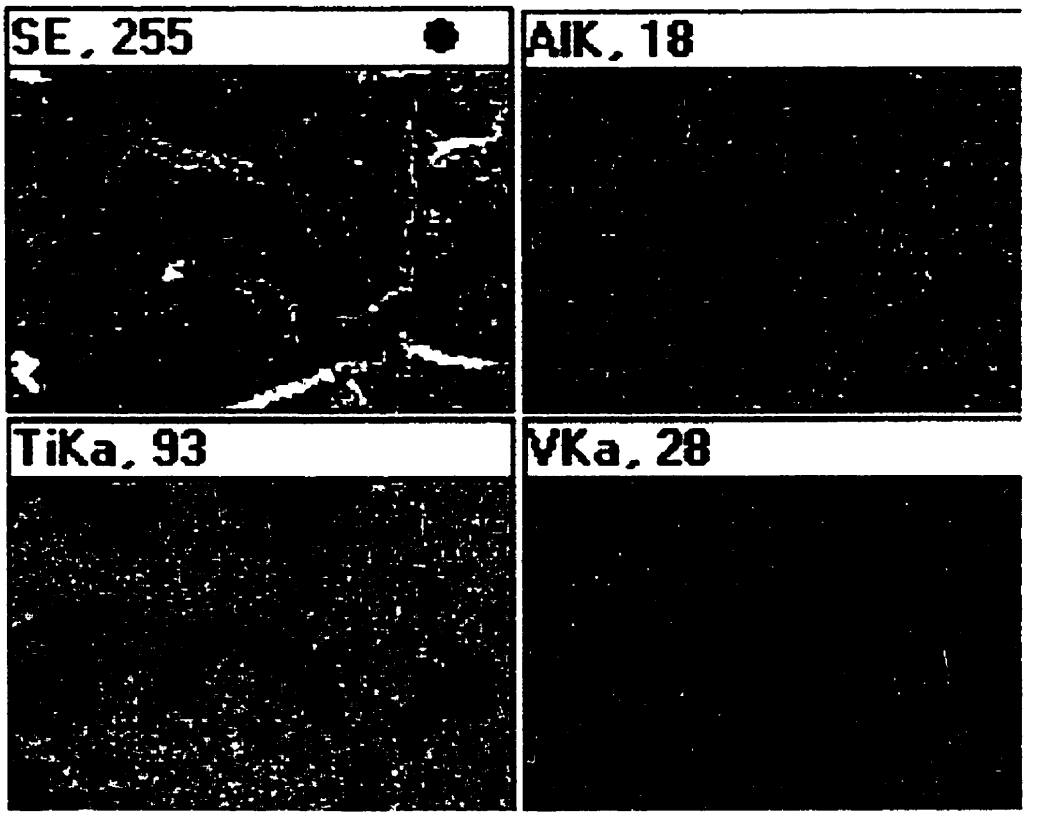

Figure 5.3: Dot mapping by EDX shows a uniform distribution of the alloying elements.

5.1.2 SIZE DISTRIBUTION

The cumulative size distribution was determined for the as received and milled powder. The raw data is compiled in Tables 5.1 and 5.2 and is presented in Figure 5.4

Table 5.1: Sizing analysis of as received titanium alloy powder

Opening (μm)	Trial 1		Trial 2		Trial 3	
	Weight (g)	Cumulative % Passing	Weight (g)	Cumulative % Passing	Weight (g)	Cumulative % Passing
> 106	0.0	100	0.0	100.0	0.0	100.0
>75	4.21	95.79	5.11	94.89	5 47	94.53
>53	88.49	7.30	87.36	7.53	86.84	7.69
>45	6.29	1.01	6.46	1.07	6.68	1.01
>38	0.94	0.07	0.98	0.09	0.94	0.07
<38	0.07		0.09		0.07	
Total	100.0		100.0		100.0	

Table 5.2: Sizing analysis of milled titanium alloy powder

Opening (μm)	Trial 1		Trial 2		Trial 3	
	Weight (g)	Cumulative % Passing	Weight (g)	Cumulative % Passing	Weight (g)	Cumulative % Passing
> 106	0.0	100.0	0.0	100.0	0.0	100.0
>75	3.16	96.84	3.35	96.65	3.48	96.52
>53	85.16	11.68	85.17	11.48	85.14	11.38
>45	9.15	2.53	9.21	2.27	9.18	2.20
>38	1.74	0.79	1.59	0.68	1.59	0.61
<38	0.79		0.68		0.61	
Total	100.0		100.0		100.0	

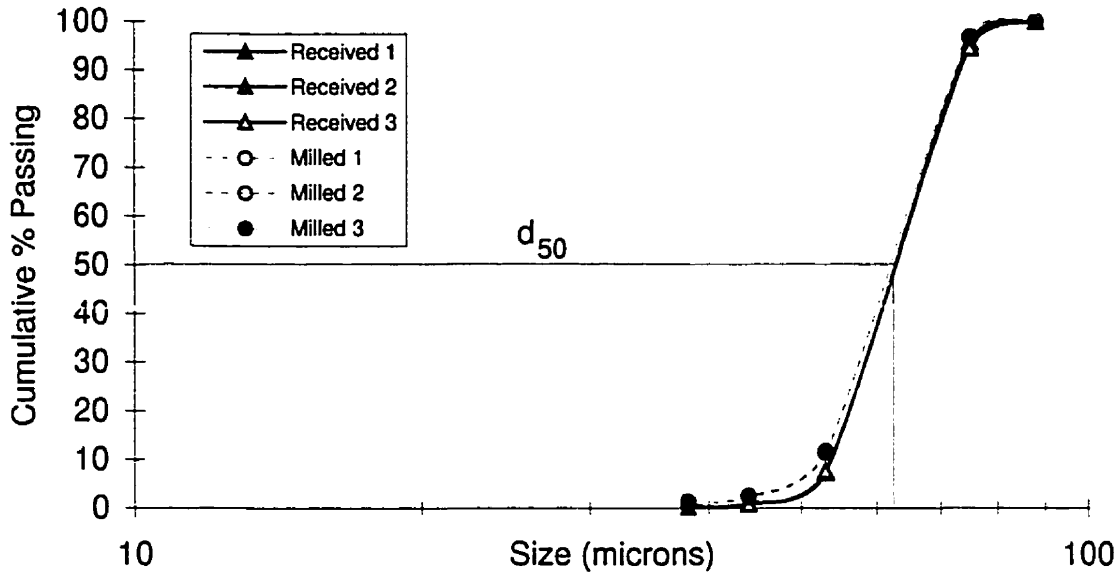

Figure 5.4: Particle size distribution of as received and milled titanium alloy powders.

From Figure 5.4, it can be seen that the as received powder has a narrow size range mainly between 75 and 45 μm. The attrition milling results in a slightly finer range of 73 to 40μm. These results suggest that attrition milling does not result in fracture of the particles but rather abrades the surface by particle/particle and particle/media contact. Surface abrasion is useful for the reduction of surface TiO_2 oxide layers, which through increased friction reduce compaction and during sintering inhibit bonding by preventing the diffusion of atoms. Based on these size distributions, the sedimentation technique, which is limited by the settling velocities to particle sizes less than 40μm, was not used.

The relatively narrow size distribution of the particles with the presence of some small particles will improve the packing characteristics of the powder. Also, the problem of bridging which can occur when using angular powders is reduced for narrow particle size distributions. Moreover, narrow size distribution result in a more uniform grain structure, which can be beneficial to the final mechanical properties of the sintered component.

Although the particle size of the hydride-dehydride powder is not as fine compared to atomized powder, the specific surface area and hence surface energy of this powder should result in a good thermodynamic driving force for the formation of bonds during sintering. In the case of titanium very small particle sizes may be deleterious to sintering as the increased reactivity promotes oxidation. Additionally, very small particles are difficult to compact and require larger compaction pressures for the collapse of fine pores. Thus the particle size and size distribution is a compromise based on tailoring the size distribution to optimize green consolidation, promote sintering and obtain a uniform grain structure and good final properties.

5.1.3 FLOW

The as received titanium powder was not free flowing due to the angular morphology of the particles which resulted in increased inter-particle friction. The addition and mixing of a lubricant such as zinc stearate can reduce the inter-particle friction such that the powder becomes free flowing. However, two parameters become important as seen from the flow test results for the various mixing times in Figure 5.5.

The first parameter is the weight percent of lubricant admixed. As the admixed lubricant content is increased, the flow rate is observed to decrease. This is due to agglomeration caused by excessive lubricant, which hinders flow. The second variable is mixing time. Initially, there is a large increase in flow rate (approx. 10%) within the first 20 minutes of mixing. As the time increases the relative increase in the flow rate diminishes. This effect is the result of the lubricant coating most of the particle surface within the first 20 minutes. Thus, the benefit obtained from longer times is limited beyond this critical mixing period. In fact, prolonged mixing increases the chance of de-mixing which is the segregation of particles due to variations in particle size, shape and density. If flow was the only criteria needed to fill a specific volume quickly, then, based

on these results, the optimum time would be approximately 20 minutes with 0.50 weight percent zinc stearate lubricant.

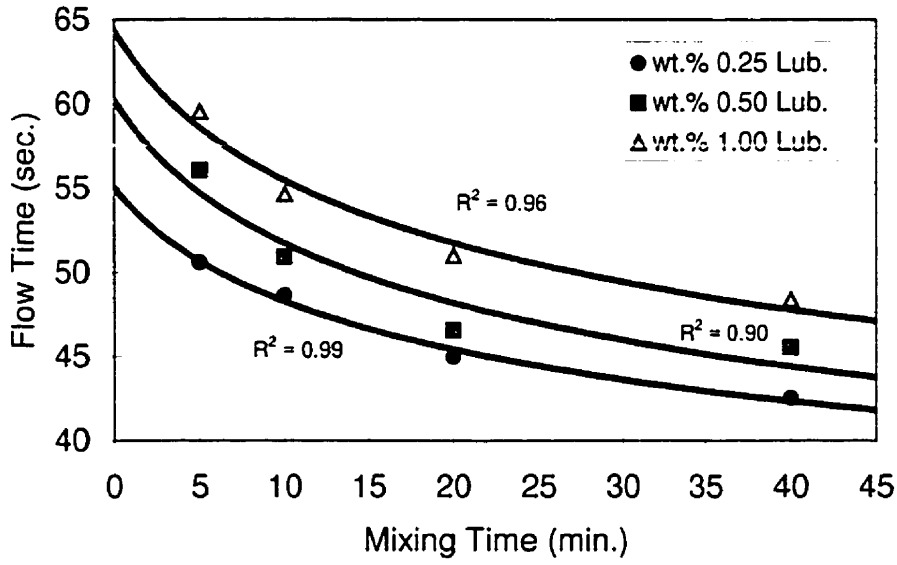

Figure 5.5: Effect of mixing time and weight percent lubricant on flow.

5.1.4 APPARENT DENSITY

In practice the apparent density is used for controlling the fill volume. This is because if the weight of the powder changes for a fixed volume, a change in the pressed density occurs. The two important parameters tailored to increase the apparent density are lubricant content and mixing time. The effects of these two parameters are shown in Figure 5.6. The effect of increasing the weight percent lubricant admixed is to decrease the apparent density. This is due to the increased volume that is being occupied by the lower density lubricant. Increasing the mixing time results in an increased apparent density. As in Figure 5.5, the largest gains (approximately7%) occur within the first 20 minutes of mixing. During this time the lubricant coats most of the particle surface and through reduced inter particle friction improves the packing characteristics.

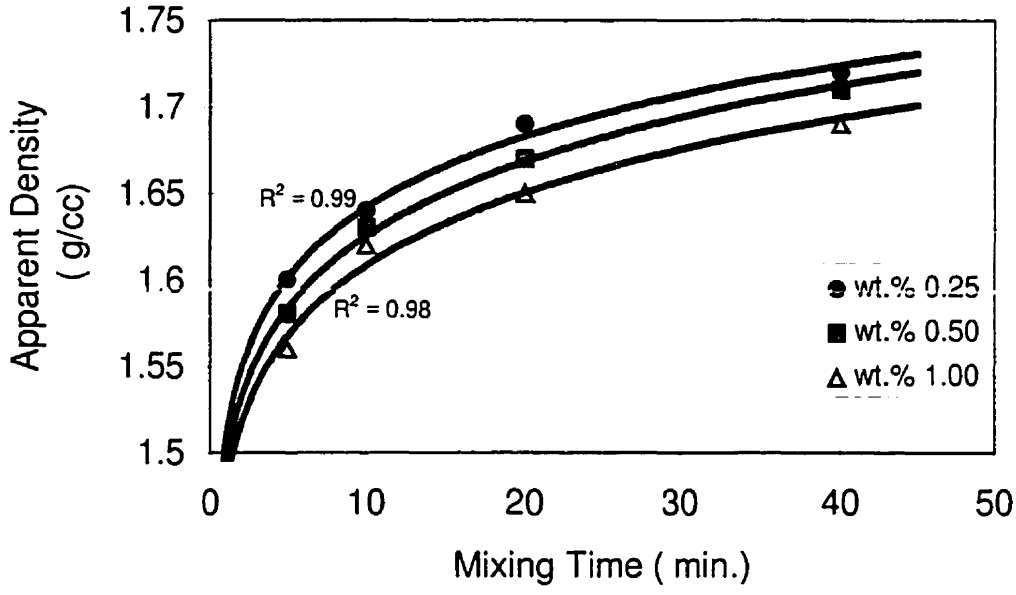

Figure 5.6: Effect of mixing time and weight percent lubricant on apparent density of the titanium alloy powder.

As the mixing time increases, the slope of the curves in Figure 5.6 begins to plateau and suggests that prolonged times result in negligible increases in the apparent density with mixing time. Based on these results, the time chosen for subsequent sample mixing was 35 minutes. Although the flow rate increases little above 20 minutes mixing, the near maximum value in the apparent density should reduce compaction requirements for uniform densification.

5.2 COMPACTION: GREEN STRENGTH AND GREEN DENSITY

Uniaxial pressing offers good dimensional control during forming and is an inexpensive and common means to compact powder, as evidenced by the large amount of pills, vitamins and candies produced by this method. However, for metallic materials the high wall friction and limited ability of angular powders to rearrange during compaction can result in density gradients, which, during sintering, produce non-uniform shrinkage.

For this reason the height to diameter ratio was kept small (approx. 0.16) to improve uniformity in the compacts and reduce shape distortion during sintering.

The compaction pressures chosen were 207, 241, 276, 310 and 343 MPa. Pressures below 207 MPa did not produce enough green strength for manipulation and pressures above 343 MPa resulted in excessive fragmentation of the particles. Initial compaction without any lubricant at 207 MPa resulted in samples that had sufficient green strength for manipulation but edge retention was minimal. Figure 5.7, is a comparison of samples as the compaction pressure increased from 207 to 343 MPa. The photograph for the 1.00 weight percent lubricant samples was chosen due to the enhanced contrast between the five compacts.

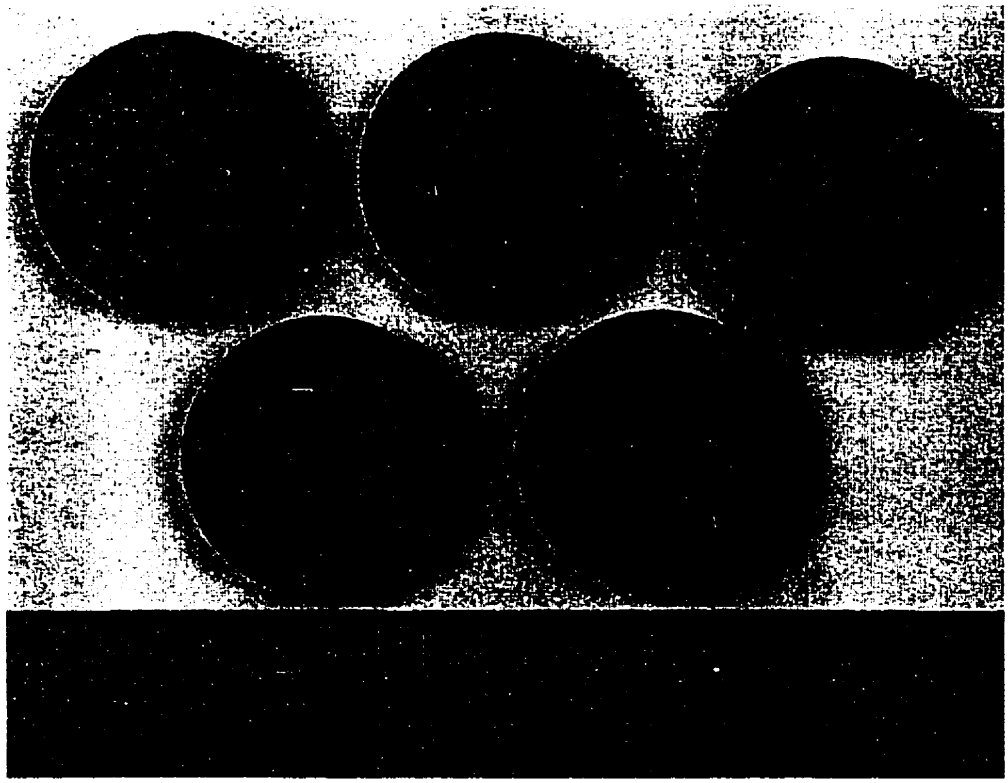

Figure 5.7: Photograph of compacted titanium alloy powder admixed with 1.00 wt.% zinc stearate lubricant. Numbers 1 to 5 correspond to compaction pressures of 207, 241, 276, 310 and 343 MPa, respectively.

Generally, the results (also Tabulated in Appendix A) were seen to be similar for all the compacts. Compact no.1, shows the most degradation with the corners fretted almost completely around. As the pressure was increased, the subsequent compacts showed greater resistance to degradation from handling, as seen with compact no.5, which has almost no fretting. This resistance is due to an increased green density as the pressure increased, and as stated in the theory, increases in the green density also produces a corresponding improvement in the green strength.

The increase in green density as pressure is increased is due to the short-range rearrangement that results from the increased particle deformation. Figure 5.8 shows a comparison of the particle rearrangement and deformation observed at 207 MPa and 343 MPa. The improved particle rearrangement at the higher compression pressure is apparent in the lower magnification micrographs, Figures 5.8a and c. The increased particle deformation with minimal fracture is apparent in the images taken at higher magnification, Figures 5.8b and d.

The addition of lubricant further encourages compaction through particle rearrangement and increased effective die pressure by reduced friction between particles and the die wall. Figure 5.9 compares the particle rearrangement and deformation observed at 207 MPa and 343 MPa with the addition of 1.00 weight percent lubricant. The effect of lubricant addition on rearrangement is apparent in Figure 5.9a and c, particularly when compared to Figure 5.8a and c. Increased compaction pressure and increased particle deformation are observed. Also, as seen in Figure 5.9b and d, the higher the compaction pressure the greater the pore filling from excess lubricant.

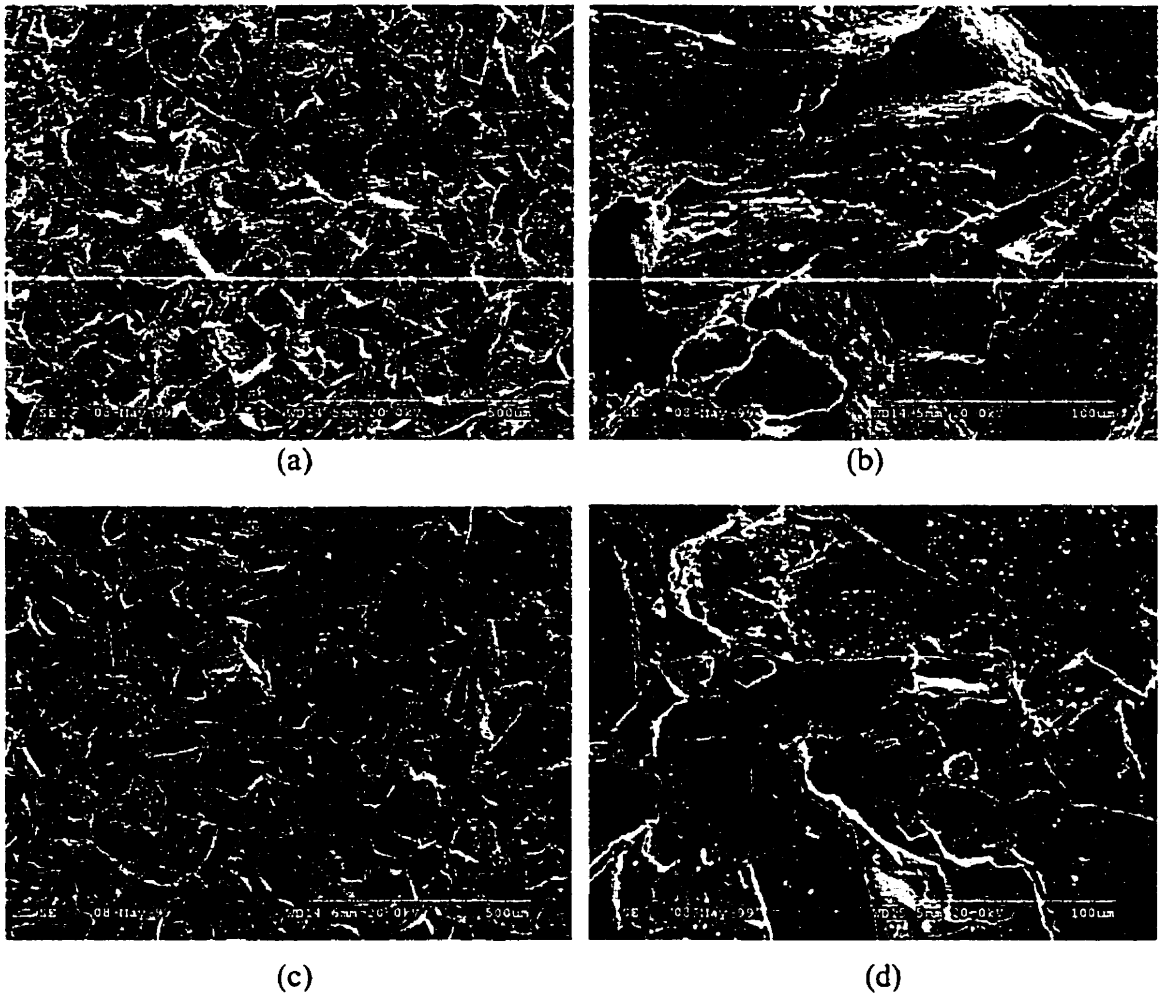

(a) (b)

(c) (d)

Figure 5.8: Effect of compaction pressure on titanium alloy powder without any lubricant: (a) 207 MPa, (b) 207 MPa, (c) 343 MPa and (d) 343 MPa.

Increased deformation also helps to penetrate the lubricant on the surface by breaking the oxide layer between the particles. Contact of the particle through deformation then achieves cold welding between particle surfaces, which is one of the characteristics of pressing responsible for the increase in green strength. The effect of increasing compaction pressure on the green density of the titanium alloy powder is shown in Figure 5.10. The results correspond to the observations noted previously; increasing the compaction pressure results in an increased green density. Regardless of the lubricant addition, an increase of approximately 11% in green density is observed

when the compaction pressure is increased from 207 MPa to 343 MPa. Also the relationship between compaction pressure and green density for the titanium alloy powder was determined to be linear over the range of pressures investigated. Consequently the compression ratio will be linear and can be used to determine the fill volume multiplier for different compaction pressures, as listed in Table 5.3. From Table 5.3 it is also apparent that similar specific fill volumes can be achieved through several compaction pressure and lubricant content combinations.

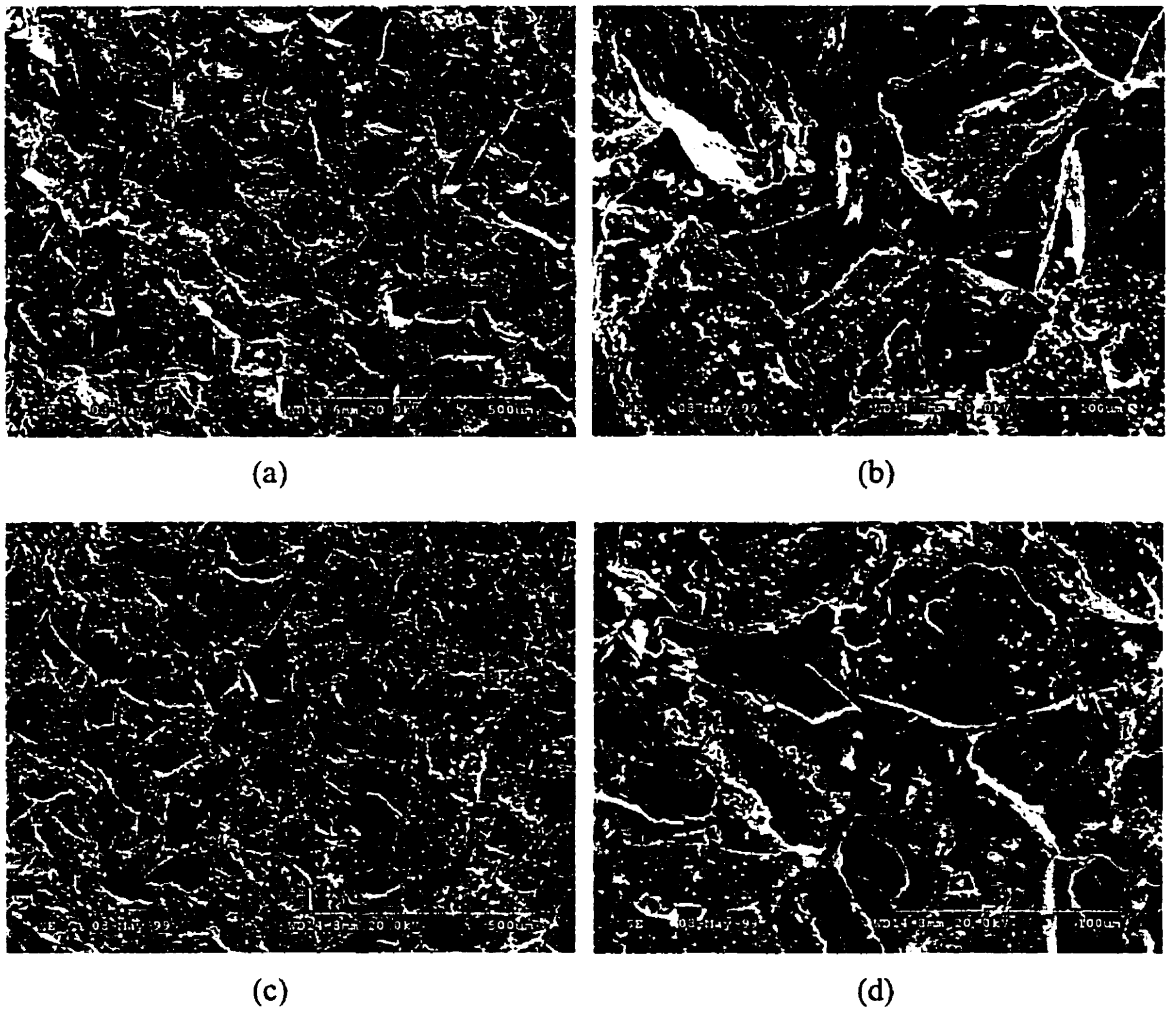

(a) (b)

(c) (d)

Figure 5.9: Effect of compaction pressure on titanium alloy powder admixed with 1.00 wt.% zinc stearate lubricant: (a) 207 MPa, (b) 207 MPa, (c) 343 MPa and (d) 343 MPa.

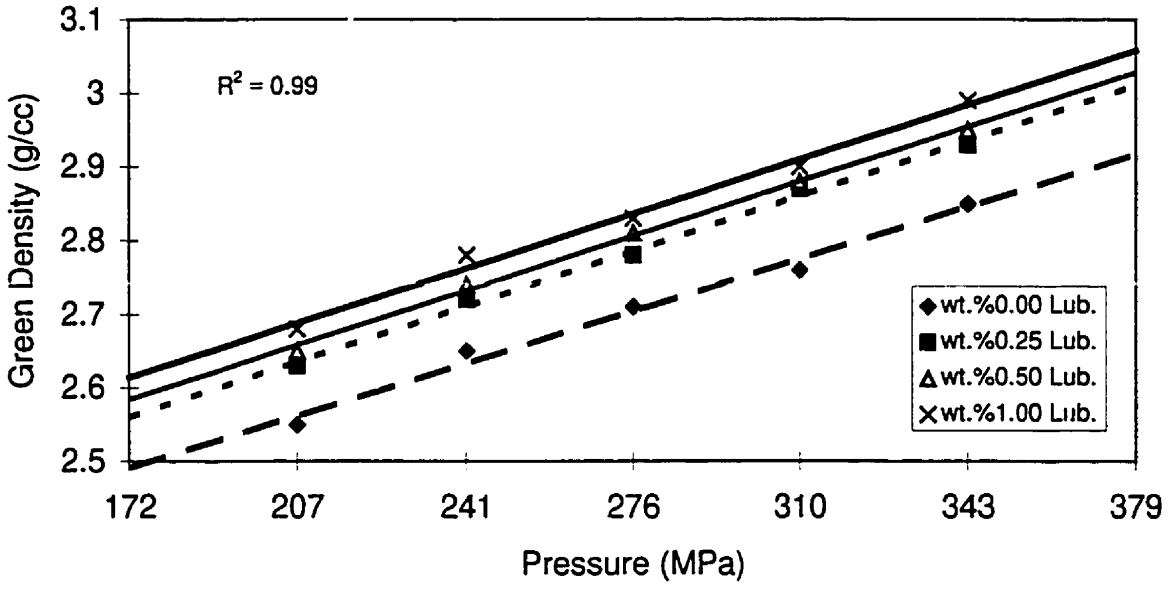

Figure 5.10: Effect of compaction pressure on the green density with for titanium alloy powder admixed with varying amounts of lubricant.

At a constant compaction pressure, increasing the lubricant content in the titanium alloy powder does not have a pronounced effect on the green density of the compact as shown in Figure 5.11. The addition of 1/4 weight percent lubricant shows an increase of approximately 4% in the green density when compared too the non-lubricated titanium alloy powder. An increase of four times the amount of lubricant to 1 weight percent, results in only an additional 2% increase in the green density. Thus, the relationship of the lubricant quantity to green density is not proportional.

As the amount of lubricant added increases, further reduction in the inter-particle friction is limited. The excess lubricant results in pore filling and reduced gains in green density

Table 5.3: Compression ratios

Apparent Density	1.72 g/cc 0.25 wt.% Lubricant	1.70 g/cc 0.50 wt.% Lubricant	1.67 g/cc 1.00 wt.% Lubricant
207 MPa	1.53	1.56	1.59
241 MPa	1.58	1.61	1.65
276 MPa	1.62	1.66	1.69
310 MPa	1.67	1.70	1.73
343 MPa	1.72	1.75	1.78

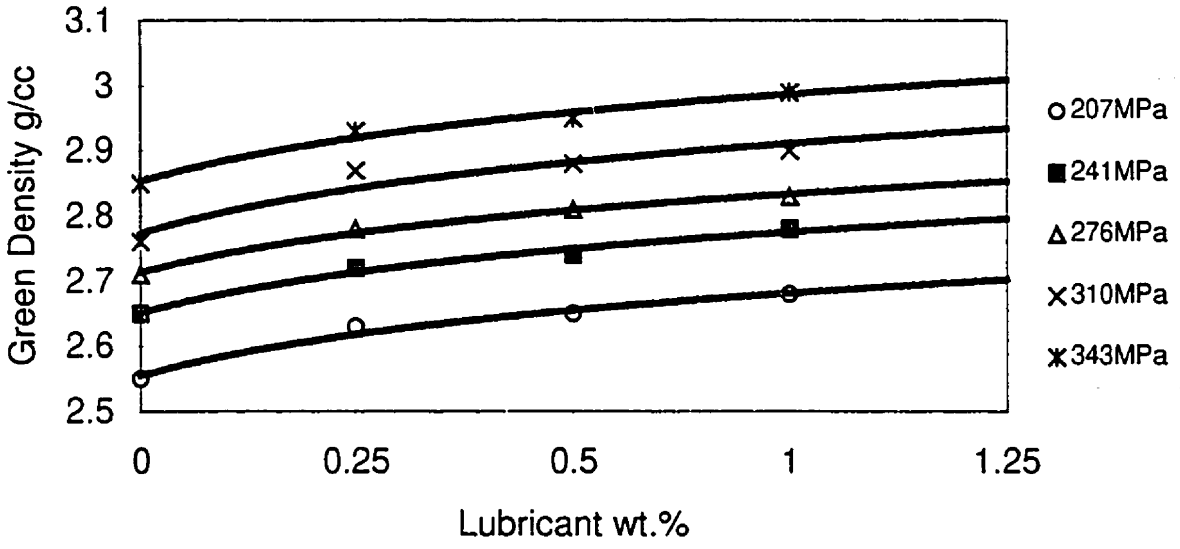

Figure 5.11: Effect of zinc stearate addition on the green density of the titanium alloy powder for different compaction pressures.

5.3 SINTERING

By measuring the sintered density and shrinkage of the consolidated components the degree of sintering can be monitored. The consolidation parameters affecting the sintered density and shrinkage include consolidation temperature, green density, lubricant addition and holding time. At any given temperature combinations of the other variables can be determined to optimize sintering. However, the main purpose of this paper was to

examine the effect of lubricant addition on the sintering of titanium alloy powder. As such, the holding time was held constant at 1 1/2 hours, on the basis of previous work[30], to enable sufficient sintering in the samples so that any changes could be monitored without over-sintering. Prior to investigating the remaining parameters, the high reactivity of titanium powders required a thorough evaluation of the burnout time, rate and temperature. This would allow tailoring of the furnace conditions to reduce the possibility of surface oxidation prior to sintering.

5.3.1 BURNOUT

The growth of titanium oxide on Ti-6%Al-4%V occurs at a logarithmic rate at temperatures below 500°C (1 atmosphere), creating a protective layer. Above this temperature the oxide layer becomes multi-layered and porous, reducing its protective qualities. As such, sintering was performed at temperatures above 1100°C in a vacuum with the intention of removing the lubricant at much lower temperatures preferably within the logarithmic growth region. Thermo-gravimetric analysis was performed to determine the temperature(s) at which the lubricant burns out. Initially samples compacted at 207 MPa and containing 0, 1/4, 1/2 and 1 weight percent lubricant were chosen. The results, shown in Figures 5.12, 5.13 and 5.14, indicate that burnout occurs between 410 to 440°C and is completed by 525°C for all the samples. At these temperatures the oxidation rate is still mostly logarithmic and since the system is under a vacuum the risk of contamination by the lubricant burnout residue through the oxide layer is minimal.

From Figure 5.12, the initial weight loss begins at around 500 seconds and corresponds to approximately 100°C, the temperature at which water begins to vaporize. Thus the weight loss at this temperature is due to evaporation of moisture within the samples. The titanium alloy powder without lubricant addition shows continued weight loss until approximately 1200 seconds after which no further drop in weight was observed. For the titanium alloy powder admixed with various amounts of zinc stearate lubricant, a second loss in weight commenced after holding between 1250 to 1500

seconds. This drop in weight is associated with the burnout of zinc stearate lubricant and the largest reduction in weight was observed for the sample with the highest lubricant content. This lubricant burnout stage is completed by 2000 seconds for all the samples.

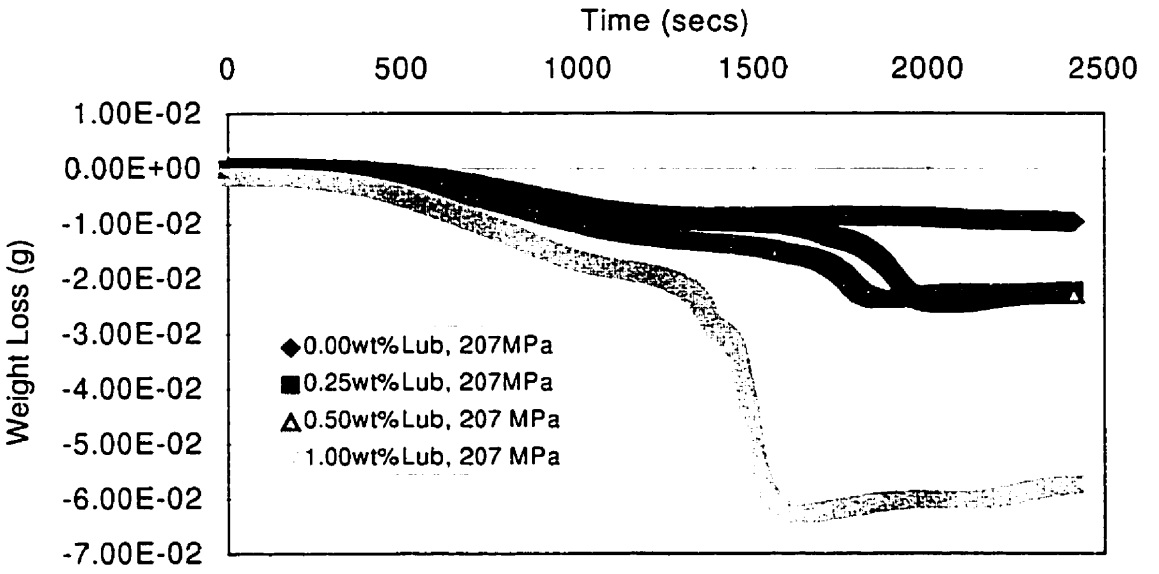

Figure 5.12: Thermo-gravimetric analysis for 0, 1/4, 1/2 and 1 weight percent lubricant addition at a constant compaction pressure of 207 MPa.

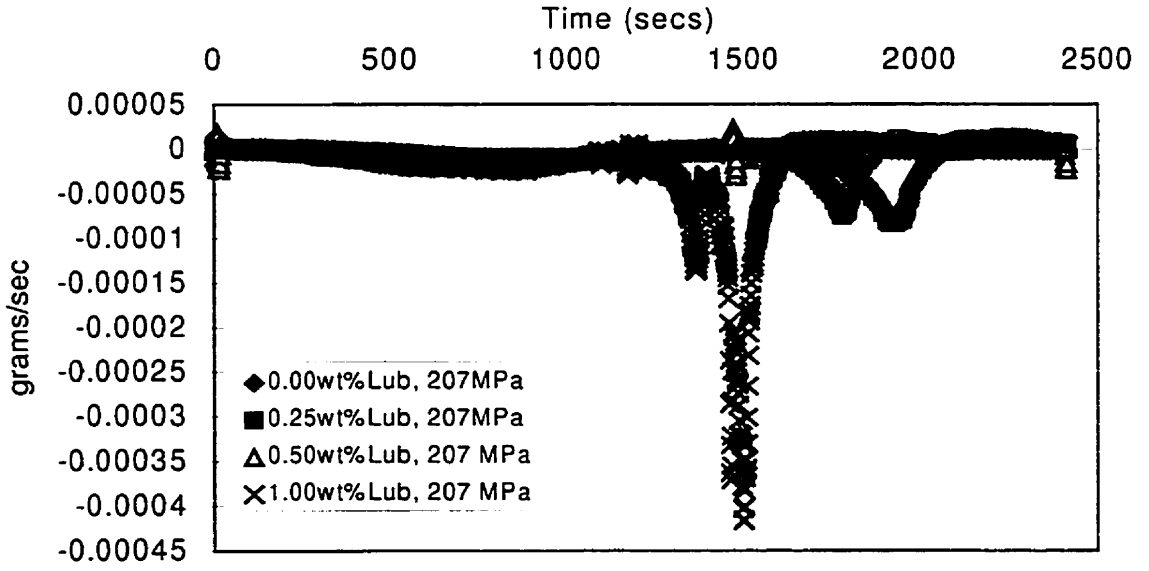

Figure 5.13: Thermo-gravimetric analysis first derivative curves for 0, 1/4, 1/2 and 1 wt.% lubricant at a constant compaction pressure of 207 MPa.

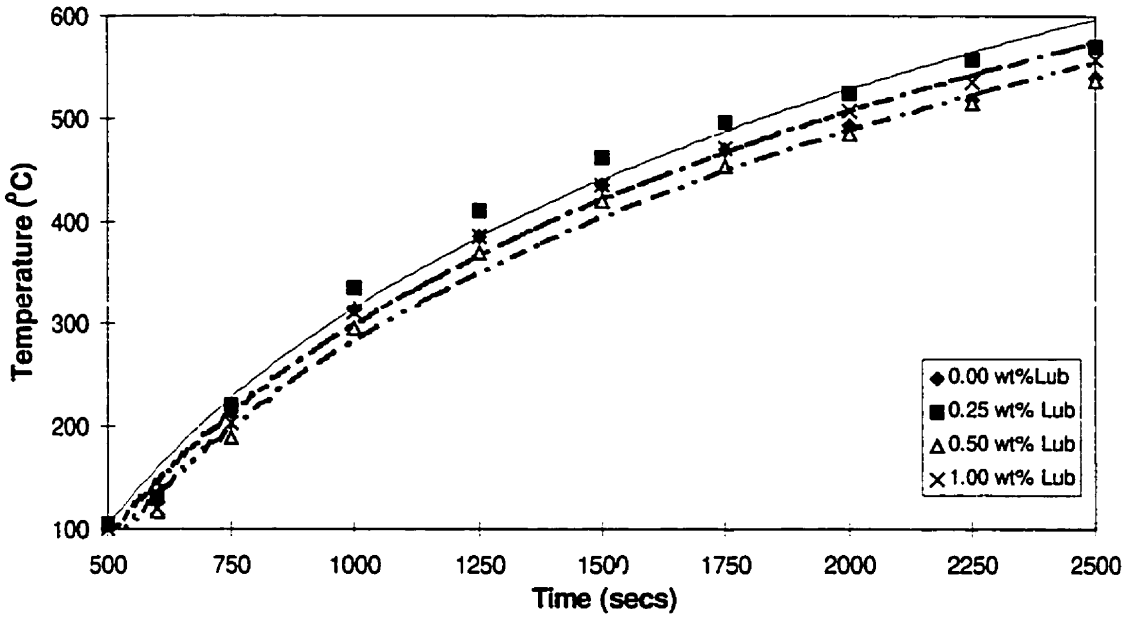

Figure 5.14: Temperature versus time curves for Figures 5.12 and 5.13.

The major inflections points in the first derivative curves plotted in Figure 5.13 (individual curves in Appendix B) corroborate with the results of Figure 5.12. The first derivative curves show that as the weight percent of zinc stearate lubricant is increased, the rate of burnout increases. However the time to complete lubricant burnout remains the independent of the zinc stearate content. The first derivative curves also indicate a small peak between 1250 and 1500 seconds (385 to 415°C), which is not immediately apparent in the curves shown in Figure 5.12. Since this peak is common to only the titanium alloy samples admixed with zinc stearate lubricant and appears to be proportional to the size of the main peak, it is likely an indication of lubricant decomposition prior to burnout.

Since the quantity of zinc stearate lubricant added results in only a change in amount of weight loss and rate of burnout, investigation of the effect of green density on sintering was performed by simply holding the weight percent lubricant constant and varying the compaction pressure. Figure 5.15 shows the temperature versus time plots for

each curve in Figures 5.16 and 5.17, which are the weight loss and rate of burnout results respectively for three 0.50 weight percent lubricant samples that had been compacted at 207, 276 and 343 MPa. Moisture loss was still observed to occur between approximately 500 and 1250 seconds and burnout commenced at around 1250 seconds (420 to 440°C) and was complete by 2100 seconds (510°C). Similar results were observed for the titanium alloy powder samples admixed with 0.00, 0.25 and 1.00 weight percent zinc stearate lubricant and compacted at various pressures. Thus, since no significant change in the weight loss behavior due to compaction pressure was observed, the burnout temperature and rate are not dependant on the green density but only the type and amount of lubricant used.

Based on the weight loss results obtained from the thermo-gravimetric analysis work, the thermal cycle profile for the sintering furnace could be defined. Basically, the titanium alloy powder samples were heated from room temperature to 540°C at a constant rate of 20°C/min, held for 10 minutes at 540°C and then heated to the required sintering temperature and held for 1.5 hours. The sintered densities were determined by the Archimedes method and are given in Appendix C.

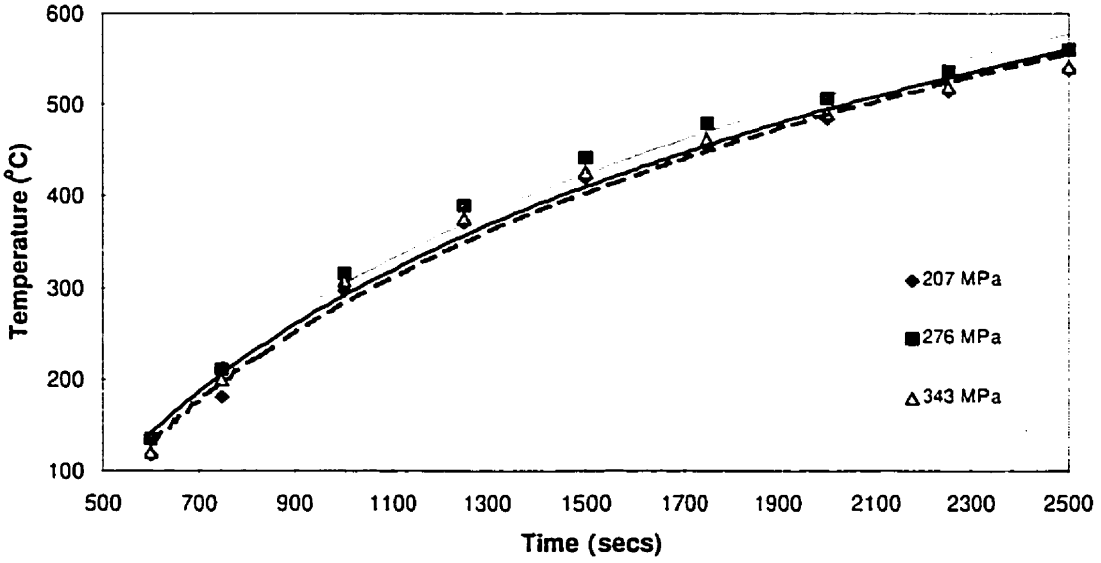

Figure 5.15: Temperature versus time curves for Figures 5.16 and 5.17.

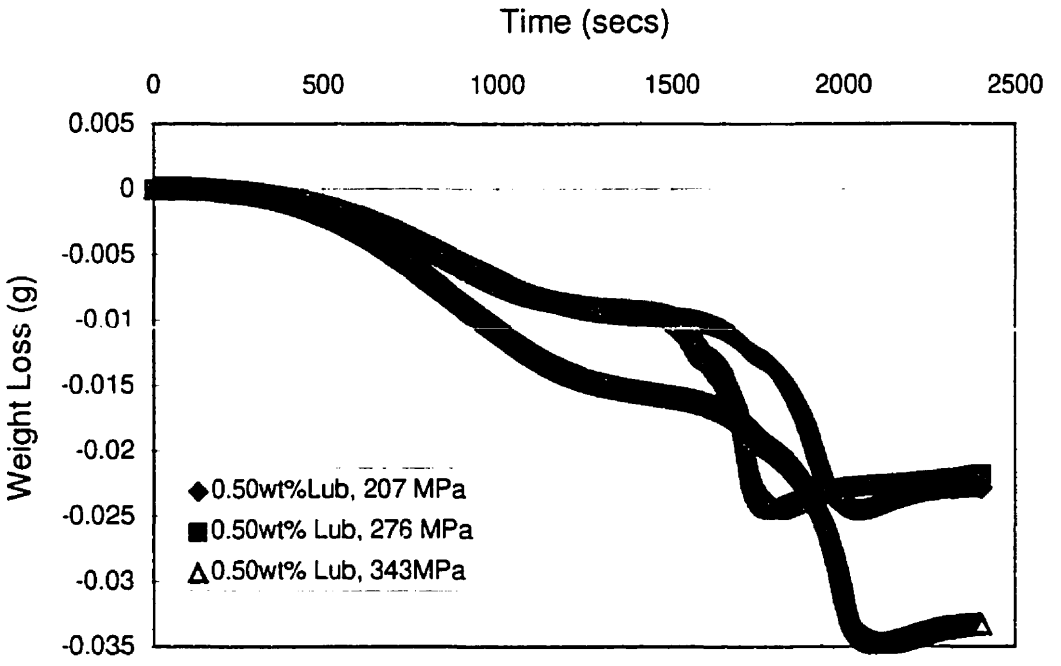

Figure 5.16: Thermo-gravimetric analysis for powder containing 0.5 wt.% lubricant and compacted at 207, 276 and 343 MPa. Note slight dip in the curves due to lubricant decomposition between 1500 and 1750 seconds.

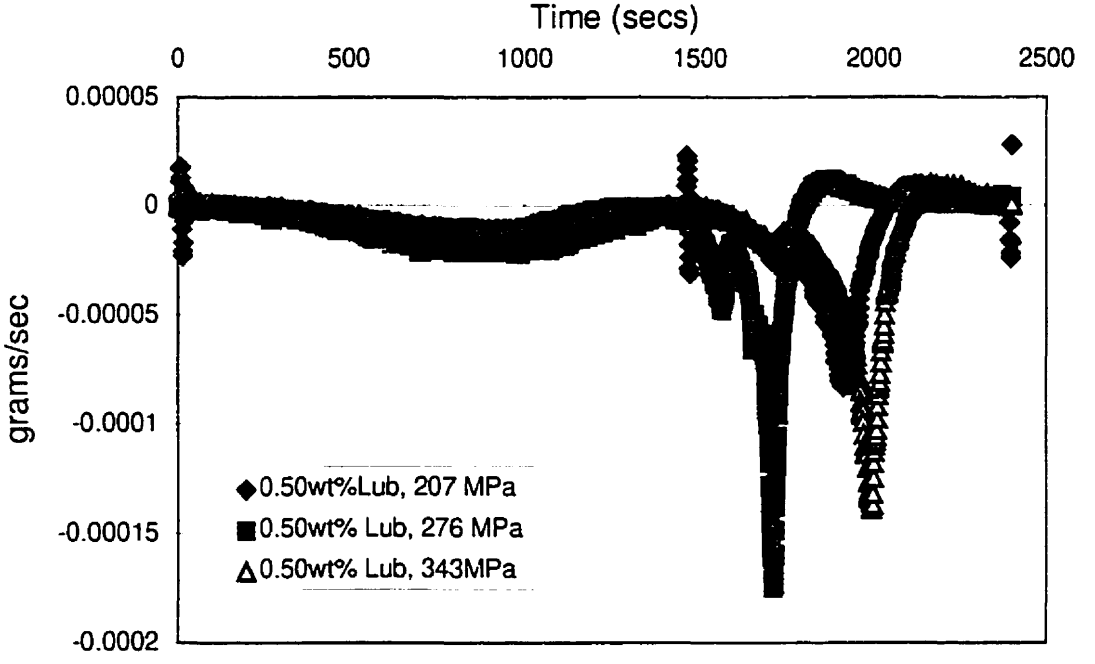

Figure 5.17: Thermo-gravimetric analysis first derivative curves for 207, 276 and 343 MPa at a constant addition of 0.5 wt.% lubricant.

5.3.2 SINTERED DENSITY

Figures 5.18 to 5.21, show the effect of temperature on the sintered density as a function of the green density for the powder containing 0.00, 0.25, 0.50 and 1.0 weight percent zinc stearate lubricant. As a means of comparison, the sintered density results are expressed as a fraction of the theoretical density (4.43 g/cm^3), also known as the relative density. At 1100°C all the graphs show a similar increase of approximately 10% in relative sintered density for a 10% increase in green density (i.e. an increase in the compaction pressure from 207 to 343 MPa). This increase in the sintered density with increasing green density is likely a result of an increasingly finer pore size and higher initial density of the green compact with increasing compaction pressure.

Under the sintering conditions investigated both surface and bulk transport mechanisms may be occurring. Although for materials such as zinc and cadmium a vapor pressure difference can lead to material transport into the neck by evaporation-condensation, for Ti-6%Al-4%V this surface mechanism is unlikely to occur at these temperatures. Of the existing surface transport mechanisms, surface diffusion, which can occur throughout consolidation, can dominate in the early stages of sintering, especially for fine powders, for which the specific surface is high. Hence, the concentration of vacancies and the presence of curvature gradients can lead to the movement of atoms from convex particle surfaces to the neck region by this mechanism even at relatively low sintering temperatures. This leads to neck growth, smoothing of the surface roughness and pore rounding. However pore shrinkage is not possible by surface diffusion transport and the increase in sintered density with holding time would be small at low temperatures. With increasing temperature a greater heat source is present to activate and maintain the atomic movement for sintering to progress. The effect of increasing the temperature by 15% to 1300°C thus resulted, on average, in a 17% increase in relative sintered density. With increasing sintering temperature, the predominant sintering mechanism for metallic materials is usually vacancy diffusion by movement along grain boundaries or lattice dislocations from the neck region to convex particle surfaces, grain boundaries (where

there is a lower concentration of vacancies) or the external surface of component (thereby enabling shrinkage). Thus, the effect of increasing the temperature is more pronounced on the relative sintered density than if the green density is increased.

The curves in Figures 5.18 to 5.21 indicate a linear relation between the sintered density and green density for all the temperatures investigated. As such, the slope of these curves were determined (Table 5.4) to examine the influence of green density at a specific temperature and lubricant addition. At a low temperature (1100°C), the sintered density is mostly dependent on the initial green density as indicated by largest slope value of unity obtained under these conditions. A decrease in slope value occurred with increasing temperature, which suggests that there is a lower dependence of the final sintered density on the initial green density. Moreover, there appears to be a trend towards decreasing slope values with increasing lubricant content at intermediate temperatures (1300°C and 1400°C) which suggest even lower dependencies on the initial density of the green compact.

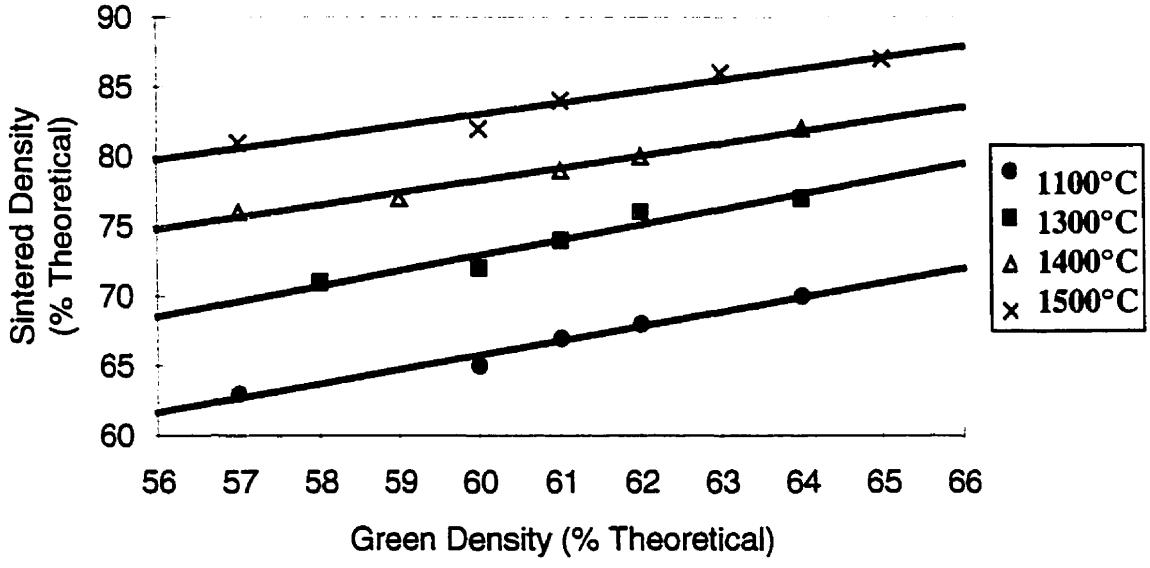

Figure 5.18: Relative sintered density as a function of green density for 1100°C, 1300°C, 1400°C and 1500°C with no lubricant.

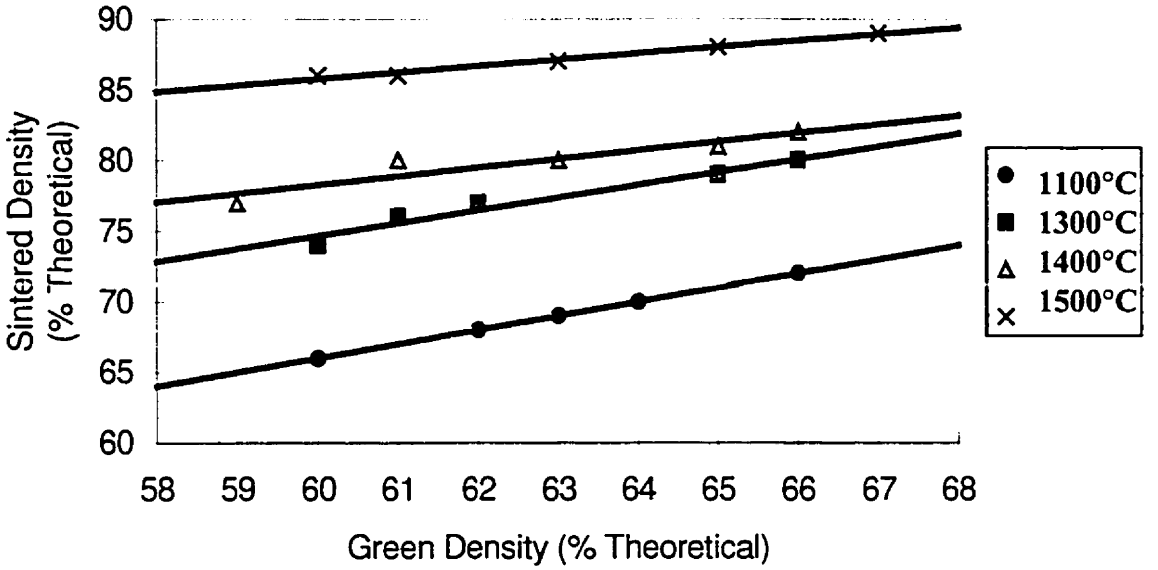

Figure 5.19: Relative sintered density as a function of green density for 1100°C, 1300°C, 1400°C and 1500°C with 0.25 weight percent lubricant.

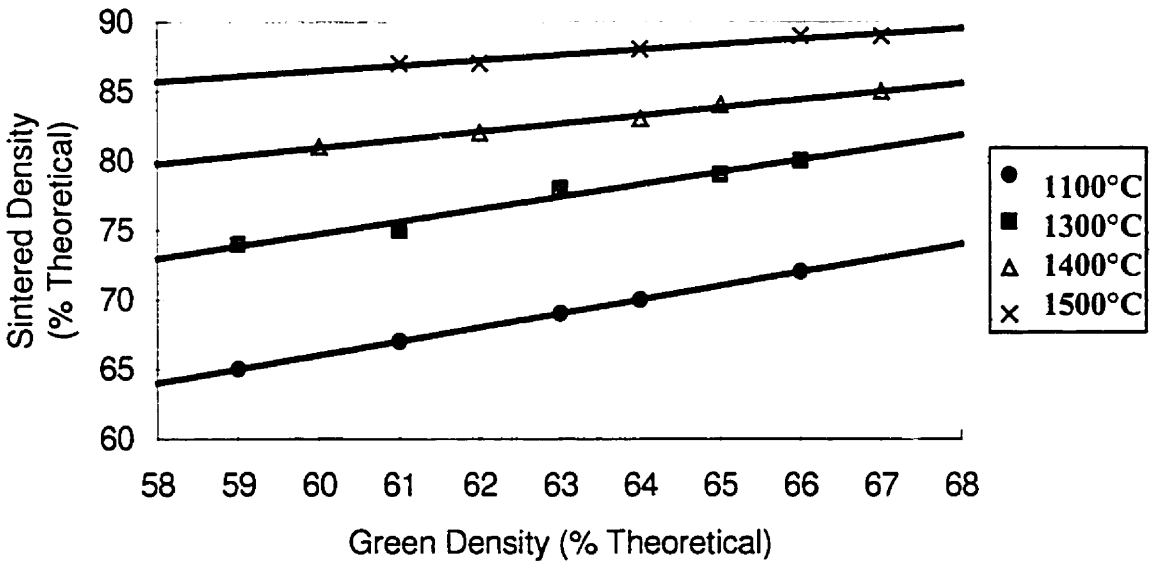

Figure 5.20: Relative sintered density as a function of green density for 1100°C, 1300°C, 1400°C and 1500°C with 0.50 weight percent lubricant.

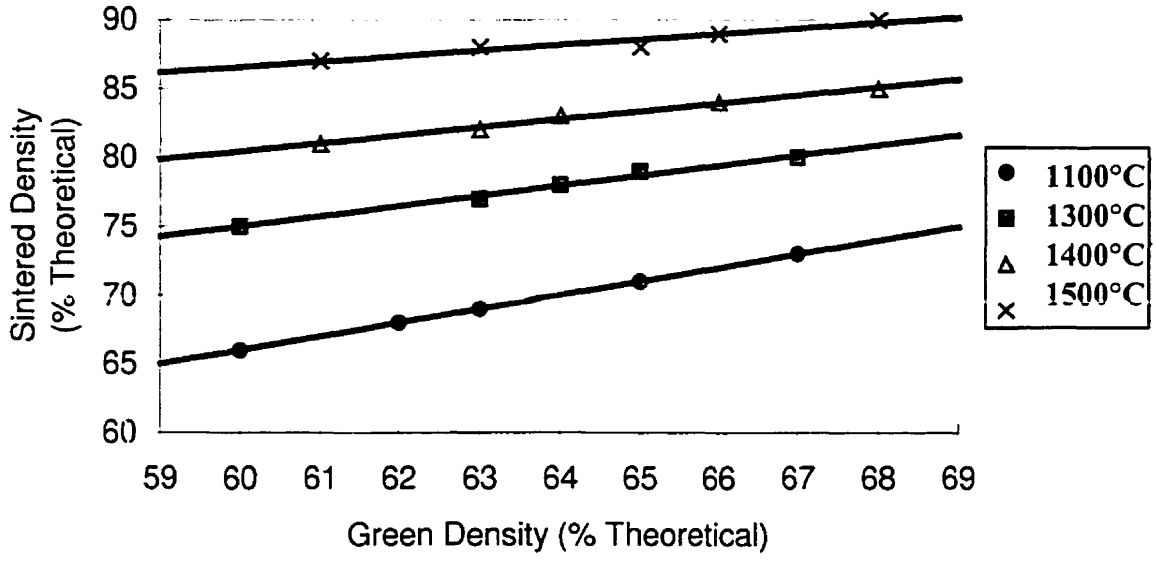

Figure 5.21: Relative sintered density as a function of green density for 1100°C, 1300°C, 1400°C and 1500°C with 1.0 weight percent lubricant.

Table 5.4: Relative sintered density versus green density slopes for the curves in Figures 5.16 to 5.19

Temperature (°C)	0.0 wt% Lubricant	0.25 wt% Lubricant	0.50 wt% Lubricant	1.0 wt% Lubricant
1100	1.0	1.0	1.0	1.0
1300	1.0	1.0	0.85	0.71
1400	0.85	0.71	0.67	0.57
1500	0.75	0.43	0.33	0.30

For a consolidation temperature of 1100°C, the relative sintered density values are plotted as a function of the green density for the various lubricant contents as shown in Figure 5.22. It is observed that the effect of adding zinc stearate lubricant to the titanium alloy powder at these low sintering temperatures has a negligible influence on the sintered density.

As the temperature is increased, the slopes of the lubricated samples decreased significantly as compared to the non-lubricated titanium alloy powder. This effect was similar for the sintering temperatures of 1300°C, 1400°C and 1500°C examined, but most prominent at 1500°C, as shown in Figure 5.23. This appears to suggest that diffusion mechanisms may be enhanced by the addition of zinc stearate lubricant though the improvement in the pressing efficiency and subsequently greater particle-particle contact. Hence, significantly less sintering would be required for a lubricated sample as compared to a non-lubricated titanium alloy powder to achieve a specific relative sintered density. Extrapolation of the non-lubricated curve shows that above a specific green density there exists a limit to the effectiveness of zinc stearate addition. Figure 5.23 shows that the increase in relative densities for the 0.50 and 1.0 weight percent are similar. Thus, for sintering of the titanium alloy powder, the maximum amount of zinc stearate lubricant appears to be 0.50 weight percent and above this content further improvement in density is minimal.

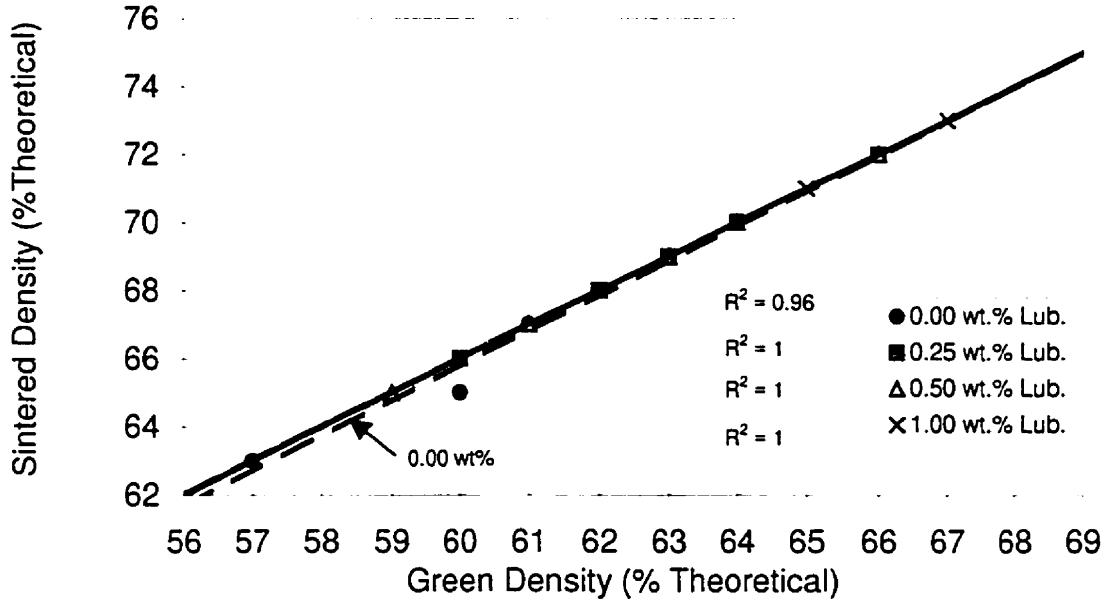

Figure 5.22: Relative sintered density as a function of green density for 0.00, 0.25, 0.50 and 1.00 weight percent lubricant at 1100°C.

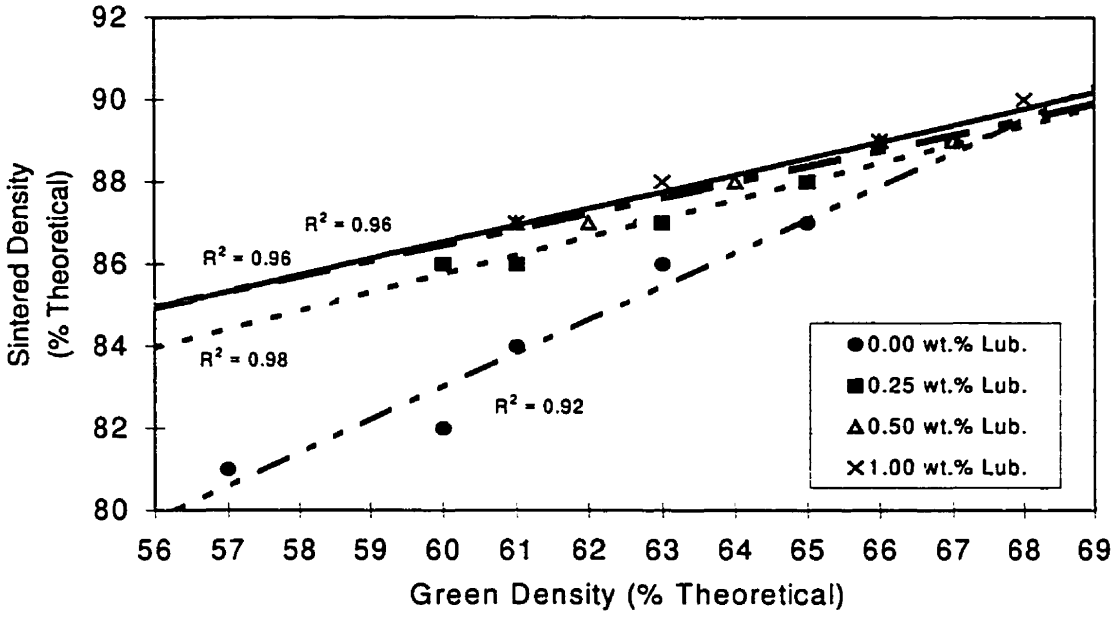

Figure 5.23: Relative sintered density as a function of green density for 0.00, 0.25, 0.50 and 1.00 weight percent lubricant at 1500°C.

Shrinkage measurements can also be used to quantify consolidation in powder metallurgy materials. Shrinkage in powder compacts is the result of the bulk transport processes, as surface transport mechanisms do not result in decreases in the pore volume. Figure 5.24 plots the amount of shrinkage for the titanium alloy powder consolidated at various temperatures for different zinc stearate lubricant additions. At low sintering temperatures (1100°C), approximately 8% shrinkage was measured for the titanium alloy powder. The amount of shrinkage was observed to increase almost linearly with increasing temperature. Specifically, a 20 % increase was observed by increasing the temperature from 1100°C to 1500°C for all the samples, regardless of lubricant content. As bulk transport mechanisms dominate sintering processes at higher temperatures, it is expected that the titanium alloy powder would exhibit less shrinkage at the lower temperatures due to slower diffusion rates. With increasing temperature, the activation of diffusion mechanisms increases material transport by vacancy movement through the lattice and along grain boundary networks that reach the exterior surface and reduce the pore volume[1].

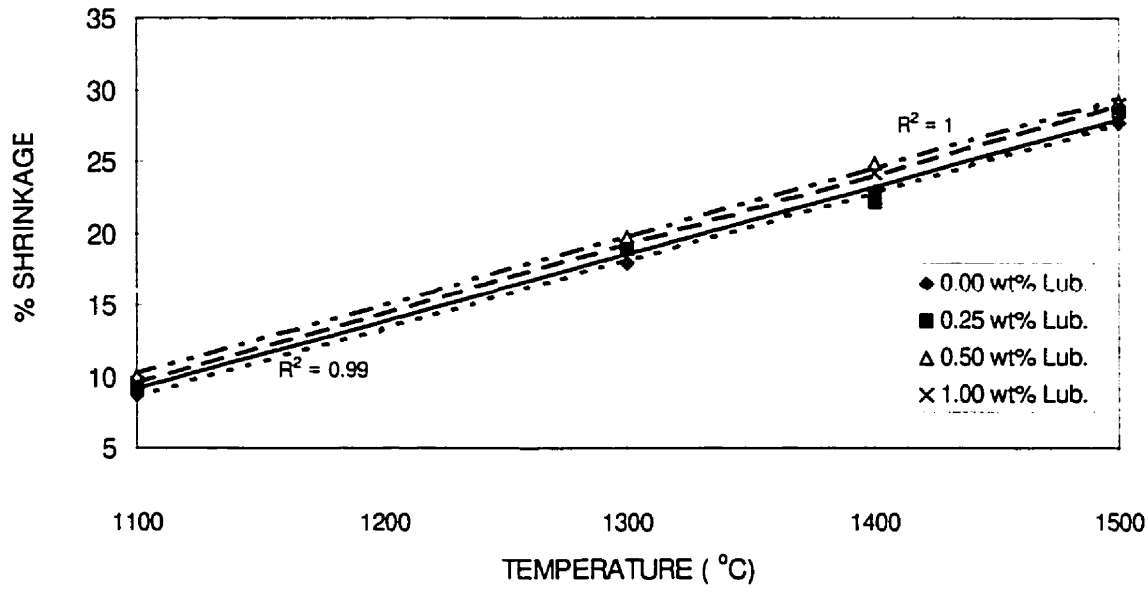

Figure 5.24: Shrinkage as a function of sintering temperature.

Figure 5.24 also shows that the linear relationship between temperature and shrinkage is regardless of lubricant content. This relationship is similar to that observed for the dependence of relative sintering density on temperature and verifies the inter-relationship of shrinkage and relative sintered density. Besides temperature, other parameters that affect shrinkage are holding time and particle size. Although these were kept constant in these experiments, the amount of shrinkage would increase with hold time and finer particle sizes, however the exact nature of the relationship of these with shrinkage would probably depend on the sintering temperature. By manipulating the various parameters the dimensions of the sintered component can be tailored and controlled to produce near net shaped parts.

Although the effect of zinc stearate lubricant addition on shrinkage is small relative to the overall effect of temperature, at the sintering temperatures above 1100°C a small variation is observed in the shrinkage when the temperature is constant and the compaction pressure (green density) is increased. Figure 5.25, shows an increased shrinkage of approximately 2% for lubricated samples as compared to non-lubricated

titanium alloy powder compacted at low pressures. As the compaction pressure is increased, the shrinkage due to lubricant addition is diminished. Similar trends for shrinkage as function of compaction pressure were observed at 1400°C and 1500°C, Figure 5.26 shows the effect for 1500°C. This suggests that the increased shrinkage is due to the higher degree of densification (better sintering kinetics) of the lubricated samples at lower green densities than the non-lubricated samples. The reduced shrinkage corresponds to the diminishing difference in the sintered densities, particularly at the highest temperature, between the lubricated and non-lubricated titanium samples. Thus, when using a lubricant at lower compaction pressures, a slight trade-off exists between shrinkage and compaction pressure (green density), although the overall sintered density is still higher than the non-lubricated samples.

Figure 5.26 also shows higher shrinkage at 0.50 weight percent lubricant addition. Since the sintered density plots do not show a similar trend and the standard deviation of the slopes was lower, no explanation can be suggested for this behavior at this point.

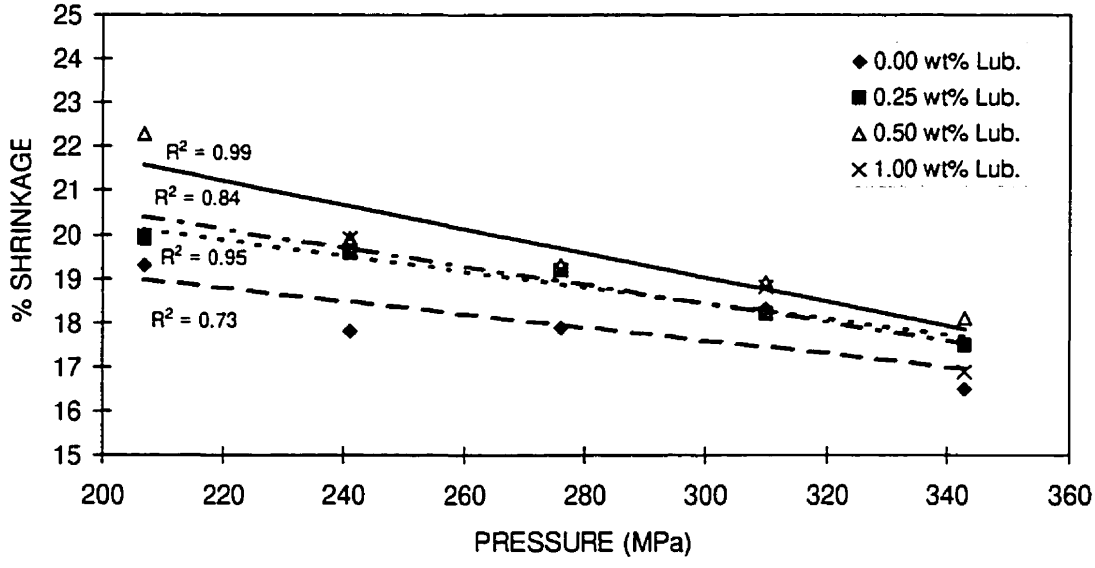

Figure 5.25: Shrinkage as a function of compaction pressure at 1300°C.

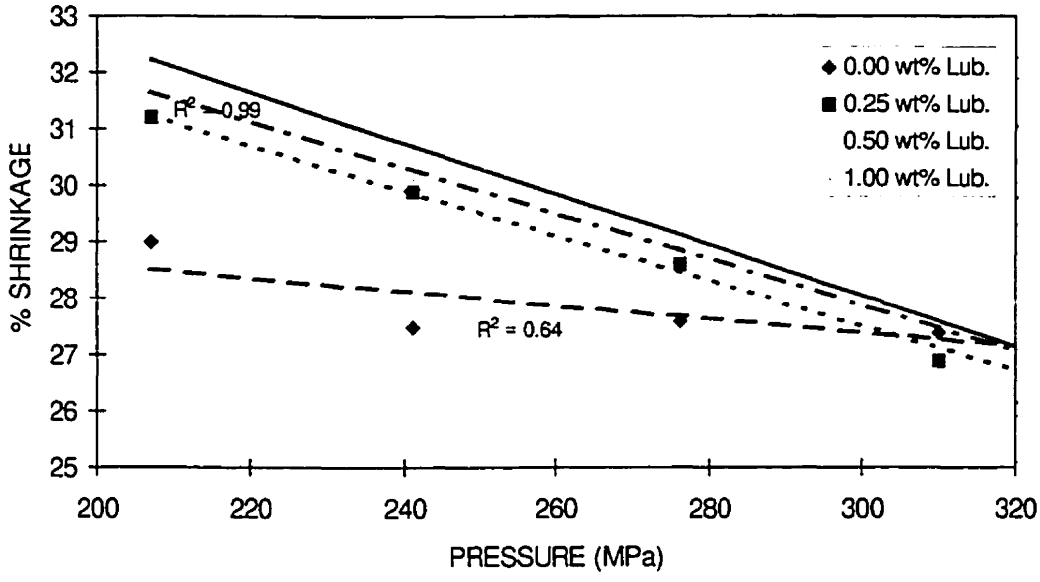

Figure 5.26: Shrinkage as a function of compaction pressure at 1500°C.

5.4 MICROSTRUCTURE

The microstructure of each sample depended mostly on its initial green density and the sintering temperature. The microstructures observed ranged from being highly porous in the sample consolidated the least (Figure 5.27) to slightly porous in the most dense sample (Figure 5.28). In these optical micrographs, the dark regions are the porosity and the bright regions are the Ti-6%Al-4%V alloy. The microstructures revealed in Figures 5.27 and 5.28 also show uneven pore size and distribution which is a consequence of uniaxial pressing. This is an indication that the sintered compact ranged in density from the top surface to the bottom. Hence, image analysis can be used for comparison of trends in the bulk density, but quantitative pore size analysis gave large errors due to this range of pore size and size distribution generated from the differences in axial pressure gradients.

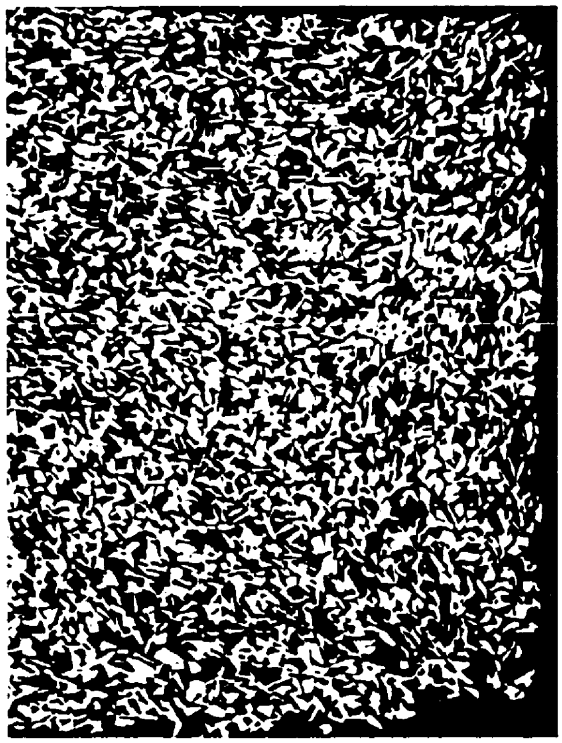

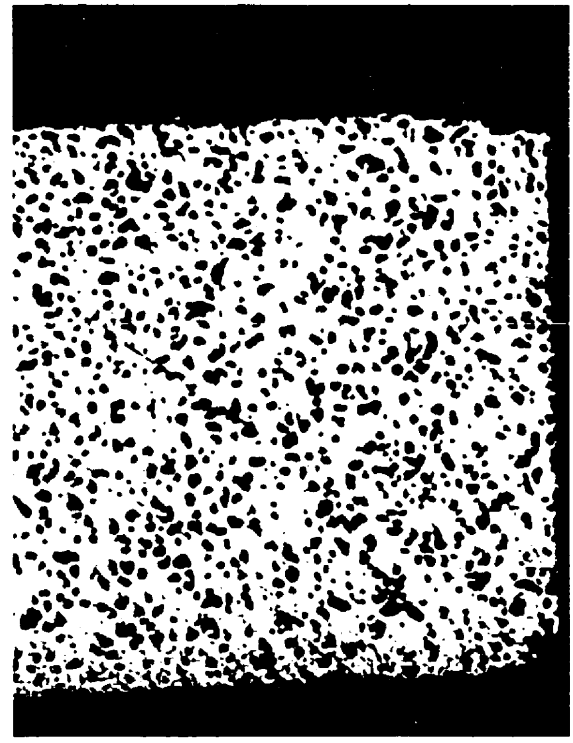

300 μm

Figure 5.27: Non-lubricated sample (207 MPa at 1100°C) with 63.4% relative density.

Figure 5.28: 1.00 wt.% lubricated sample (343 MPa at 1500°C) with 87.1% relative density.

To demonstrate the density trends observed by image analysis, two extremes in temperature were chosen, specifically 1100°C and 1500°C. The density results obtained by image analysis for all additions of zinc stearate lubricant at a particular sintering temperature were determined to be similar (Appendix D), therefore only the 0.00 wt.% and 1.00 wt.% lubricant results are given in Table 5.5. The density trends obtained are in good agreement with those determined by the Archimedes method, however the bulk density obtained by image analysis is on average 4 to 14% higher.

This difference in density is due to the reliance of the Archimedes method in obtaining the measured volume for determining the density. If the surface of the sample is more porous, the measured volume over estimates the amount of porosity, as was the case in the present work. This in turn results in a lower bulk density than may be

expected. The surface effect was noted for all the samples and a typical porous surface layer, regardless of lubricant addition and temperature, of approximately 100 to 250 μm was observed as shown in Figures 5.29 and 5.30.

Table 5.5: COMPARISON OF TRENDS BY IMAGE ANALYSIS AND ARCHIMEDES METHOD

Condition Lub. wt% Addition at Temperature °C	Relative Density % (Archimedes)	Relative Density % (Image analysis)	Difference (%)	Porosity (%)
0.00wt%@ 1100°C				
207MPa	63.4	72.7	9.3	27.3
241MPa	65.0	76.8	11.8	23.2
276MPa	66.1	77.6	11.5	22.4
310MPa	67.7	82.3	14.6	17.7
343MPa	70.4	83.6	13.2	16.4
1.00wt%@1100°C				
207MPa	66.1	77.1	11.0	22.9
241MPa	67.5	81.7	14.2	18.3
276MPa	69.3	84.1	14.8	15.9
310MPa	71.3	86.1	14.8	13.9
343MPa	72.7	86.4	13.7	13.6
0.00wt%@1500°C				
207MPa	81.3	89.0	7.7	11.0
241MPa	82.4	90.5	8.1	9.5
276MPa	84.4	90.2	5.8	9.8
310MPa	85.8	90.7	4.9	9.3
343MPa	87.1	91.9	4.8	8.1
1.00wt%@1500°C				
207MPa	86.2	92.5	6.3	7.5
241MPa	87.6	92.6	5.0	7.4
276MPa	88.3	92.6	4.3	7.4
310MPa	88.7	92.6	3.9	7.4
343MPa	89.6	93.6	4.0	6.4

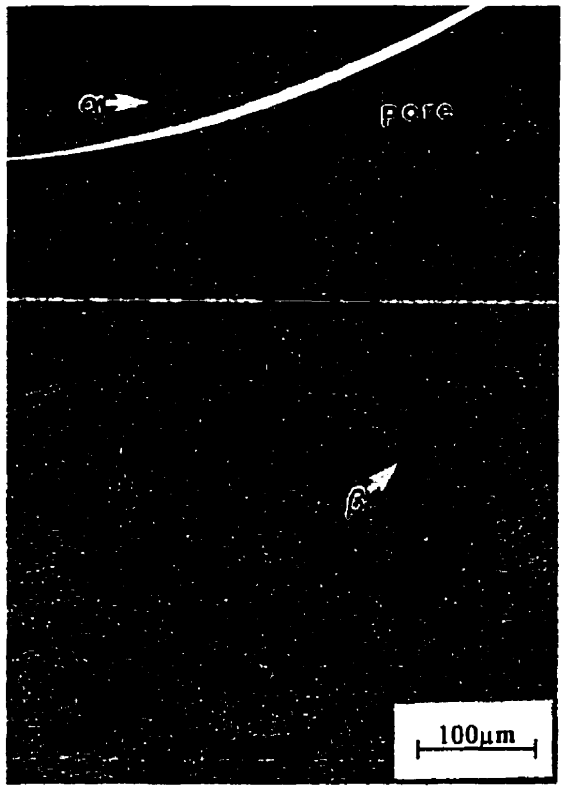

Figure 5.29: Micrograph of non lubricated Ti-6%Al-4%V (343 MPa, 1100°C)

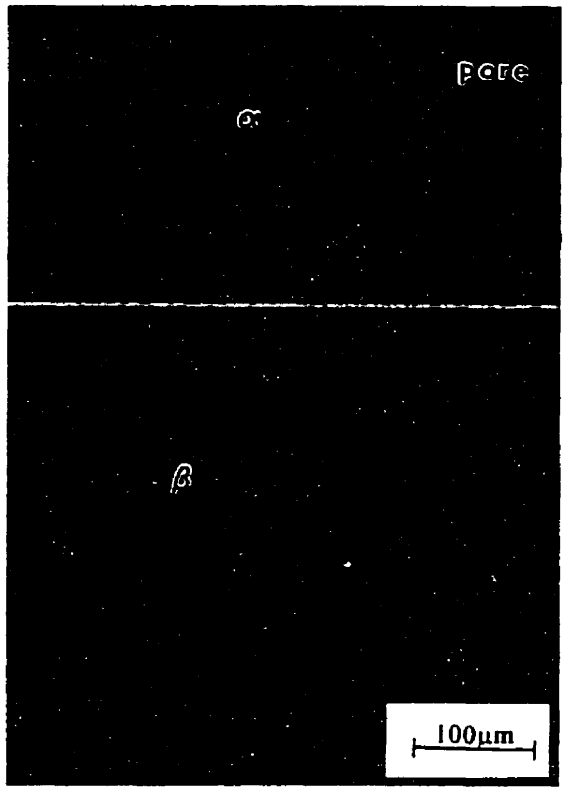

Figure 5.30: Micrograph of lubricated Ti-6%Al-4%V (1.00 wt%, 343 MPa, 1500°C)

The porous layer near the surface of the samples is the result of poor sintering due to surface oxidation. The presence of some oxygen with the furnace can directly or indirectly lead to the formation of this porous layer. The latter would be due to reactions with residual gases within the furnace. The residual gases are most likely from the reaction of oxygen with carbon introduced from the graphite elements of the furnace. The resulting gaseous mixture of CO/CO_2 gas interferes with the sintering process and would contribute to the formation of a porous layer. This was verified by energy dispersive x-ray microanalysis of the surface layer and bulk matrix of the Ti-6%Al-4%V samples both with and without zinc stearate lubricant addition. The results revealed the presence of dissolved carbon in the region of the porous layer as shown in Figure 5.31.

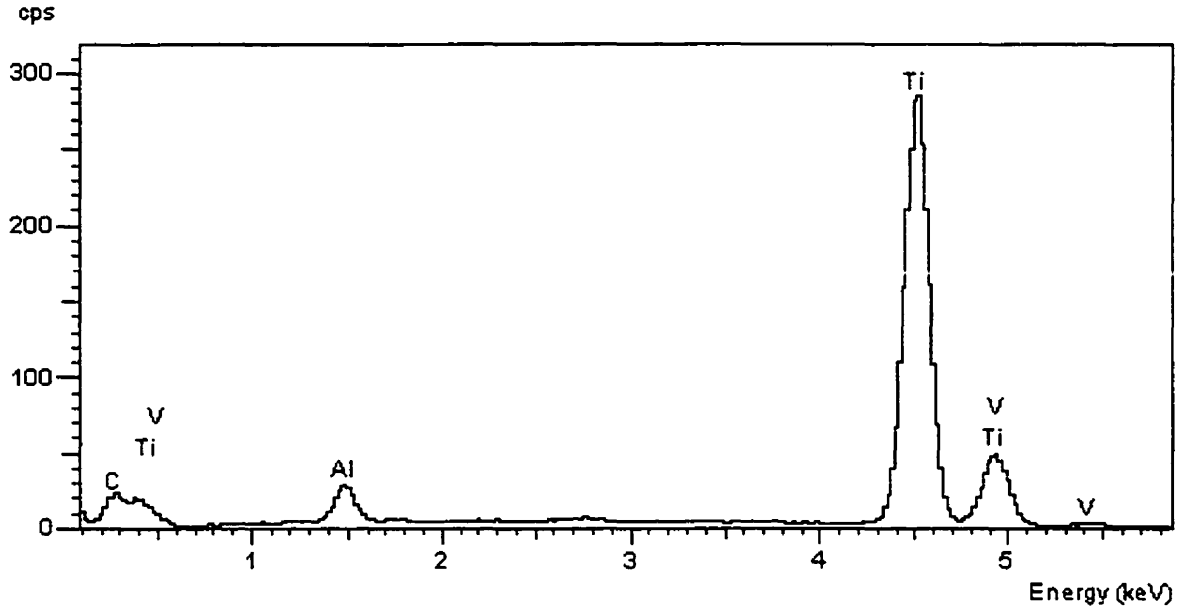

Figure 5.31: Energy dispersive x-ray analysis in the region of the porous surface layer, showing the presence of carbon.

Another difference observed between the porous surface region and the interior of the Ti-6%Al-4%V sample is in the morphology of the lamellar microstructure. The microstructure in both regions is typical of lamellar Ti-6%Al-4%V, which consists of plate-like alpha phase separated by inter-plate beta phase[31]. (In optical micrographs, the alpha plates are lighter in phase contrast and the inter-plate beta phase is darker.) However, the alpha platelets were generally slightly coarser within the porous surface as compared to that of the inner bulk microstructure. This phenomenon may be related to the presence of dissolved carbon and dissolved oxygen within the porous layer, both of which would increase the beta transition temperature, particularly the oxygen as shown in Figure 5.32. Thus, during cooling, even though the dissolved carbon can act as a grain refiner, the coarser grain structure may be the result of the beta phase within the surface layer transforming to the alpha phase at a higher temperature. Which in turn results in a longer grain growth period than the bulk microstructure.

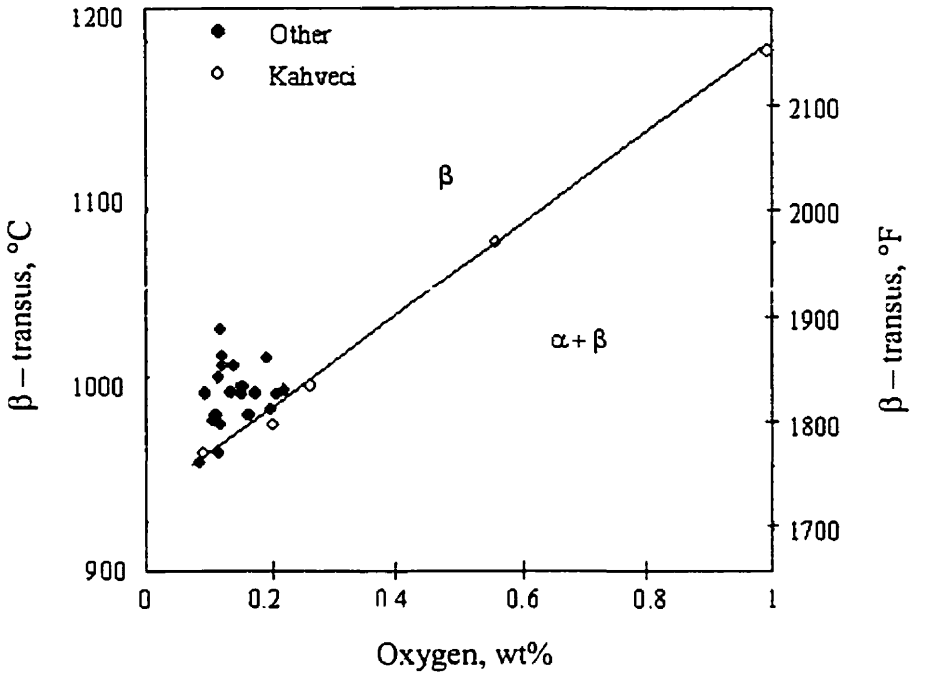

Figure 5.32: Beta transus versus oxygen content[5]

For the same consolidation temperature, the morphology of the pores in the Ti-6%Al-4%V alloy did not change appreciably with increasing compaction pressure (green density) and zinc stearate lubricant addition rendering comparison between the samples difficult as illustrated in Figures 5.33 and 5.34. Even comparing the two extremes in compaction pressure and zinc stearate lubricant addition, the differences in size and shape of the pores are small. (It should be noted that the relative densities are given in parentheses.) For varying sintering temperatures, comparison of the samples for monitoring the change in morphology is possible. With increasing temperature, the pore structure evolves from being interconnected and irregular in shape to gradually becoming isolated and spherical in shape.

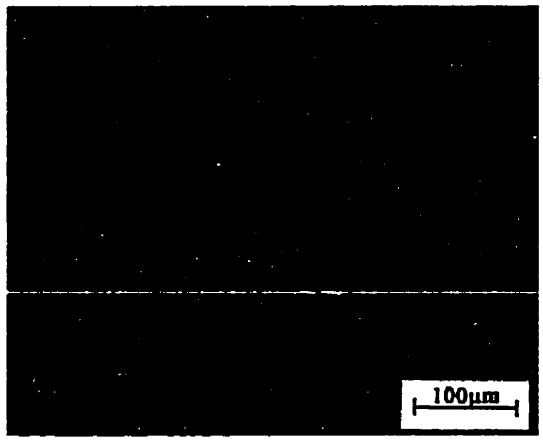

Figure 5.33a: Micrograph showing non-lubricated sample (63%), 207 MPa, 1100°C.

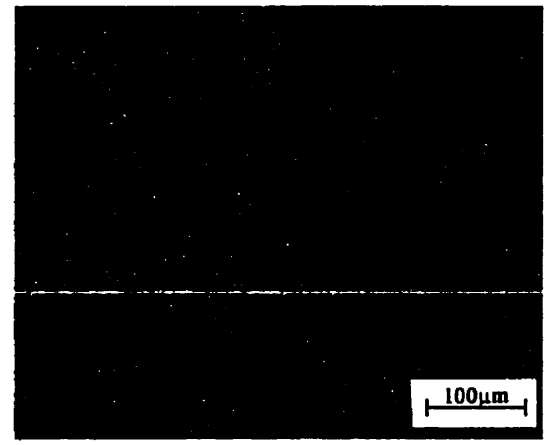

Figure 5.33b: Micrograph for 1.00 wt.% lubricated sample (66%), 207 MPa, 1100°C.

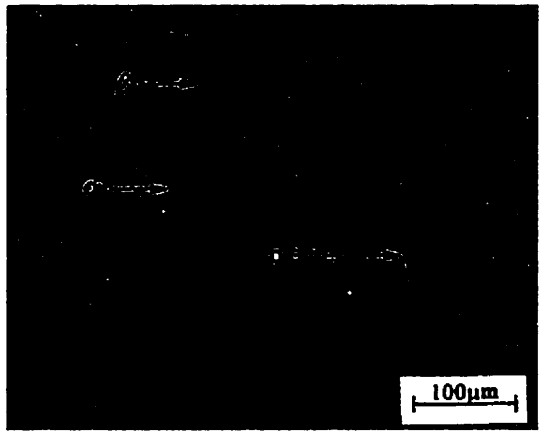

Figure 5.33c: Micrograph showing non-lubricated sample (70%), 343 MPa, 1100°C.

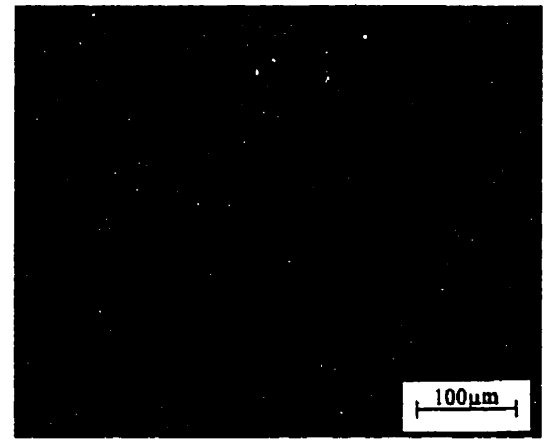

Figure 5.33d: Micrograph for 1.00 wt.% lubricated sample (73%), 343 MPa, 1100°C.

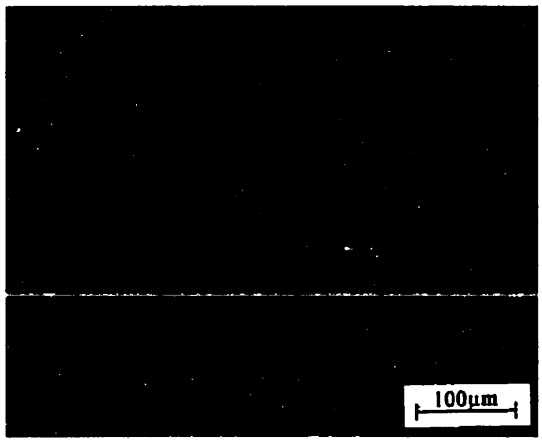

Figure 5.34a: Micrograph showing non-lubricated sample (81%), 207 MPa, 1500°C.

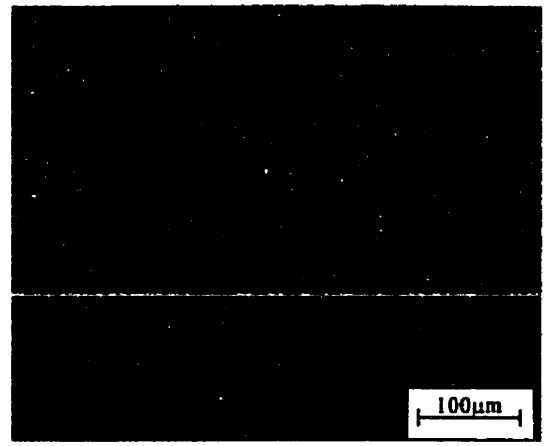

Figure 5.34b: Micrograph for 1.00 wt.% lubricated sample (86%), 207 MPa, 1500°C.

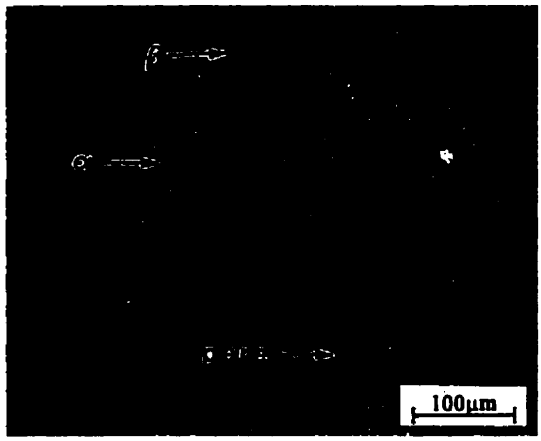

Figure 5.34c: Micrograph showing non-lubricated sample (87%), 343 MPa, 1500°C.

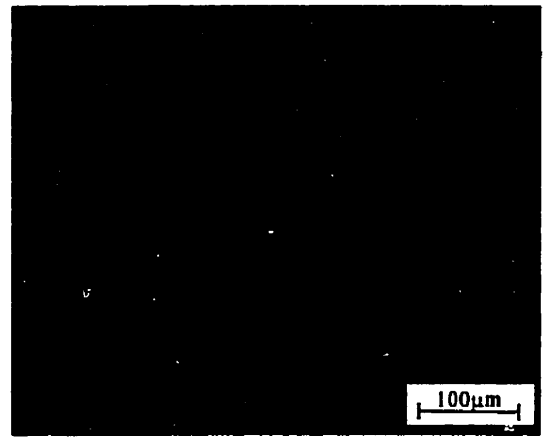

Figure 5.34d: Micrograph for 1.00 wt.% lubricated sample (89%), 343 MPa, 1500°C.

The effect of zinc stearate addition on the microstructure of Ti-6%Al-4%V alloy compacted at the highest pressure (343 MPa) is illustrated in Figures 5.35 to 5.38 for the various sintering temperatures examined (i.e. 1100°C, 1300°C, 1400°C and 1500°C, respectively). It should be mentioned that the overall effect of increasing the compaction pressures on the microstructure is smaller than that of increasing the temperature. Also, the highest compaction pressure minimizes the density gradients within the samples.

At 1100°C (Figure 5.35), substantial porosity is present in all the samples as the activation energy available at this temperature is small and negligible increases in density are obtained by bulk transport mechanisms. This microstructural observation is supported by the small shrinkage values obtained for the Ti-6%Al-4%V samples at this temperature. The microstructural appearance of the porosity suggests that the samples sintered at 1100°C are still in the neck growth stage where the pores are open and interconnected and there is little change in the irregular pore morphology. However, due to better particle-particle contact, the samples with zinc stearate lubricant addition (5.35b, c and d) show slightly less overall porosity then the non-lubricated Ti-6%Al-4%V alloy. This is supported by the similar densification results of the samples with zinc stearate additions. The lamellar microstructure at 1100°C consists of relatively fine alpha platelets separated by the beta phase.

At 1300°C (Figure 5.36), The Ti-6%Al-4%V alloy without lubricant addition contains substantial porosity after consolidation as shown in Figure 5.36a. For the Ti-6%Al-4%V samples containing zinc stearate, Figures 5.36b, c and d, the pores appear slightly coarser for 0.25 weight percent lubricant addition as compared to those with higher lubricant contents. However, the relative densities at 1300°C for all Ti-6%Al-4%V were determined to be similar with the addition of zinc stearate. At this temperature, a significant increase in diffusion occurs by bulk transport mechanisms and the microstructure shows a reduction in the porosity, which is supported by the relative densities and shrinkage values. Figure 5.39 is a high-resolution photograph of a particle surface that shows the formation of growth steps due to diffusion by bulk transport

mechanisms. Moreover, the pore structure revealed in Figure 5.36 show less interconnected pores and somewhat smoother pore morphology as compared to sintering at 1100°C. This indicates a progression into the intermediate stage of sintering at this temperature. In this stage, pore closure is the dominant effect. The change in the lamellar microstructure of the Ti-6%Al-4%V alloy with increasing temperature appears to be related to the gradual coarsening of the alpha platelets. At this temperature this process has begun and occasionally coarser alpha platelets are observed dispersed amongst fine alpha plates.

Increasing the sintering temperature to 1400°C (Figure 5.37), results in the pore structure of the Ti-6%Al-4%V alloy without zinc stearate lubricant addition becoming gradually spherical in shape and isolated (Figure 5.37a). However, the microstructure still remains porous in the absence of the lubrication as was reflected in the relative density values. For the Ti-6%Al-4%V alloy lubricated with zinc stearate, the pore structure is mostly closed and pore rounding is evident indicating the sintering has progressed to the final stage. The lamellar microstructure of the Ti-6%Al-4%V alloy reveals a mix of coarser and fine alpha platelets.

At 1500°C (Figure 5.38), the Ti-6%Al-4%V alloy without zinc stearate addition, Figure 5.38a, was slightly more porous than the samples with lubricant. At this consolidation temperature, the pore structure for all the Ti-6%Al-4%V samples (with and without lubricant) was mostly closed with rounded pore morphology. Substantial shrinkage has occurred and the samples are in the final stage of sintering as evidenced by the presence of isolated pores, especially in the case of the Ti-6%Al-4%V alloy containing zinc stearate lubricant. Figures 5.38b, c and d show pore break away from the grain boundaries. This suggests that prolonged holding at this temperature would result in small improvements in the density because isolated pores must diffuse vacancies to distant grain boundaries by volume diffusion, which is a relatively slow process. This suggests that although some gains in the density can definitely be achieved in the non-

lubricated Ti-6%Al-4%V alloy, prolonged holding of the lubricated samples may not be as useful.

The effect of lubricant addition is particularly evident at 1500°C with an increase in the zinc stearate content leading to better sintering kinetics, finer pore size and lower porosity levels. However, above 0.50 weight percent lubricant addition, there appears to a saturation of this effect and doubling of the zinc stearate content causes negligible changes to the pore size and morphology, as illustrated in Figure 5.38d. Hence lubricant additions above 0.50 weight percent may not be particularly beneficial.

At 1500°C, the microstructure of the Ti-6%Al-4%V samples with and without zinc stearate additions show coarse alpha platelets separated by the beta phase. Coarsening of the lamellar microstructure may deteriorate the mechanical properties and albeit the potential for high sintered densities at high sintering temperatures, the overall benefits may be reduced. Alternatively, finer grain structures can be achieved by varying the sintering parameters to achieve similar densities. For example, comparing Figures 5.37d and 5.38a, the relative densities are similar for the two temperatures examined (1400°C and 1500°C, respectively). At a constant compaction pressure, the addition of 1 weight percent lubricant at the lower sintering temperature of 1400°C produced an equivalent relative density to sintering at 1500°C without lubricant addition. At an equivalent density, the microstructure of the Ti-6%Al-4%V alloy sintered at 1400°C is finer than that obtained by sintering at 1500°C.

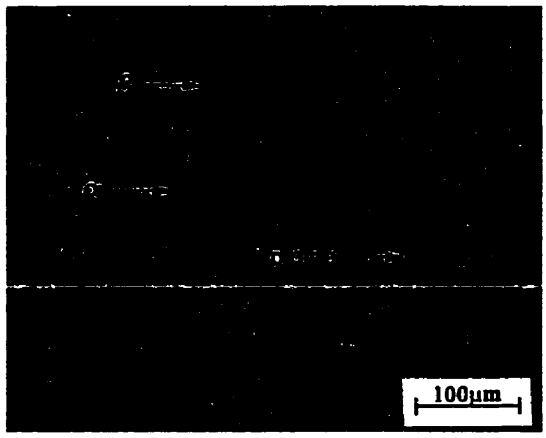

Figure 5.35a: Micrograph showing non-lubricated sample (70%), 343 MPa, 1100°C.

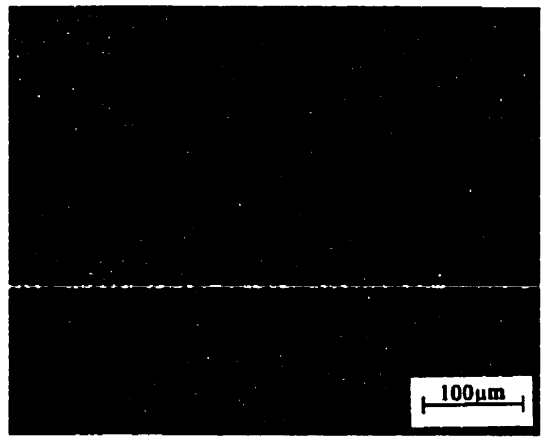

Figure 5.35b: Micrograph for 0.25 wt.% lubricated sample (72%), 343 MPa, 1100°C.

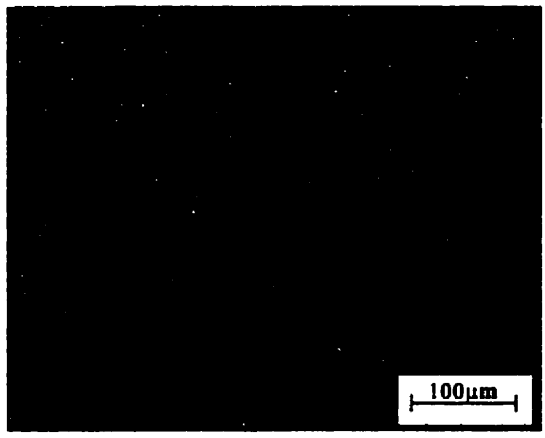

Figure 5.35c: Micrograph for 0.50 wt.% lubricated sample (72%), 343 MPa, 1100°C.

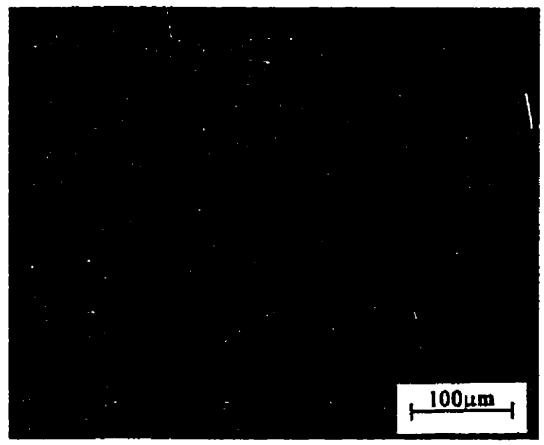

Figure 5.35d: Micrograph for 1.00 wt.% lubricated sample (73%), 343 MPa, 1100°C.

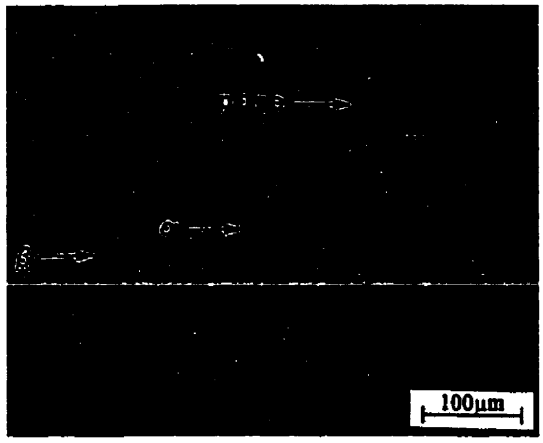

Figure 5.36a: Micrograph showing non-lubricated sample (77%), 343 MPa, 1300°C.

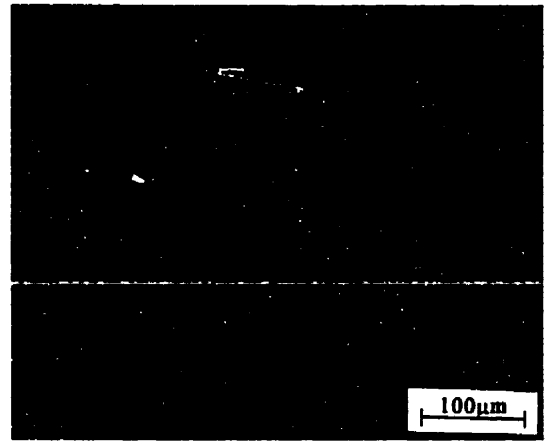

Figure 5.36b: Micrograph for 0.25 wt.% lubricated sample (80%), 343 MPa, 1300°C.

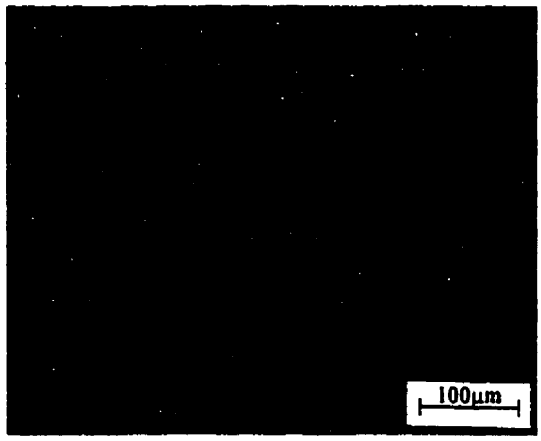

Figure 5.36c: Micrograph for 0.50 wt.% lubricated sample (80%), 343 MPa, 1300°C.

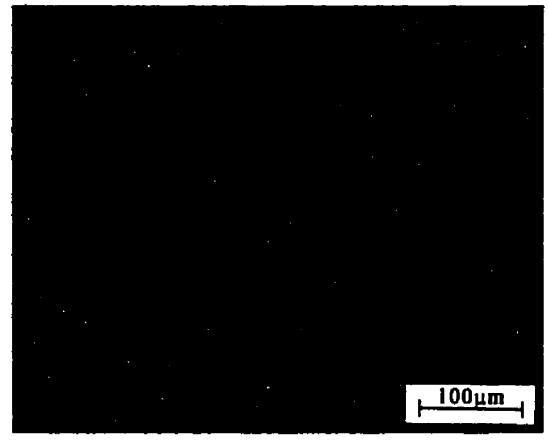

Figure 5.36d: Micrograph for 1.00 wt.% lubricated sample (80%), 343 MPa, 1300°C.

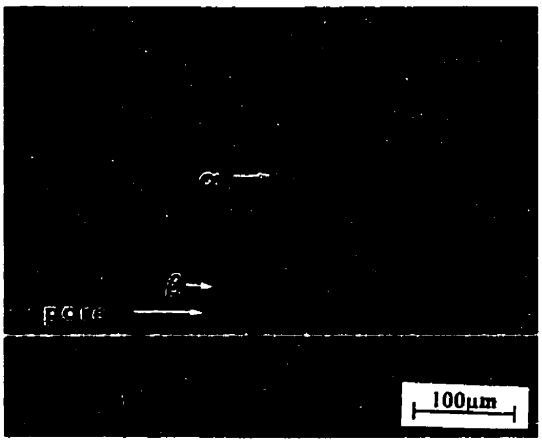

Figure 5.37a: Micrograph showing non-lubricated sample (81%), 343 MPa, 1400°C.

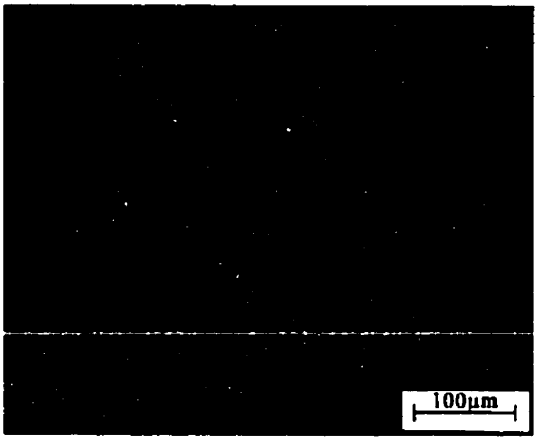

Figure 5.37b: Micrograph for 0.25 wt.% lubricated sample (82%), 343 MPa, 1400°C.

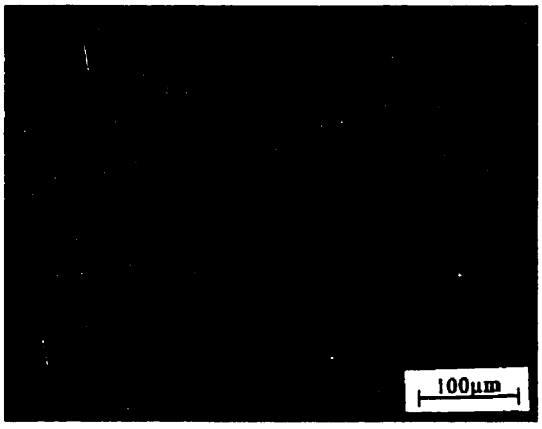

Figure 5.37c: Micrograph for 0.50 wt.% lubricated sample (85%), 343 MPa, 1400°C.

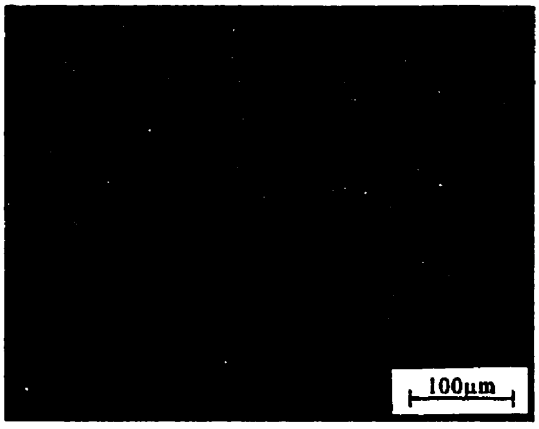

Figure 5.37d: Micrograph for 1.00 wt.% lubricated sample (85%), 343 MPa, 1400°C.

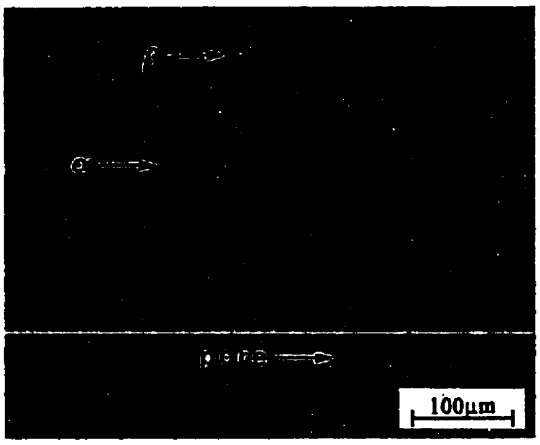

Figure 5.38a: Micrograph showing non-lubricated sample (87%), 343 MPa, 1500°C.

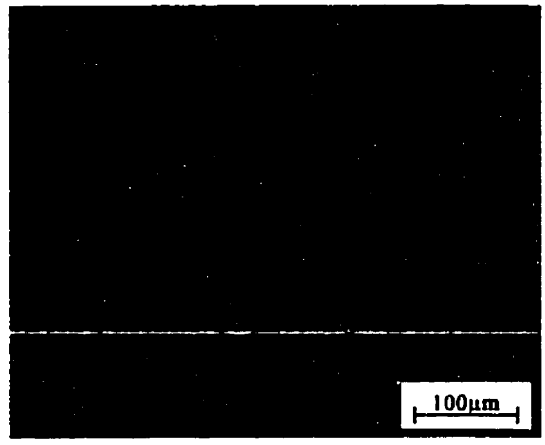

Figure 5.38b: Micrograph for 0.25 wt.% lubricated sample (89%), 343 MPa, 1500°C.

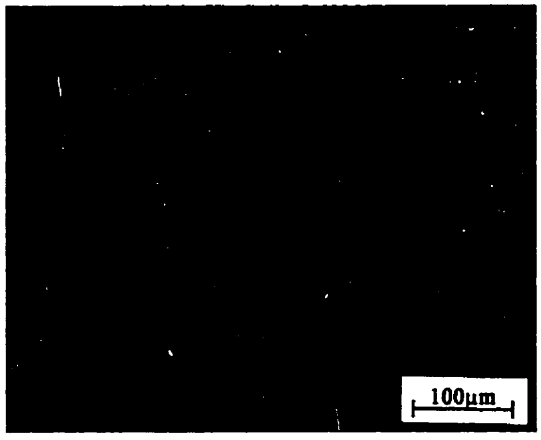

Figure 5.38c: Micrograph for 0.50 wt.% lubricated sample (89%), 343 MPa, 1500°C.

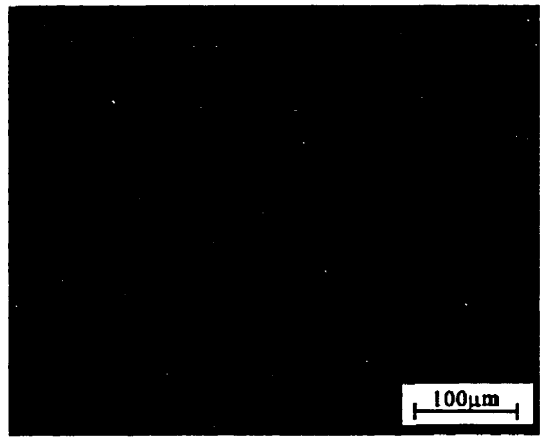

Figure 5.38: Micrograph for 1.00 wt.% lubricated sample (90%), 343 MPa, 1500°C

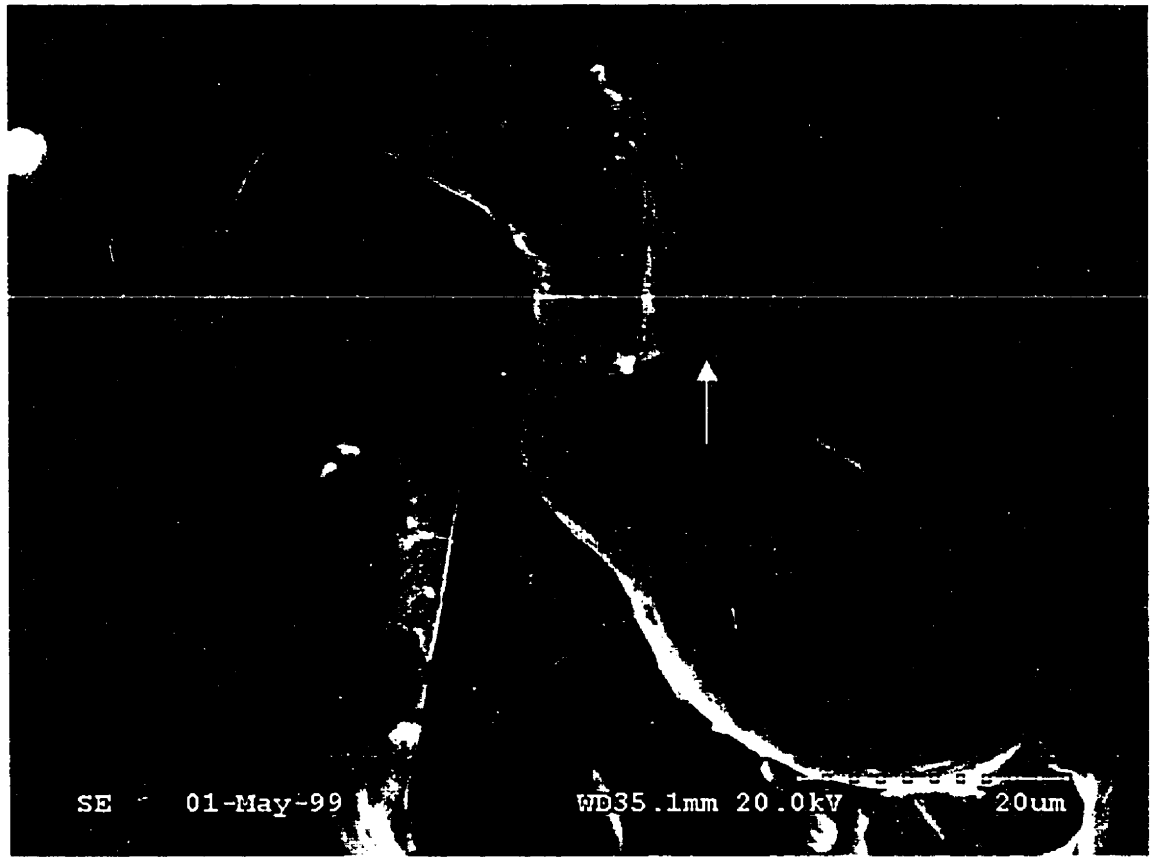

Figure 5.39: Micrograph of 1.00 weight percent lubricant sample compacted at 343 MPa sintered at 1300°C showing growth steps (arrow) on the particle surface related to bulk diffusion.

5.5 MICROHARDNESS

The differences in densification, quantified by the density and shrinkage measurements as well as that observed by microstructural analysis, caused by varying the sintering conditions will result in changes to the mechanical properties of the Ti-6%Al-4%V alloy. Through microhardness measurements sintering conditions that improve the properties can be assessed. However, the shortcoming of this measurement technique is in the assessment of inhomogeneous material, such as in the case of samples with excessive porosity and density gradients. Indentation distortion from underlying porosity

can prevent accurate measurements, while density gradients can result in higher or lower values than the overall bulk density. These problems were evident in the measurement of samples with less than 72% relative density. Consequently almost no microhardness values were obtained for the samples sintered at 1100°C. Even for the samples consolidated under more favorable sintering conditions, the absolute values (Appendix E) are not directly compared, but rather the trend at each temperature are compared.

Figure 5.40 shows the variation in the microhardness with increasing compaction pressure for the samples sintered at 1300°C. The increase in microhardness values with increasing compaction pressure (or green density) agrees well with the trends observed for the microstructure and relative sintered densities. Additionally the beneficial effect of lubricant addition is indicated by the higher microhardness values of these as compared to the non-lubricated Ti-6%Al-4%V alloy. Moreover, the microhardness values measured for 0.50 and 1.00 weight percent lubricants addition are almost identical. This finding is consistent with that observed previously between the green density and sintered density in Figure 5.23.

Figures 5.41 and 5.42 are the microhardness values as a function of the compaction pressure for the samples sintered at 1400°C and 1500°C, respectively. The trends are similar to those observed at 1300°C. Basically the plots of microhardness versus compaction pressure for all the sintering conditions suggests that the densification and properties improve up to 0.50 weight percent lubricant addition. Further addition of zinc stearate lubricant does not lead to substantial changes for the Ti-6%Al-4%V alloy and suggests, from the measured additions, that 0.5 weight percent lubrication is optimal. When comparing the effect of increasing the temperature, the hardness values exhibit a larger increase than that resulting from increased compaction pressure. This is consistent with the results obtained from the sintered densities and microstructures, and confirms the high dependence of sintering on temperature.

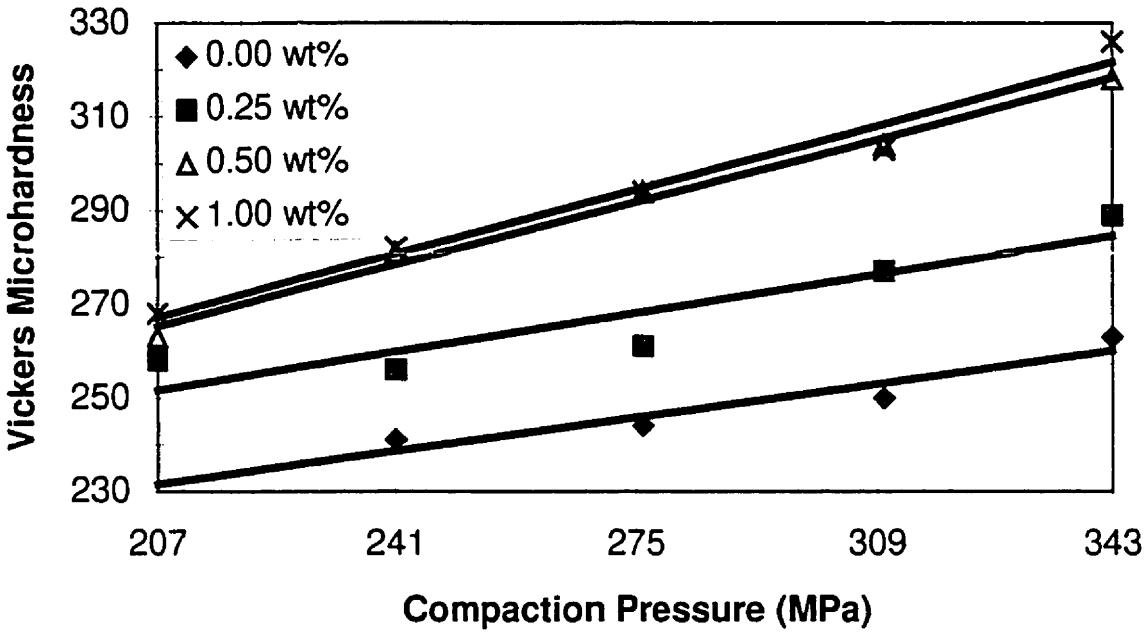

Figure 5.40: Vickers microhardness as a function of compaction pressures at 1300°C.

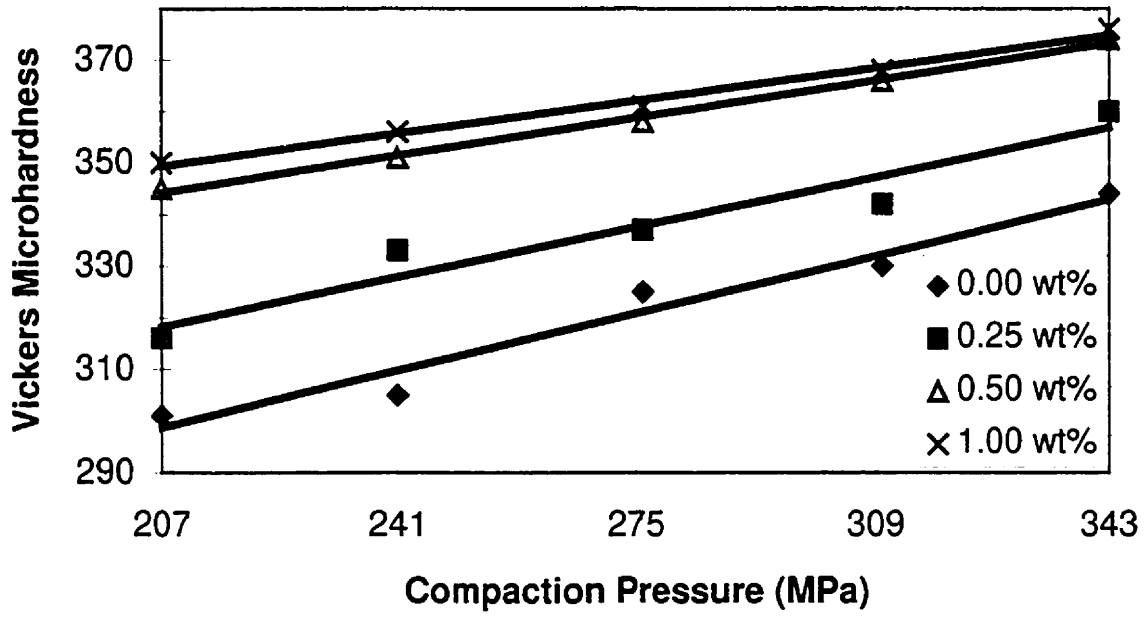

Figure 5.41: Vickers microhardness as a function of compaction pressure at 1400°C.

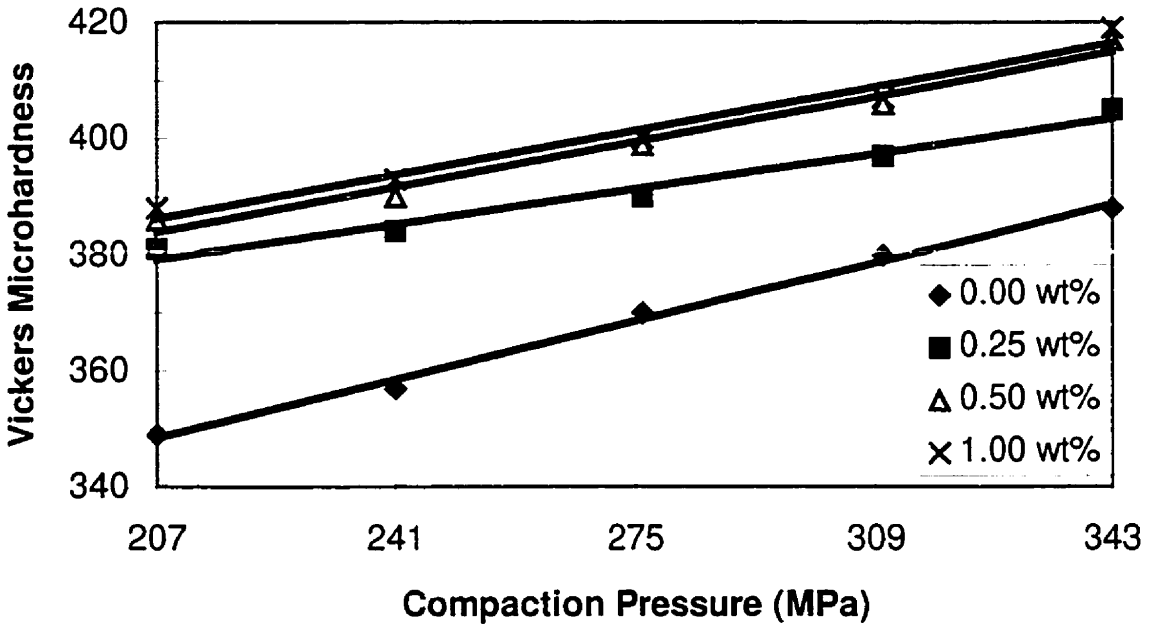

Figure 5.42: Vickers microhardness as a function of compaction pressure at 1500°C.

5.6 NON-DESTRUCTIVE X-RAY ANALYSIS

The results from x-ray analysis of the Ti-6%Al-4%V samples sintered at 1100°C, 1300°C, 1400°C and 1500°C are shown in Figures 5.43 to 5.46, respectively. Figure 5.43 shows bulk densities that correspond to between the 0.05" and 0.08" steps of the wedge block. Since the 1T of the 0.08" penetrameter is visible, defects as small as approximately 0.003" can be seen. The non-lubricated samples in the first two rows tend to exhibit density gradients, which are particularly evident in the sample in the second row and column 280 MPa. The top left side reveals a lighter color (indicating higher density) than the bottom right side, which is slightly darker (indicating lower density).

The 0.25 weight percent lubricant addition samples shown in rows three and four do not show the large density gradients observed in the non-lubricated samples. However, below 307 MPa the centers of the samples show occasional small dark regions,

which are localized areas of low density. This is particularly evident for the sample in the fourth row and column 240 MPa. This suggests that 0.25 weight percent lubricant addition helps reduce the overall density gradient but is insufficient for producing a completely homogeneous structure with uniaxial pressing.

The Ti-6%Al-4%V samples containing 0.50 weight percent zinc stearate addition are shown in rows five and six. Immediately evident at the 207 and 241 MPa compaction pressures are regions of higher density. As observed previously in the sintering section, the shrinkage values for the 0.50 weight percent lubricant addition were slightly higher than the other samples. Since shrinkage depends on the ability to densify, regions of higher density would result in better sintering and an overall higher reduction in size. The regions of higher density, as suggested by the x-ray results, are unlikely a direct result of the compaction or burnout processes, since similar effects should have then been observed for the other lubricant additions. Instead these localized density gradients could be the result of lubricant agglomeration, which may have occurred during mixing by contact of the zinc stearate with excessive moisture.

Ti-6%Al-4%V alloy samples containing 1.00 weight percent zinc stearate lubricant are shown in the last two rows. These samples show the best density distribution and appear generally unremarkable.

For the samples sintered at 1300°C, Figure 5.44, the x-ray image is both lighter and smaller in size as compared to the samples consolidated at 1100°C. This is a good visual correlation supporting the generally large increase in density and shrinkage observed for the samples when the sintering temperature is increased sufficiently for bulk transport mechanisms to be active. The densities correspond closer to the 0.08" step of the wedge block where the 1T penetrameter is visible, indicating a 0.03" minimum defect size sensitivity.

The first two rows for the non-lubricated samples show a similar trend in the bulk density gradient observed at 1100°C. For the 0.25 weight percent lubricant, rows three and four, show overall less localized density gradients. However occasional small defects of up to 0.004" (column 280 MPa, row four and column 350 MPa, row one) are now observed. Because of their small sizes, attempts to locate and qualify the defects were unsuccessful.

The 0.50 weight percent lubricant samples seen in rows five and six again showed similar regions of localized higher density gradients. Cross sections through these regions confirmed the existence of small areas of varying densities (Figure 5.47). Energy dispersive x-ray analysis did not reveal any impurities in the regions of the higher density. The localized pore morphologies observed in Figure 5.48 show larger interconnected pores with typical lower density regions amongst regions of smaller and less interconnected pores. This supports the possibility of lubricant agglomeration. The 1.00 weight percent lubricant addition gave similar results to that observed at 1100°C, specifically showing the most homogeneous density distribution.

For the samples sintered at 1400°C, Figure 5.45, bulk densities between the 0.08" and 0.10" steps of the wedge block were observed. Since the 1T of the 0.08" penetrameter is visible, defects as small as approximately 0.003" can be detected. At this temperature, the Ti-6%Al-4%V samples appear to have more homogeneous density distribution as compared to that observed at 1100°C and 1300°C. (Care must be exercised when analyzing the results for this temperature because boron nitride residue from the sintering plate results in less x-ray penetration and gives the appearance of a darker or less dense material.

At 1400°C, the Ti-6%Al-4%V alloy without zinc stearate addition (first two rows) shows the greatest bulk density gradients but these are greatly diminished when compared to low sintering temperature conditions. The Ti-6%Al-4%V alloy with 0.25 weight percent zinc stearate lubricant no longer shows any "defects" and the samples are almost

completely homogeneous. The samples with 0.50 weight percent lubricant addition (in rows five and six) are similarly homogenous, which is expected since the bulk transport diffusion mechanism is now predominant at this temperature. Finally, the samples containing 1.00 weight percent zinc stearate addition, which are shown in the last two rows, appear completely uniform.

For the samples consolidated at 1500°C, Figure 5.46 shows that the bulk sintered densities correspond to 0.08" and 0.12" steps of the wedge block. Since the 1T of the 0.08" penetrameter is visible, defects as small as approximately 0.003" can be detected. Evident for both the non-lubricated and lubricated samples is the occasional defect. Careful sectioning and progressive polishing revealed that the defect seen near the edge of the sample at column 280 MPa, row two was in fact a larger internal pore as shown in Figure 5.49. However, most of the observed defects were not internal porosity. The sample at column 350 MPa, row four, was examined and found to have a surface rupture that coincides with the defect seen on the x-ray (Figure 5.50). This type of defect was the largest and most commonly observed at this temperature. The defect is typical of "popcorning"[32], an excessive gas pressure buildup in closed or partially closed pores that results in a surface rupture. The increase in gas pressure may have been due to a marginal increase in furnace heating rate, trapped lubricant or reduction of TiO_2 by C (CO/CO_2 gas).

Another evident observation is that of the circular density effect caused by the boron nitride sintering plate as observed for the samples consolidated at 1400°C. At 1500°C, this effect is more prominent. However, no large differences in the density could be observed between the various samples examined. Therefore holding at 1500°C was observed to result in the most homogeneous structure, albeit the disadvantages of uniaxial pressing.

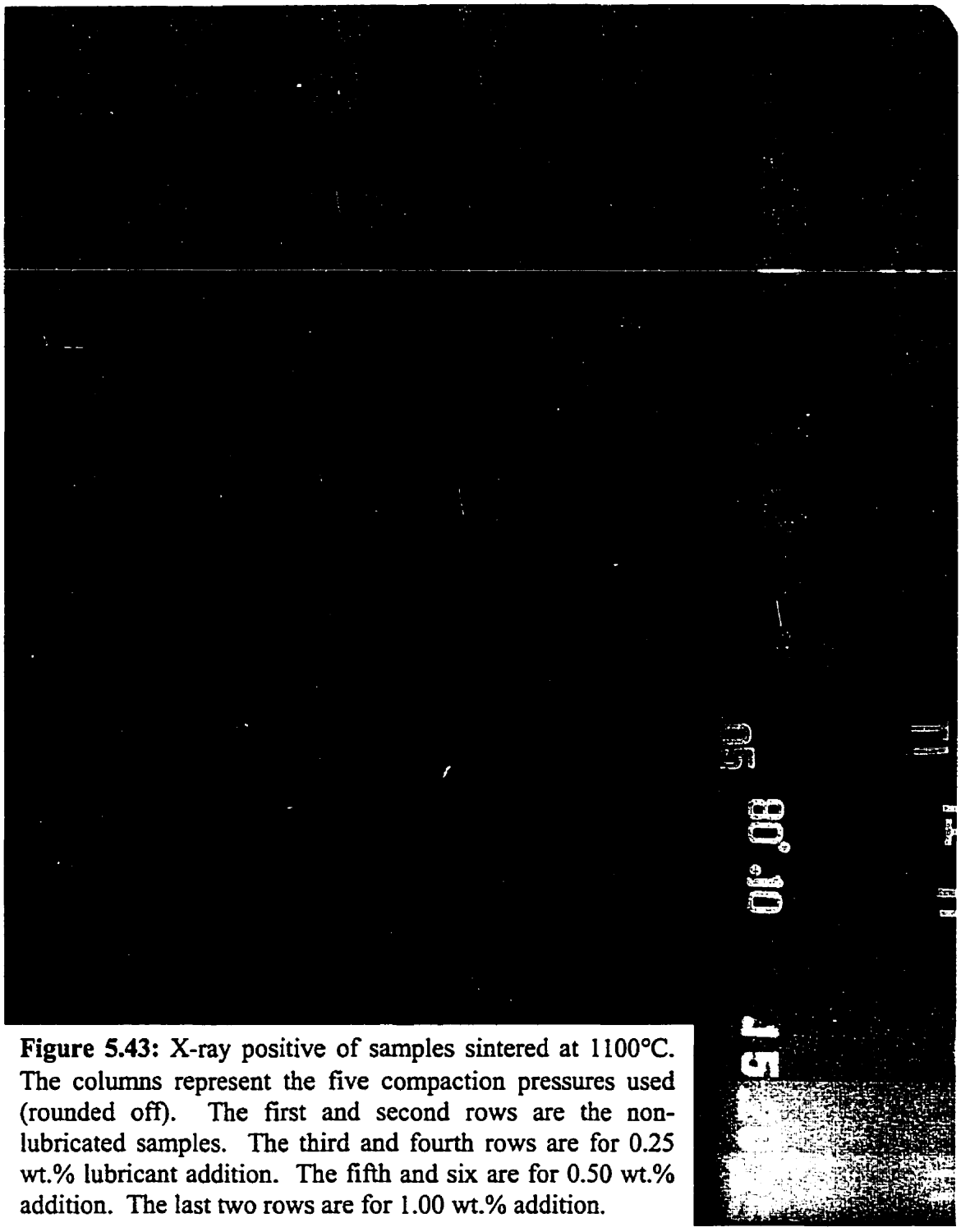

Figure 5.43: X-ray positive of samples sintered at 1100°C. The columns represent the five compaction pressures used (rounded off). The first and second rows are the non-lubricated samples. The third and fourth rows are for 0.25 wt.% lubricant addition. The fifth and six are for 0.50 wt.% addition. The last two rows are for 1.00 wt.% addition.

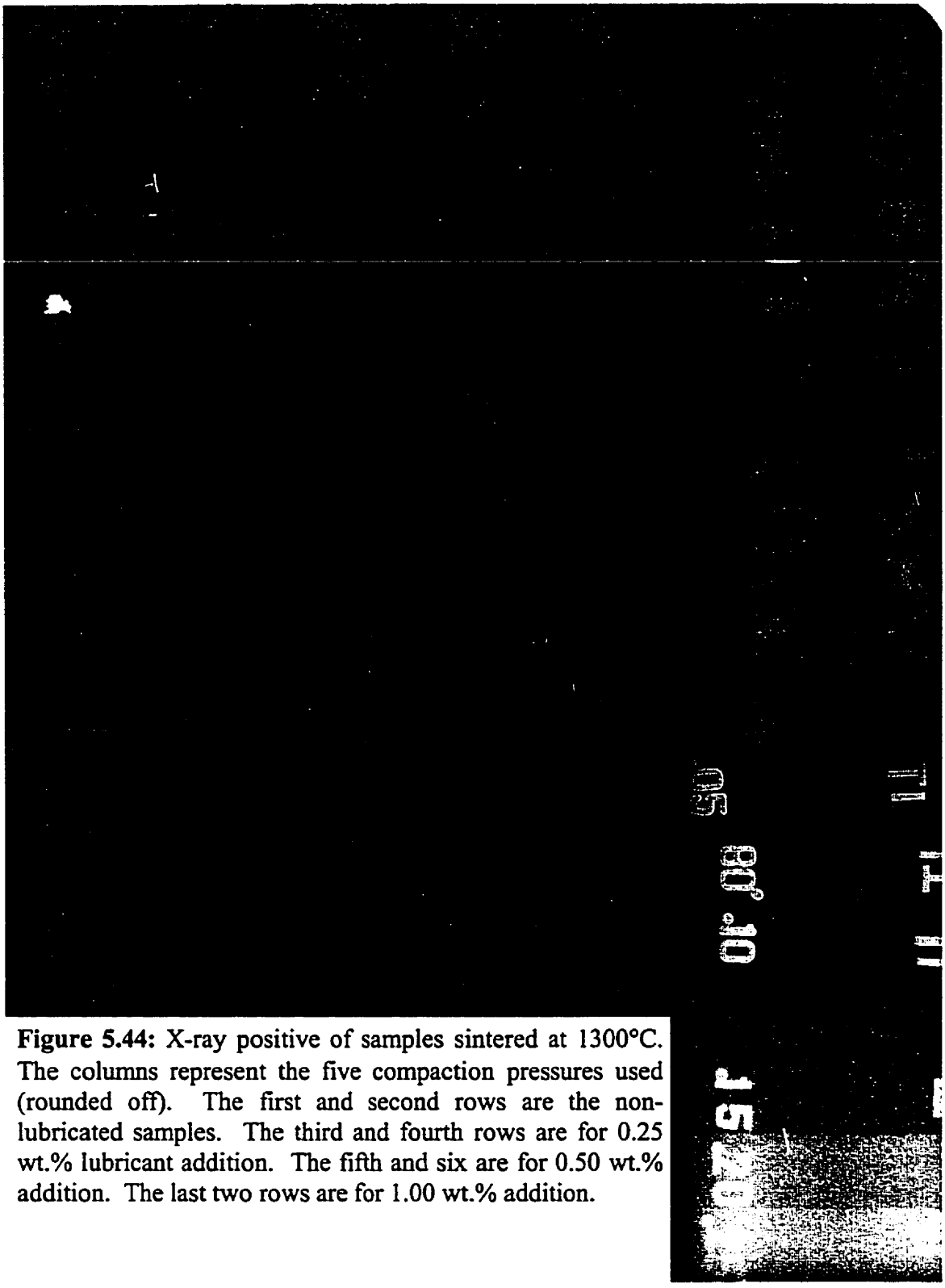

Figure 5.44: X-ray positive of samples sintered at 1300°C. The columns represent the five compaction pressures used (rounded off). The first and second rows are the non-lubricated samples. The third and fourth rows are for 0.25 wt.% lubricant addition. The fifth and six are for 0.50 wt.% addition. The last two rows are for 1.00 wt.% addition.

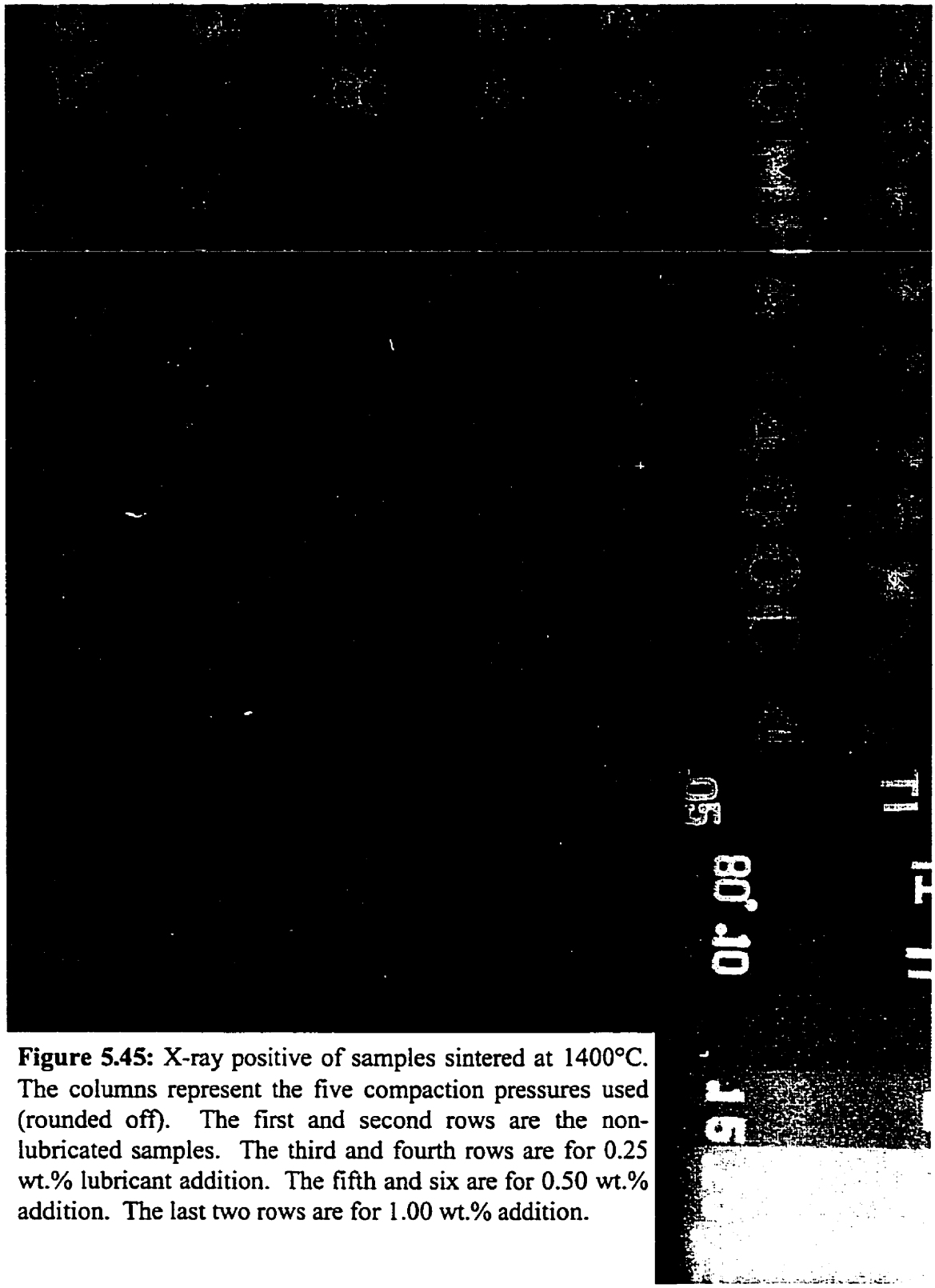

Figure 5.45: X-ray positive of samples sintered at 1400°C. The columns represent the five compaction pressures used (rounded off). The first and second rows are the non-lubricated samples. The third and fourth rows are for 0.25 wt.% lubricant addition. The fifth and six are for 0.50 wt.% addition. The last two rows are for 1.00 wt.% addition.

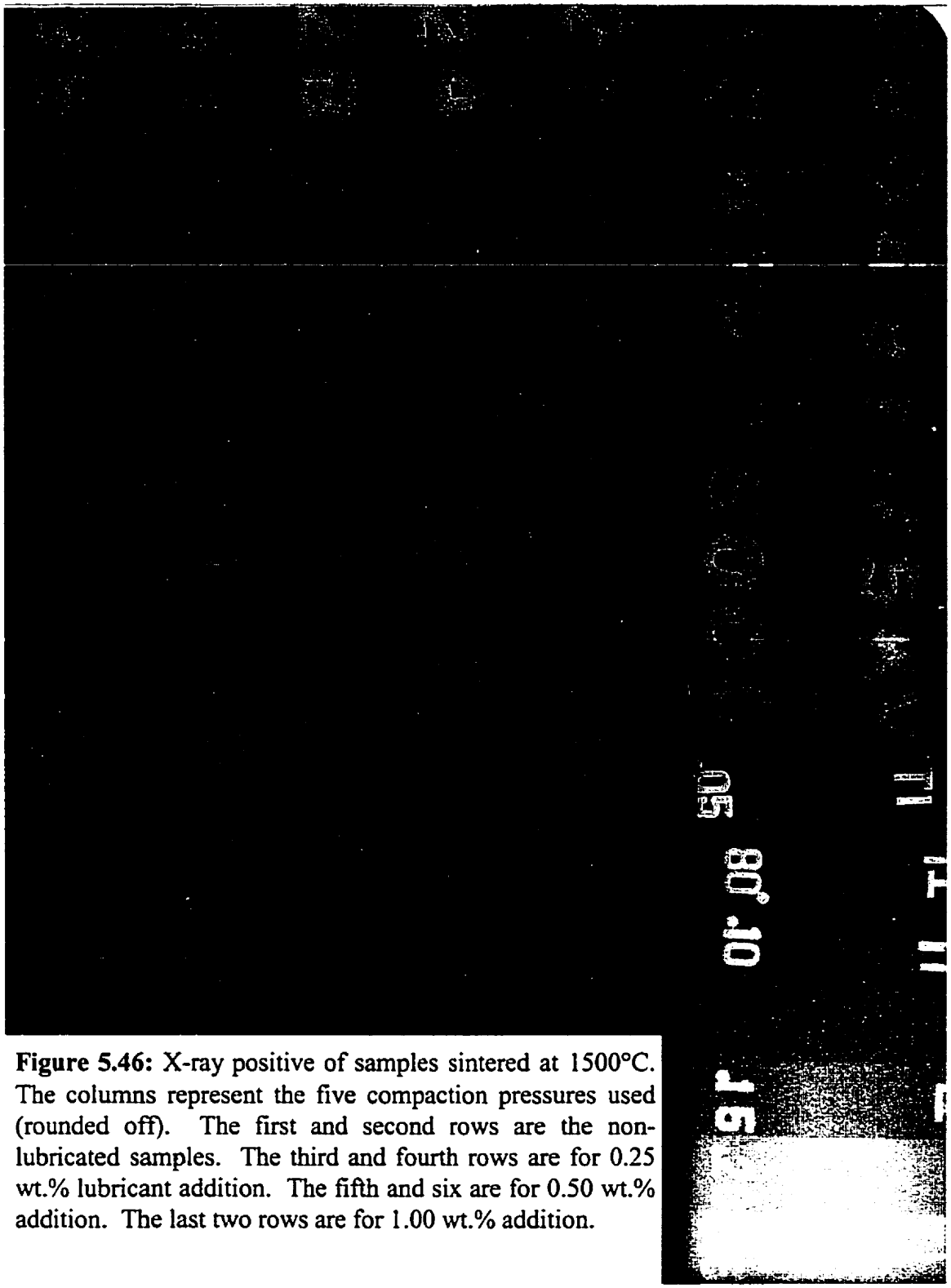

Figure 5.46: X-ray positive of samples sintered at 1500°C. The columns represent the five compaction pressures used (rounded off). The first and second rows are the non-lubricated samples. The third and fourth rows are for 0.25 wt.% lubricant addition. The fifth and six are for 0.50 wt.% addition. The last two rows are for 1.00 wt.% addition.

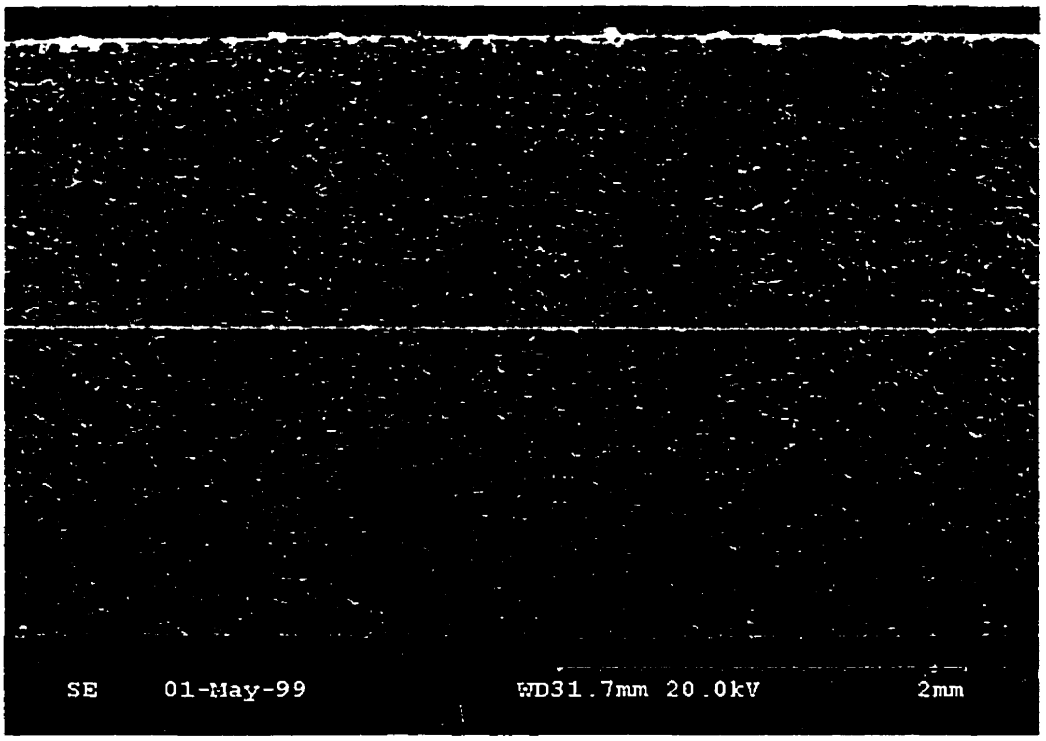

Figure 5.47: Sample cross-section (76% relative density) observed in Figure 5.44, column 240 MPa, row six showing localized regions of varying densities.

Figure 5.48: Higher magnification of Figure 5.47, showing a central region of large interconnected pores surrounded by smaller less interconnected pores.

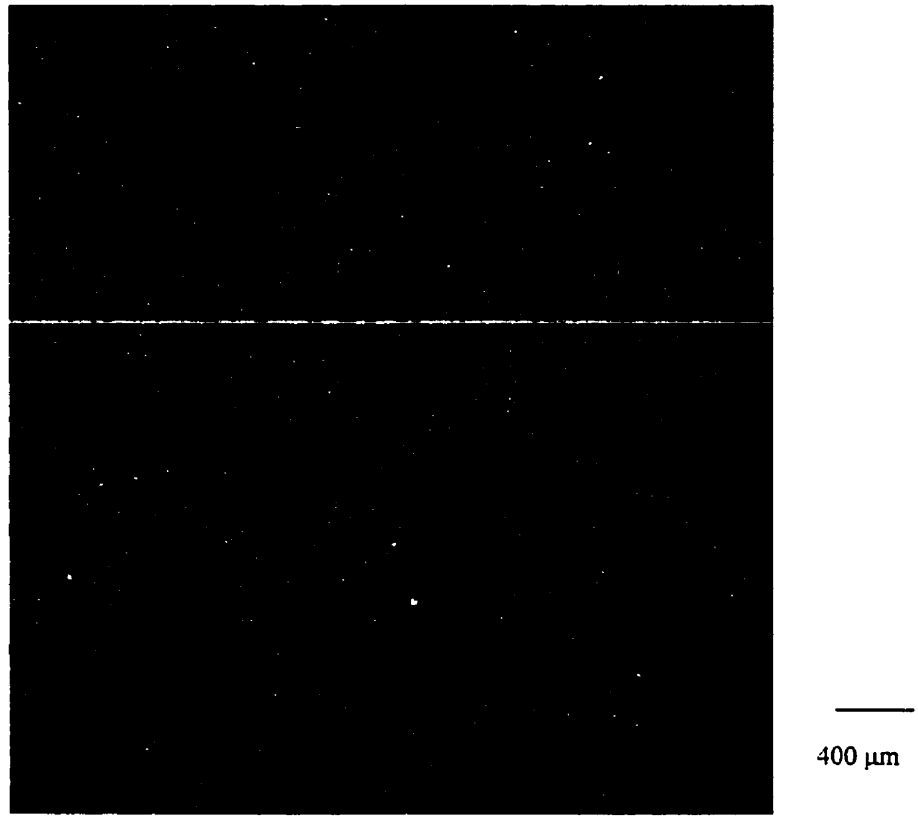

Figure 5.49: Cross section showing a large internal pore in the region where a defect was found for the sample (85%) in Figure 5.46 column 280 MPa, row 2.

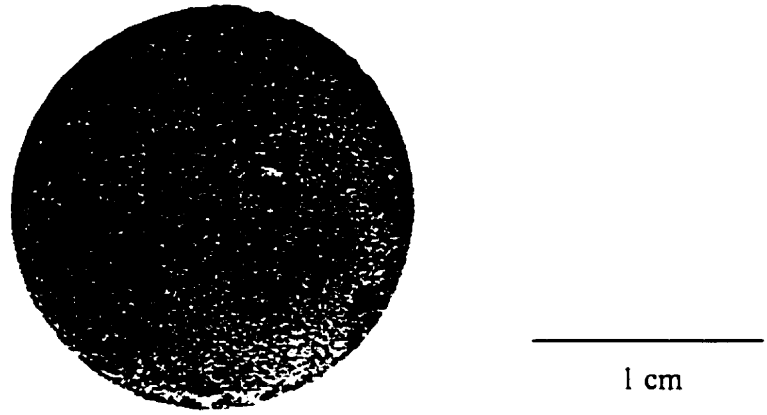

Figure 5.50: Sample (89%) showing a surface rupture in the region where a defect was observed for Figure 5.46; column 350 MPa, row 4.

CHAPTER 6:

CONCLUSIONS

1. The as received Ti-6%Al-4%V powder was not free flowing. The addition of zinc stearate resulted in a free flowing powder with improved flow and apparent density. The greatest increase in these parameters occurred within the first 20 minutes of mixing and at 35 minutes an optimum flow rate and apparent density were found.
2. As the compaction pressure was increased, the pressed samples showed a greater resistance to handling degradation. Below 207 MPa, insufficient green strength was observed, whilst above 343 MPa particle fracture was apparent.
3. Regardless of the lubricant content, the relationship between compaction pressure and green density was linear.
4. The addition of zinc stearate resulted in an increase in the green density. This increase was not proportional to the amount of zinc stearate added.
5. Optimum lubricant addition for good apparent and green densities was determined to be 0.50 weight percent with subsequent additions producing negligible increases.
6. The rate of burnout was not affected by the green density of the compact, but by the amount of zinc stearate used.
7. The zinc stearate burnout began at approximately 425°C and was completed by 525°C, below 595°C the temperature at which the oxidation rate becomes parabolic.

8. The sintered density linearly increased with increasing green density.
9. The improved compaction effect of zinc stearate addition resulted in a 3 to 6 percent increase in the sintered density.
10. The predominant parameter for densification was determined to be temperature as the sintered density for a corresponding increase in temperature was greater than the effect of increased green density. However, for maximum densification the two parameters are interlinked.
11. Due to the improved densification of the lubricated samples, the shrinkage regardless of temperature was 2 to 4 percent greater than the non-lubricated samples. This amount decreased as the initial compaction pressure used was increased.
12. The sintered microstructure confirmed that below 1300°C the activation energy was insufficient to cause significant diffusion by bulk transport mechanisms. As the temperature was increased the corresponding change in microstructure was more apparent as was the improved densification attributed to the lubricant additions.
13. The microstructures of the 0.50 and 1.00 weight percent lubricant additions confirmed the similar trends observed in the sintered density values. Therefore, the optimum amount of zinc stearate was found to be 1/2 weight percent. Above this amount, the degree of improvement in green and sintered densities was relatively small.
14. Although the highest increases in relative sintered densities and Vickers microhardness values were obtained using a sintering temperature of 1500°C, the effect of varying the holding time was not investigated. Thus, 1500°C is the optimum temperature only when a holding time of 1.5 hours is used.
15. The combination of sintering parameters can lead to similar properties for the sintered density, microstructure or microhardness.
16. The importance of proper mixing was demonstrated by the density gradients observed in the X-ray analysis.

RECOMMENDATIONS

Although a significant portion of the investigation into the effect of zinc stearate lubricant addition on sintering of Ti-6%Al-4%V was achieved, the following are suggestions that would help complete this evaluation:

1. The effect and optimization of the holding time employing 1300°C, 1400°C and 1500°C, while using the optimum lubricant addition of 0.50 weight percent and a compaction pressure of 343 MPa.
2. The evaluation and comparison of the mechanical properties using the optimized lubricant versus non lubricated parameters, by such methods as tensile testing, stress rupture and toughness.
3. Cost estimation of using the optimized lubricant in Ti-6%Al-4%V versus no lubricant addition to achieve the same required final properties.

REFERENCES

1. R.M. German, Powder Metallurgy Science, Metal Powder Industries Federation, Princeton, New Jersey, USA, 1984.
2. J.S. Hirschorn, Introduction to Powder Metallurgy, American Powder Metallurgy Institute, New York, New York, USA, 1969.
3. F. Thümmler and R. Oberacker, An Introduction to Powder Metallurgy, Eds. I. Jenkins and J.V. Wood, The Institute of Materials, London, United Kingdom, 1993.
4. F.H. Froes and John E. Smugeresky, Powder Metallurgy of Titanium Alloys, Proceedings of a symposium sponsored by the Powder Metallurgy Committee and the Titanium Committee of The Metallurgical Society of AIME at the 109th AIME Annual Meeting, AIME, New York, USA, 1980.
5. ASM International Handbook Committee, Materials Properties Handbook: Titanium Alloys, Eds. R. Boyer, G. Welsch and E.W. Collings, ASM International, Materials Park, Ohio, USA, 1994.
6. Metals & Minerals Annual Review, 1995, p. 67.
7. AAM, Titanium Profile, 1994, p. 186.
8. Micron Metals Inc., 7186 West Gates Avenue, Salt Lake City, Utah, 1995.
9. ASM, *Advanced Material Processes - Cost of Titanium Powder cut by Hydride- Dehydride Process*, Vol. 149, No. 3, March 1996, p. 18.
10. J.S. Reed, Introduction to Principles of Ceramic Processing, John Wiley and Sons, New York, New York, USA, 1988.
11. C.G. Johnson and W.R. Weeks, Metallurgy, American Technical Publishers Inc., Chicago, Illinois, USA, 1988.
12. M.J. Donachie Jr., Titanium a Technical Guide, ASM International, Materials Park, Ohio, USA, 1988.
13. M.J. Donachie Jr., Titanium and Titanium Alloys Source Book, ASM International, Materials Park, Ohio, USA, 1982.
14. G. Lütjering, U. Zwicker and W. Bunk, Titanium Science and Technology, Vol. 1, Proceedings of the Fifth International Conference on Titanium, Deutsche Gesellschaft für Metallukunde, Munich, 1984.
15. M. Entezarian, F. Allaire, P. Tsantrizos, and R. Drew, "Plasma Atomization", *Journal of Metals*, June 1996, p. 53.
16. K.B. Patel and D.J. Lloyd, Evaluation of Rapidly Solidified Metal Powders Produced by a Rotary Atomizer, Alcan, 1986.
17. H.H. Hausner, Handbook of Powder Metallurgy, Chemical Publishing Co. Inc., New York, New York, USA, 1973

18. F.H. Froes and D. Eylon, "Powder Metallurgy of Titanium Alloys", *International Materials Reviews*, 1990, Vol. 35, No. 3, pp. 162-182.

19. D. Yarnton and M. Argyle, A Practicle Course in Powder Metallurgy, Cassel, London, Great Britain, 1962.

20. F.V. Lenel, Overview of Powder Metallurgy Products and Processing, ASM International, Materials Park, Ohio, USA, 1990.

21. ASTM, Annual Book of ASTM Standards, Vol. 02.05, 1989.

22. A.R. Poster, Handbook of Metal Powders, Reinhold Publishing Corporation, New York, New York, USA, 1966.

23. F.V. Lenel, Powder Characterization II, ASM International, Materials Park, Ohio, USA, 1990.

24. R.M. German, Particle Packing Characteristics, Metal Powder Industries Federation, Princeton, New Jersey, USA, 1989.

25. F. Clark, Advanced Techniques in Powder Metallurgy, Rowan and Littlefield, New York, New York, USA, 1963.

26. F.V. Lenel, Compacting I, ASM International, Materials Park, Ohio, USA, 1990.

27. D.W. Richerson, Modern Ceramic Engineering, Second Edition, Marcel Dekker Inc., New York, New York, USA, 1992.

28. A. Lawley, "Chapter 5: Powder Consolidation", Advances in Powder Technology, Ed. G.Y. Chin, American Society for Metals, Metals Park, Ohio, USA, 1982, pp. 75-97.

29. H.A. Kuhn and A. Lawley, Powder Metallurgy Processing, Academic Press, New York, New York, USA, 1978, pp. 99-170.

30. S. Débouzy, Sintering of Ti-TiC Metal Matrix Composites, M. Eng. Thesis, McGill University, Montreal, Quebec, Canada, 1994.

31. E.W. Collings, The Physical Metallurgy of Titanium Alloys, American Society for Metals, Metals Park, Ohio, USA, 1984.

32. S. Bradbury, Source Book on Powder Metallurgy, American Society for Metals, Metals Park, Ohio, USA, 1979.

APPENDICES

Appendix A: MEASURED GREEN DENSITIES

No Lubricant							
Pressure (MPa)	1100°C			Pressure (MPa)	1300°C		
	Sample 1 (g/cc)	Sample 2 (g/cc)	Sample 3 (g/cc)		Sample 1 (g/cc)	Sample 2 (g/cc)	Sample 3 (g/cc)
207	2.53	2.53	2.49	207	2.56	2.56	2.56
241	2.64	2.64	2.66	241	2.65	2.64	2.65
276	2.69	2.71	2.71	276	2.69	2.69	2.70
310	2.74	2.77	2.77	310	2.75	2.76	2.76
343	2.83	2.83	2.83	343	2.85	2.85	2.86
Pressure (MPa)	1400°C			Pressure (MPa)	1500°C		
	Sample 1 (g/cc)	Sample 2 (g/cc)	Sample 3 (g/cc)		Sample 1 (g/cc)	Sample 2 (g/cc)	Sample 3 (g/cc)
207	2.52	2.52	2.53	207	2.57	2.57	2.58
241	2.63	2.63	2.62	241	2.67	2.67	2.67
276	2.71	2.71	2.71	276	2.73	2.71	2.72
310	2.75	2.74	2.74	310	2.77	2.76	2.77
343	2.84	2.84	2.84	343	2.86	2.86	2.85

0.25 % Lubricant							
Pressure (MPa)	1100°C			Pressure (MPa)	1300°C		
	Sample 1 (g/cc)	Sample 2 (g/cc)	Sample 3 (g/cc)		Sample 1 (g/cc)	Sample 2 (g/cc)	Sample 3 (g/cc)
207	2.58	2.63	2.63	207	2.64	2.65	2.66
241	2.73	2.73	2.73	241	2.73	2.71	2.69
276	2.82	2.77	2.77	276	2.75	2.75	2.75
310	2.88	2.85	2.85	310	2.87	2.87	2.86
343	2.92	2.94	2.94	343	2.92	2.93	2.93
Pressure (MPa)	1400°C			Pressure (MPa)	1500°C		
	Sample 1 (g/cc)	Sample 2 (g/cc)	Sample 3 (g/cc)		Sample 1 (g/cc)	Sample 2 (g/cc)	Sample 3 (g/cc)
207	2.63	2.63	2.63	207	2.65	2.64	2.64
241	2.71	2.70	2.71	241	2.71	2.72	2.74
276	2.77	2.77	2.77	276	2.81	2.79	2.80
310	2.87	2.87	2.87	310	2.88	2.88	2.88
343	2.92	2.93	2.91	343	2.97	2.95	2.95

0.50 % Lubricant							
Pressure (MPa)	1100°C			Pressure (MPa)	1300°C		
	Sample 1 (g/cc)	Sample 2 (g/cc)	Sample 3 (g/cc)		Sample 1 (g/cc)	Sample 2 (g/cc)	Sample 3 (g/cc)
207	2.61	2.62	2.59	207	2.64	2.62	2.63
241	2.72	2.72	2.72	241	2.72	2.72	2.72
276	2.79	2.79	2.79	276	2.81	2.80	2.81
310	2.85	2.83	2.82	310	2.87	2.87	2.88
343	2.92	2.91	2.93	343	2.95	2.93	2.93
Pressure (MPa)	1400°C			Pressure (MPa)	1500°C		
	Sample 1 (g/cc)	Sample 2 (g/cc)	Sample 3 (g/cc)		Sample 1 (g/cc)	Sample 2 (g/cc)	Sample 3 (g/cc)
207	2.67	2.66	2.66	207	2.69	2.68	2.67
241	2.73	2.75	2.73	241	2.77	2.75	2.77
276	2.81	2.82	2.82	276	2.84	2.83	2.83
310	2.90	2.87	2.89	310	2.90	2.91	2.91
343	2.95	2.96	2.95	343	2.96	2.98	2.98

1.00 % Lubricant							
Pressure (MPa)	1100°C			Pressure (MPa)	1300°C		
	Sample 1 (g/cc)	Sample 2 (g/cc)	Sample 3 (g/cc)		Sample 1 (g/cc)	Sample 2 (g/cc)	Sample 3 (g/cc)
207	2.68	2.68	2.67	207	2.68	2.69	2.62
241	2.76	2.77	2.77	241	2.77	2.77	2.77
276	2.80	2.81	2.81	276	2.83	2.82	2.82
310	2.88	2.87	2.87	310	2.88	2.90	2.90
343	2.98	2.97	2.97	343	2.99	2.98	2.98
Pressure (MPa)	1400°C			Pressure (MPa)	1500°C		
	Sample 1 (g/cc)	Sample 2 (g/cc)	Sample 3 (g/cc)		Sample 1 (g/cc)	Sample 2 (g/cc)	Sample 3 (g/cc)
207	2.69	2.69	2.69	207	2.70	2.65	2.71
241	2.77	2.78	2.79	241	2.78	2.79	2.78
276	2.83	2.84	2.84	276	2.87	2.84	2.86
310	2.91	2.91	2.92	310	2.94	2.93	2.92
343	2.99	3.00	2.99	343	3.02	3.00	3.03

Appendix B: THERMO-GRAVIMETRIC FIRST DERIVATIVE RESULTS

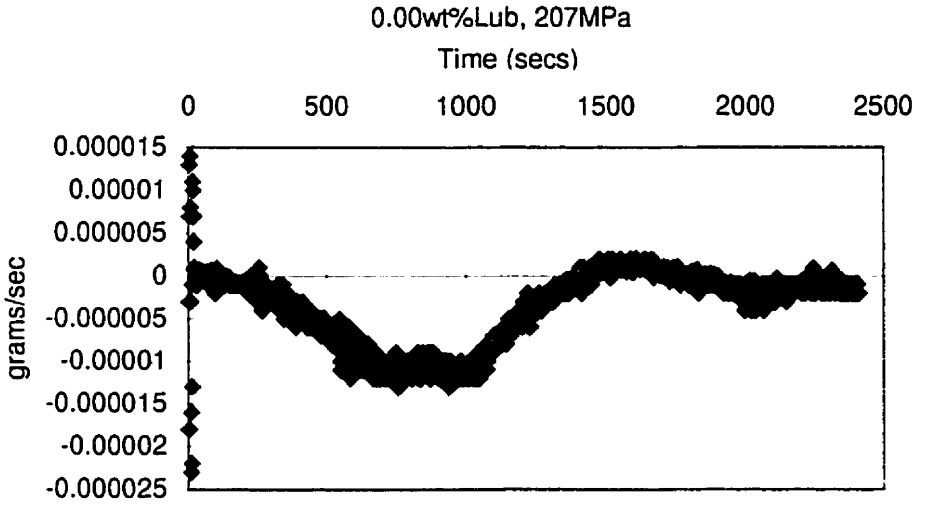

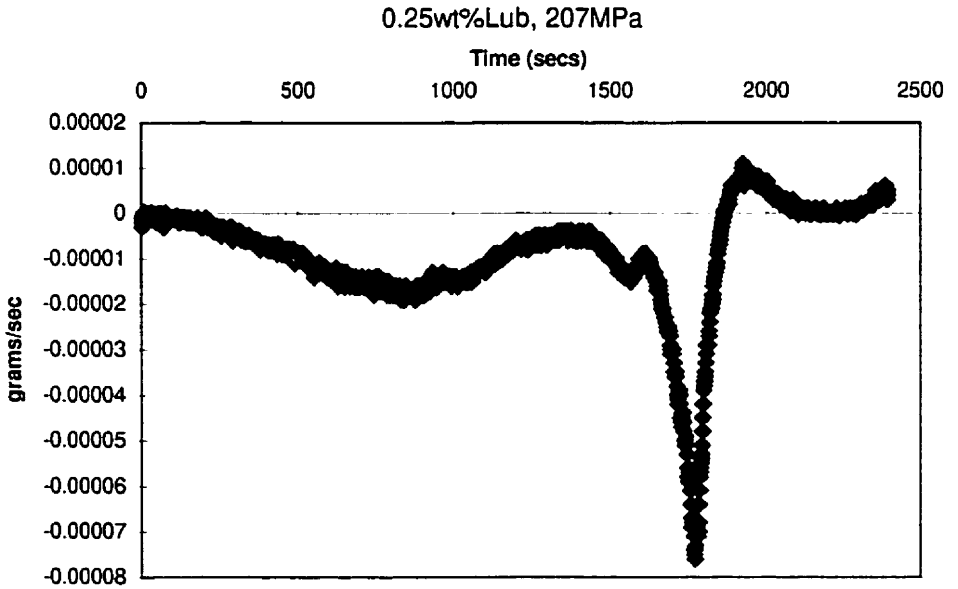

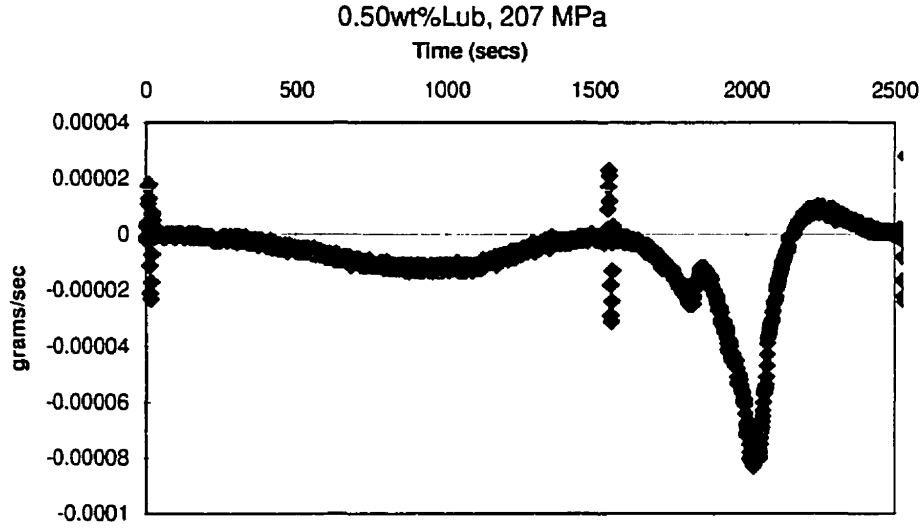
0.50wt%Lub, 207 MPa
Time (secs)
0
500
1000
1500
2000
2500
0.00004
0.00002
0
-0.00002
-0.00004
-0.00006
-0.00008
-0.0001
grams/sec

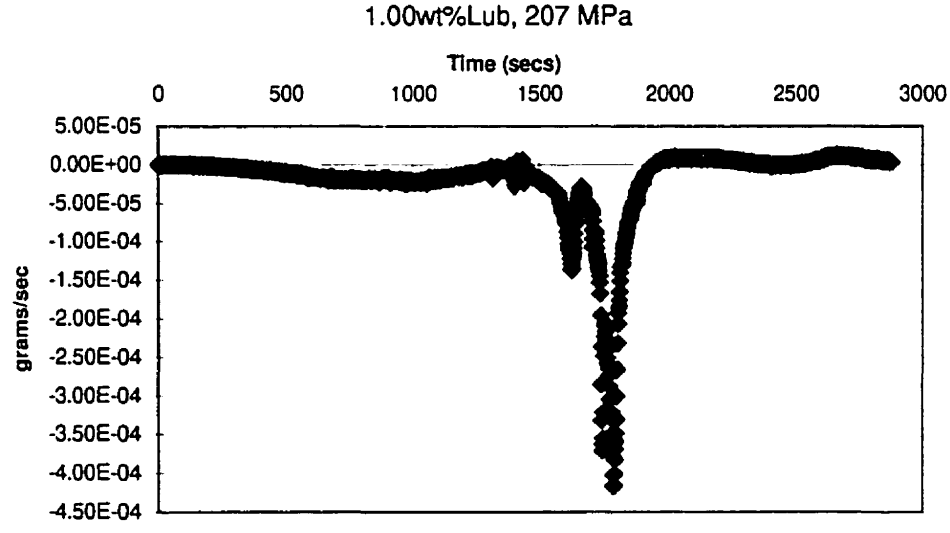
1.00wt%Lub, 207 MPa
Time (secs)
0
500
1000
1500
2000
2500
3000
5.00E-05
0.00E+00
-5.00E-05
-1.00E-04
-1.50E-04
-2.00E-04
-2.50E-04
-3.00E-04
-3.50E-04
-4.00E-04
-4.50E-04
grams/sec

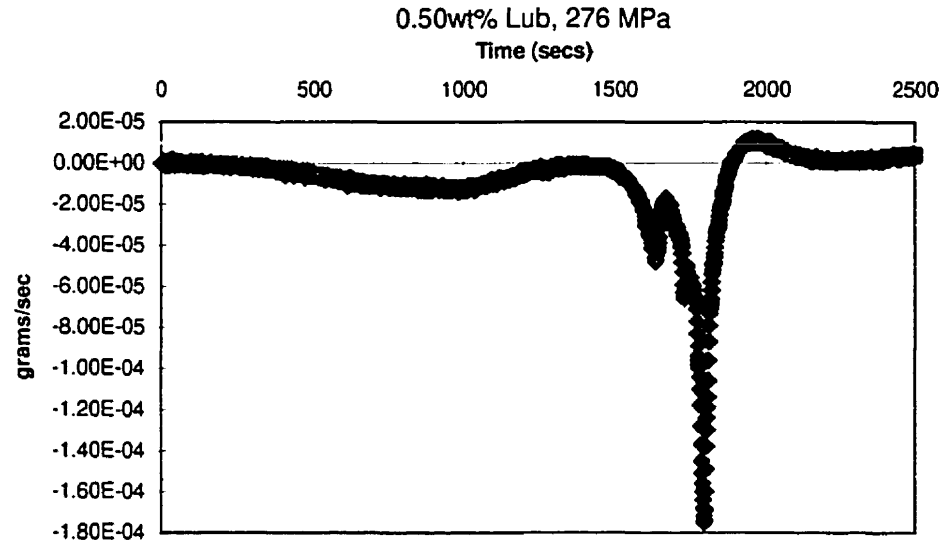
0.50wt% Lub, 276 MPa
Time (secs)
0
500
1000
1500
2000
2500
2.00E-05
0.00E+00
-2.00E-05
-4.00E-05
-6.00E-05
-8.00E-05
-1.00E-04
-1.20E-04
-1.40E-04
-1.60E-04
-1.80E-04
grams/sec

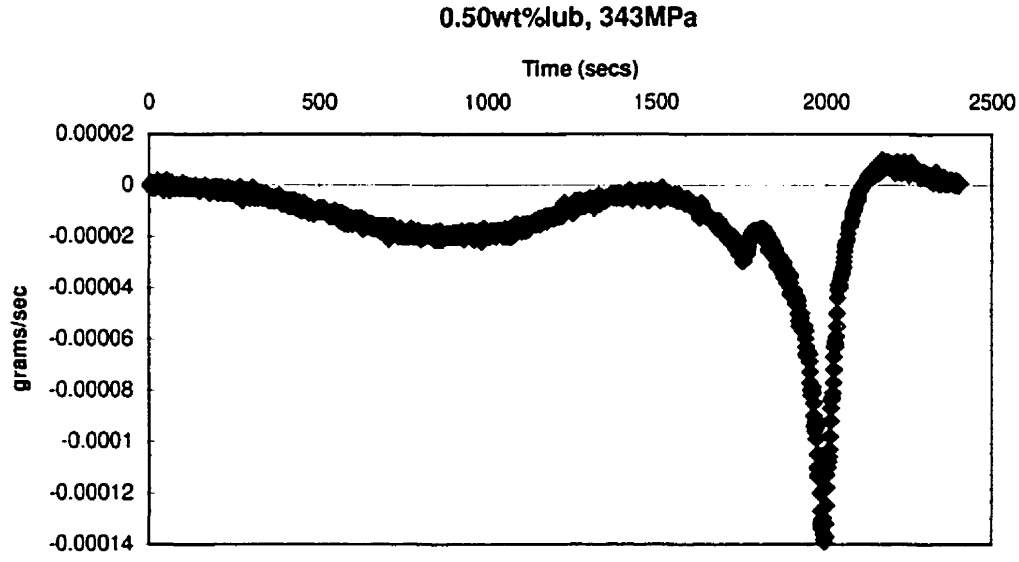
0.50wt%lub, 343MPa
Time (secs)
0
500
1000
1500
2000
2500
0.00002
0
-0.00002
-0.00004
-0.00006
-0.00008
-0.0001
-0.00012
-0.00014
grams/sec

Appendix C: ARCHIMEDES SINTERED DENSITIES

No Lubricant							
Pressure (MPa)	1100°C Sample 1 (g/cc)	1100°C Sample 2 (g/cc)	1100°C Sample 3 (g/cc)	Pressure (MPa)	1300°C Sample 1 (g/cc)	1300°C Sample 2 (g/cc)	1300°C Sample 3 (g/cc)
207	2.82	2.81	2.80	207	3.14	3.14	3.15
241	2.89	2.88	2.87	241	3.21	3.19	3.20
276	2.93	2.95	2.91	276	3.25	3.26	3.27
310	2.99	3.00	3.02	310	3.36	3.35	3.37
343	3.12	3.11	3.12	343	3.41	3.45	3.41
Pressure (MPa)	1400°C Sample 1 (g/cc)	1400°C Sample 2 (g/cc)	1400°C Sample 3 (g/cc)	Pressure (MPa)	1500°C Sample 1 (g/cc)	1500°C Sample 2 (g/cc)	1500°C Sample 3 (g/cc)
207	3.36	3.35	3.34	207	3.60	3.61	3.60
241	3.40	3.40	3.37	241	3.66	3.64	3.65
276	3.49	3.51	3.46	276	3.74	3.74	3.75
310	3.54	3.53	3.56	310	3.79	3.77	3.83
343	3.61	3.60	3.60	343	3.87	3.84	3.86

0.25 % Lubricant							
Pressure (MPa)	1100°C Sample 1 (g/cc)	1100°C Sample 2 (g/cc)	1100°C Sample 3 (g/cc)	Pressure (MPa)	1300°C Sample 1 (g/cc)	1300°C Sample 2 (g/cc)	1300°C Sample 3 (g/cc)
207	2.89	2.90	2.91	207	3.28	3.28	3.29
241	2.99	2.97	3.01	241	3.34	3.35	3.35
276	3.04	3.04	3.03	276	3.39	3.39	3.40
310	3.11	3.09	3.12	310	3.50	3.50	3.50
343	3.19	3.17	3.18	343	3.53	3.54	3.54
Pressure (MPa)	1400°C Sample 1 (g/cc)	1400°C Sample 2 (g/cc)	1400°C Sample 3 (g/cc)	Pressure (MPa)	1500°C Sample 1 (g/cc)	1500°C Sample 2 (g/cc)	1500°C Sample 3 (g/cc)
207	3.42	3.46	3.42	207	3.79	3.80	3.80
241	3.54	3.53	3.54	241	3.81	3.81	3.84
276	3.56	3.55	3.56	276	3.85	3.87	3.86
310	3.58	3.61	3.60	310	3.90	3.88	3.89
343	3.64	3.64	3.63	343	3.93	3.92	3.95

0.50 % Lubricant							
Pressure (MPa)	1100°C			Pressure (MPa)	1300°C		
	Sample 1 (g/cc)	Sample 2 (g/cc)	Sample 3 (g/cc)		Sample 1 (g/cc)	Sample 2 (g/cc)	Sample 3 (g/cc)
207	2.89	2.88	2.89	207	3.30	3.31	3.30
241	2.98	2.98	2.97	241	3.35	3.36	3.32
276	3.05	3.04	3.05	276	3.45	3.44	3.46
310	3.11	3.11	3.11	310	3.52	3.51	3.51
343	3.19	3.18	3.21	343	3.56	3.55	3.56
Pressure (MPa)	1400°C			Pressure (MPa)	1500°C		
	Sample 1 (g/cc)	Sample 2 (g/cc)	Sample 3 (g/cc)		Sample 1 (g/cc)	Sample 2 (g/cc)	Sample 3 (g/cc)
207	3.59	3.57	3.60	207	3.85	3.85	3.84
241	3.63	3.65	3.61	241	3.86	3.88	3.86
276	3.70	3.70	3.68	276	3.90	3.89	3.91
310	3.74	3.72	3.75	310	3.93	3.92	3.94
343	3.77	3.76	3.78	343	3.96	3.95	3.95

1.00 % Lubricant							
Pressure (MPa)	1100°C			Pressure (MPa)	1300°C		
	Sample 1 (g/cc)	Sample 2 (g/cc)	Sample 3 (g/cc)		Sample 1 (g/cc)	Sample 2 (g/cc)	Sample 3 (g/cc)
207	2.94	2.93	2.92	207	3.29	3.33	3.30
241	2.99	2.99	2.99	241	3.39	3.37	3.40
276	3.07	3.06	3.07	276	3.46	3.44	3.42
310	3.15	3.16	3.17	310	3.50	3.52	3.50
343	3.23	3.22	3.22	343	3.56	3.56	3.54
Pressure (MPa)	1400°C			Pressure (MPa)	1500°C		
	Sample 1 (g/cc)	Sample 2 (g/cc)	Sample 3 (g/cc)		Sample 1 (g/cc)	Sample 2 (g/cc)	Sample 3 (g/cc)
207	3.58	3.60	3.61	207	3.82	3.83	3.82
241	3.62	3.64	3.64	241	3.88	3.88	3.87
276	3.69	3.67	3.67	276	3.91	3.91	3.90
310	3.73	3.73	3.74	310	3.94	3.94	3.92
343	3.78	3.79	3.78	343	3.98	3.96	3.97

Appendix D: IMAGE ANALYSIS

1100°C								
Compact. Pressure (MPa)	Lubricant 0.00wt%		Lubricant 0.25wt%		Lubricant 0.50wt%		Lubricant 1.00wt%	
	Porosity (%)	± %	Porosity (%)	± %	Porosity (%)	± %	Porosity (%)	± %
207	27.34	2.20	24.21	2.08	22.98	1.34	22.89	1.64
241	23.16	1.19	20.30	1.58	17.93	1.41	18.29	1.09
276	22.39	2.04	16.86	1.18	15.67	1.54	15.91	1.13
310	17.71	1.62	15.37	1.26	14.89	1.35	13.90	1.18
343	16.36	1.97	14.22	1.35	14.28	1.14	13.56	0.95
1500°C								
Compact. Pressure (MPa)	Lubricant 0.00wt%		Lubricant 0.25wt%		Lubricant 0.50wt%		Lubricant 1.00wt%	
	Porosity (%)	± %	Porosity (%)	± %	Porosity (%)	± %	Porosity (%)	± %
207	11.00	1.02	8.74	0.63	8.62	0.74	7.50	0.83
241	9.54	1.15	8.75	0.78	8.95	0.63	7.37	0.67
276	9.79	0.91	9.20	0.81	7.91	0.69	7.42	0.54
310	9.32	1.08	8.91	0.60	8.61	0.94	7.41	0.65
343	8.10	0.82	7.10	0.54	6.64	0.55	6.36	0.57

Appendix E: MICROHARDNESS

1100°C								
Compact. Pressure (MPa)	Lubricant 0.00wt%		Lubricant 0.25wt%		Lubricant 0.50wt%		Lubricant 1.00wt%	
	Micro-Hardness Vickers	Std. Dev. Hv	Micro-Hardness Vickers	Std. Dev. Hv	Micro-Hardness Vickers	Std. Dev. Hv	Micro-Hardness Vickers	Std. Dev. Hv
207	-	-	-	-	-	-	-	-
241	-	-	-	-	-	-	-	-
276	-	-	-	-	-	-	-	-
310	-	-	-	-	-	-	-	-
343	-	-	-	-	244	56	242	36

1300°C								
Compact. Pressure (MPa)	Lubricant 0.00wt%		Lubricant 0.25wt%		Lubricant 0.50wt%		Lubricant 1.00wt%	
	Micro-Hardness Vickers	Std. Dev. Hv	Micro-Hardness Vickers	Std. Dev. Hv	Micro-Hardness Vickers	Std. Dev. Hv	Micro-Hardness Vickers	Std. Dev. Hv
207			258	39	263	27	268	22
241	241	35	256	24	281	22	282	20
276	244	55	261	37	294	23	294	20
310	250	27	277	27	304	22	303	25
343	263	30	289	33	318	24	326	17

1400°C								
Compact. Pressure (MPa)	Lubricant 0.00wt%		Lubricant 0.25wt%		Lubricant 0.50wt%		Lubricant 1.00wt%	
	Micro-Hardness Vickers	Std. Dev. Hv	Micro-Hardness Vickers	Std. Dev. Hv	Micro-Hardness Vickers	Std. Dev. Hv	Micro-Hardness Vickers	Std. Dev. Hv
207	301	22	316	13	345	11	350	10
241	305	16	333	17	351	14	356	16
276	325	16	337	11	358	16	361	8
310	330	18	342	13	366	11	368	10
343	344	14	360	14	374	10	376	6

1500°C								
Compact. Pressure (MPa)	Lubricant 0.00wt%		Lubricant 0.25wt%		Lubricant 0.50wt%		Lubricant 1.00wt%	
	Micro-Hardness Vickers	Std. Dev. Hv	Micro-Hardness Vickers	Std. Dev. Hv	Micro-Hardness Vickers	Std. Dev. Hv	Micro-Hardness Vickers	Std. Dev. Hv
207	349	13	381	10	386	5	388	6
241	357	14	384	9	390	6	393	5
276	370	9	390	6	399	5	400	4
310	380	8	397	5	406	4	407	4
343	388	6	405	5	417	5	419	3